

Excitation Energies and Properties of Large Molecules from *ab-initio* Calculations



Dissertation

zur Erlangung des Doktorgrades der Naturwissenschaften (Dr. rer. nat.)
der Fakultät
- Chemie und Pharmazie -
der Universität Regensburg

vorgelegt von

Danylo Kats

aus Regensburg

Regensburg 2010

Promotionsgesuch eingereicht am:	25.01.2010
Tag des kolloquiums:	18.03.2010
Diese Arbeit wurde eingeleitet von:	Prof. Dr. Martin Schütz

Promotionsausschuss

Vorsitzender:	Prof. Dr. Hans-Achim Wagenknecht
Erstgutachter:	Prof. Dr. Martin Schütz
Zweitgutachter:	Dr. Tatiana Korona
Drittprüfer:	Prof. Dr. Bernhard Dick

Die Ergebnisse dieser Arbeit sind bereits veröffentlicht worden:

Chapter 2

D. Kats, T. Korona and M. Schütz

"Local CC2 electronic excitation energies for large molecules with density fitting"

The Journal of Chemical Physics

125, 104106 (2006), doi: 10.1063/1.2339021

Chapter 3

D. Kats, T. Korona and M. Schütz

"Transition strengths and first-order properties of excited states from local coupled cluster CC2 response theory with density fitting"

The Journal of Chemical Physics

127, 064107 (2007), doi: 10.1063/1.2755778

Chapter 4

D. Kats, D. Usvyat and M. Schütz

"On the use of the Laplace transform in local correlation methods"

Physical Chemistry Chemical Physics

10, 3430 (2008), doi: 10.1039/b802993h

Chapter 5

D. Kats, D. Usvyat, S. Loibl, T. Merz and M. Schütz

"Comment on 'Minimax approximation for the decomposition of energy denominators in Laplace-transformed Møller-Plesset perturbation theories' [J. Chem. Phys. 129, 044112 (2008)] "

The Journal of Chemical Physics

130, 127101 (2009), doi: 10.1063/1.3092982

Chapter 6

D. Kats and M. Schütz

"A multistate local coupled cluster CC2 response method based on the
Laplace transform"

The Journal of Chemical Physics

131 , 124117 (2009), doi: 10.1063/1.3237134

Chapter 7

D. Kats and M. Schütz

"Local Time-Dependent Coupled Cluster Response for properties of
excited

states in large molecules"

Zeitschrift für physikalische Chemie

(2010)

Acknowledgements

This thesis would not have been completed without guidance and support from my colleges, friends and family.

First of all I would like to express my gratitude to my supervisor, Prof. Dr. Martin Schütz, for his excellent guidance, encouragement and support throughout the whole period of my PhD studentship.

I would like to thank Dr. Tatiana Korona for deep and extremely fruitful collaboration and also having good time during several conferences.

I am obliged to many of my colleagues from the theoretical chemistry group of the University Regensburg who supported me throughout the past few years, especially Dr. Denis Usvyat for interesting and fruitful discussions and Dr. Keyarash Sadeghian for his tricky test molecules, which never worked from the first time.

I am grateful to all my colleges for understanding and patience during our "russian" conversations, for the nice atmosphere here in our cozy corridor on the third floor of the chemistry building, and for pleasant tea rounds.

I also would like to thank my parents and sisters for their patience, believe in me and encouraging me with their best wishes.

This project was funded by the Deutsche Forschungsgemeinschaft (DFG) in the context of the priority program SPP1145, which is gratefully acknowledged.

Contents

1	Introduction	3
1.1	Coupled Cluster Theory and Diagrams	4
1.1.1	Fundamentals of the Coupled Cluster Theory	4
1.1.2	Diagrammatic technique for spatial orbitals	5
1.1.3	MP2 and CC2 methods	7
1.2	Linear Response theory	8
1.2.1	Time-dependent formalism	8
1.2.2	Time-averaging and response functions	10
1.2.3	Excitation energies	12
1.3	Density fitting approximation	13
1.4	Local methods	14
1.5	Laplace transform	16
1.6	Structure of the thesis	17
2	Local CC2	18
2.1	Introduction	18
2.2	Theory	19
2.2.1	The local CC2 model	21
2.2.2	Local CC2 excitation energies	26
2.3	Test Calculations	29
2.4	Conclusions	43
3	Properties of excited states	45
3.1	Introduction	45
3.2	Theory	45
3.2.1	Transition strengths	49
3.2.2	First-order properties	52
3.2.3	CP domains for property calculations	53
3.3	Test Calculations	55
3.4	Conclusions	63

4	Laplace Transform in local methods	66
4.1	Introduction	66
4.2	Theory	68
4.3	Test Calculations	79
4.4	Conclusions	88
5	Integration Points for Laplace Transform	89
6	Local CC2 with Laplace Transform	94
6.1	Introduction	94
6.2	Theory	95
6.2.1	Direct diagonalization of the Jacobian	98
6.2.2	The right matrix-vector product	100
6.2.3	Local approximations for excited states	102
6.2.4	Complex eigenvalues and -vectors	104
6.2.5	Rescaling of matrix-vector product after refresh	106
6.3	Test Calculations	106
6.4	Conclusions	113
7	LCC2 vs. LT-LCC2	115
7.1	Introduction	115
7.2	Theory	117
7.2.1	Excitation energies	117
7.2.2	Transition strengths and first-order properties	121
7.3	Test Calculations	124
7.4	Conclusions	127
8	Summary	129
	Bibliography	131

Chapter 1

Introduction

Electronic excitations play an important role in the physical and chemical processes in the universe, from chemistry taking place in all life-forms to Fraunhofer lines in the optical spectrum of the Sun, etc. It is evident, that we need reliable theoretical methods to study properties of electronically excited states, which can be used to interpret experimental data, to understand mechanisms of complex photo-reactions, to predict spectra from not (yet) synthesized molecules etc. Over the last decades an arsenal of different *ab initio* methods for excited state calculations has been developed, ranging from rather inexpensive but often unreliable approaches (like Configuration Interaction Singles, CIS [1]) to highly accurate but very expensive methods (like multi-reference CI [2–5] or Coupled Cluster (CC) [6] with the inclusion of triples excitations). One of the most commonly used methods for calculating the excitation spectra of large molecules is the Time-Dependent Density Functional Theory (TD-DFT) [7, 8]. However TD-DFT, used with the common exchange-correlation functionals based on the generalized gradient approximation (including hybrids like B3LYP), is not capable to provide a qualitatively correct spectrum of a molecular system, as concerns charge transfer (CT) or Rydberg states, or excitations of larger π systems play a role [8, 9]. Errors in excitation energies of CT states can easily exceed 2 eV [10], with TD-DFT drawing a picture of the photophysics of a system which is quite different from that provided by more reliable methods and incompatible to experimental findings [11]. Although very recently several new functionals have appeared, which were especially tailored to overcome these deficiencies (see e.g. the CAM-B3LYP method [12]), the TD-DFT approach should be still used with caution and is far from being a *black-box* method. For instance the CAM-B3LYP functional was reported to reproduce the correct behaviour of a low-lying CT band of the zincbacteriochlorin-bacteriochlorin complex [13], yet another

recent study [14] shows that it systematically underestimates the lowest excitation energies for a series of anthraquinones (one of the most important classes of industrial dyes). A functional capable of properly treating valence, CT, and Rydberg states still is unavailable. This is a rather unsatisfactory situation, since the interest in excited states of extended molecules, where CT and excitations of larger π systems play the decisive role for the photophysical processes, is rapidly growing.

Successful methods (in a sense of making a reasonable compromise between cost and accuracy and therefore used frequently for molecules of medium sizes) are: CASSCF/CASPT2 (Complete Active Space SCF and CAS with the second order perturbation theory) [15], Equation-of-Motion Coupled Cluster theory (EOM-CC) [16, 17], and linear-response CC (LR-CC) theory [18–20], both restricted to single and double excitations. In particular the LR-CC approach offers a general framework for the calculation of various time-independent and time-dependent molecular properties and has been successfully applied to several approximate models such as CC2 [21], CCSD [19], and CC3 [22]. The important advantage of LR-CC over the EOM-CC method is that the former provides properties such as transition moments, which scale correctly with the molecular size [23] (note that for both methods the excitation energies of valence states are size-intensive while the properties expressed as energy derivatives are size-extensive). For the calculation of excitation energies EOM-CCSD and CCSD response theories are equivalent and the computational task in both cases consists of finding a few lowest eigenvalues of the CCSD Jacobian.

1.1 Coupled Cluster Theory and Diagrams

1.1.1 Fundamentals of the Coupled Cluster Theory

Coupled Cluster (CC) methods are based on exponential ansatz of the wavefunction [24]:

$$|CC\rangle = \exp(T)|0\rangle = \exp\left(\sum_{\mu} t_{\mu}\tau_{\mu}\right)|0\rangle, \quad (1.1)$$

where $T = T_1 + T_2 + \dots$ denotes the cluster operator, T_1 is the singles operator, T_2 is the doubles operator and so on, and $|0\rangle$ is the reference wavefunction (usually the Hartree-Fock wavefunction). If one cancels T after T_1 , one gets the CCS method (with the ground-state energy equal to the reference and the excitation energies equal to CIS); after T_2 - CCSD etc.

The CC methods have several important advantages in comparison to Configuration Interaction (CI) and Perturbative (MP2, MP4) methods. The CC methods are size-extensive and, due to the similarity transformation of the Hamiltonian with the exponent of T_1

$$\hat{H} = \exp(-T_1)H\exp(T_1), \quad (1.2)$$

partly orbital relaxed, which is crucial for response theory [20]. If one combines CC and perturbative methods, the higher order excitations can be treated at the level of the perturbation theory (e.g. CC2, CCSD(T), etc.).

The CC ground-state energy is defined as

$$\langle \overline{CC} | H | CC \rangle = \langle 0 | H | CC \rangle = E_{CC} \quad (1.3)$$

with

$$\langle \overline{CC} | = \langle 0 | \exp(-T),$$

and the amplitudes of the cluster operators can be obtained from the equations

$$\langle \mu_i | \exp(-T)H\exp(T) | 0 \rangle = 0, \quad (1.4)$$

where μ_i denote the singly ($i = 1$), doubly ($i = 2$), etc., excited configuration state functions (CSFs). After applying the Baker-Campbell-Hausdorff-expansion

$$\exp(-T)H\exp(T) = H + [H, T] + \frac{1}{2!}[[H, T], T] + \frac{1}{3!}[[[H, T], T], T] + \dots \quad (1.5)$$

the expressions (1.3) and (1.4) are reduced to polynomial commutator expressions.

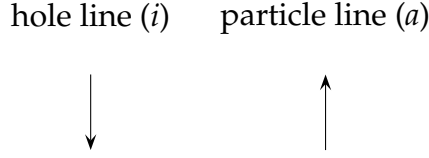
The working equations in terms of integrals and amplitudes can be easily obtained from the commutator expressions via the diagrammatic technique [25, 26]. Here we use diagrams for deriving the spatial orbital formulation of the coupled cluster equations.

1.1.2 Diagrammatic technique for spatial orbitals

In the diagrammatic technique the **operators** are drawn as horizontal (interaction) lines, e.g.,

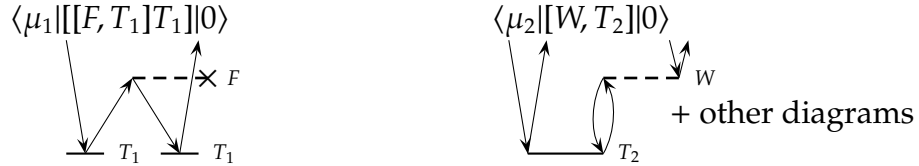
Fock	Fluctuation	Singles	Doubles
--- \times F	--- W	— T_1	— T_2

and are connected with vertical (hole/particle) lines.



The fluctuation operator is defined as the difference between the Hamiltonian and the Fock operator. Here and in the following $i, j, k...$ and $a, b, c...$ denote occupied and virtual orbital indices, respectively. The interaction lines are coupled over hole/particle (h/p) lines on vertices (Fock and singles operators have one vertex, fluctuation and doubles operators have two etc.). On each vertex there have to be exactly two lines (one incoming and one outgoing).

The *bra* side of the expression is on the top of the diagram and the *ket* side is on the bottom. If the *bra* side is a non-reference CSF (like in (1.4)), then the h/p lines can leave the diagram (external lines), e.g.,



In the case of the CC model the diagrams have to be *connected*, i.e. a diagram cannot comprise disconnected parts.

The analysis of the diagrams is carried out in accordance with the following rules:

1. hole and particle lines correspond to the occupied ($i, j, k...$) and virtual ($a, b, c...$) orbital indices, respectively;
2. the summation runs over indices coming from h/p lines, which connect two vertices (internal lines);
3. each interaction line constitutes an integral (lines from Fock or fluctuation operators) or amplitude (lines from cluster operators);
4. the outgoing lines correspond to indices from complex conjugated orbitals (the first indices) in the integrals, e.g.,

$$\begin{aligned} & \langle 0 | [W, T_2] | 0 \rangle \rightarrow \\ & \begin{array}{c} \text{---}^W \text{---} \\ \text{---}^i \text{---}^a \text{---}^j \text{---}^b \\ \text{---}^T_2 \text{---} \end{array} \\ & \rightarrow \sum_{iajb} T_{ab}^{ij} (ia|jb) = \sum_{iajb} T_{ab}^{ij} \int \phi_i^*(\mathbf{r}_1) \phi_a(\mathbf{r}_1) \frac{1}{|\mathbf{r}_1 - \mathbf{r}_2|} \phi_j^*(\mathbf{r}_2) \phi_b(\mathbf{r}_2) d\mathbf{r}_1 d\mathbf{r}_2 \end{aligned}$$

5. The resulting sign is given by $(-1)^{h+L}$, where h is the number of hole lines, and L is the number of loops in the diagram (including "loops" of external lines);
6. each internal loop (i.e. not over external lines) yields a factor of two in the final expression;
7. equivalent vertices on the interaction line (i.e. vertices with incoming and outgoing lines coming from/going to the same cluster operator) divide the final expression by factor of two, i.e.

$$\begin{array}{c}
 \text{Diagram: A rectangle with a dashed top line labeled } W \text{ and a solid bottom line labeled } T_2. \text{ Arrows on the vertical lines indicate a clockwise loop.} \\
 + 2 * 2 * \frac{1}{2} \sum_{iajb} (ia|jb) T_{ab}^{ij}
 \end{array}$$

We should also mention, that external "vertices" are not equivalent (on the contrary to spin-orbital formalism [26]), i.e. diagrams

$$\begin{array}{c}
 \text{Diagram 1: A vertex } T_1 \text{ with two incoming lines from the left and one outgoing line to the right labeled } W. \\
 \sum_c (ai|bc) t_c^j
 \end{array}
 +
 \begin{array}{c}
 \text{Diagram 2: A vertex } T_1 \text{ with one incoming line from the left and two outgoing lines to the right labeled } W. \\
 \sum_c (bj|ac) t_c^i
 \end{array}
 \rightarrow V_{ab}^{ij}$$

lead to two different terms.

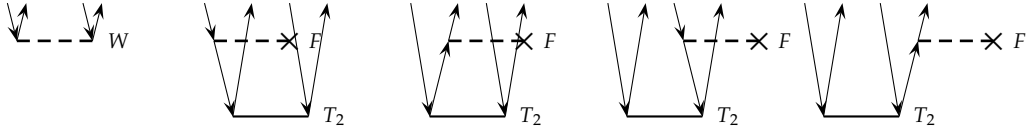
1.1.3 MP2 and CC2 methods

In the Møller-Plesset perturbation theory the Fock operator is of the zeroth order and the fluctuation operator is of the first order. The MP2 energy is correct to the second order, i.e. all terms with orders higher than the second are neglected,

$$\begin{array}{c}
 \text{Diagram 1: Same as above (rectangle with dashed top line } W \text{ and solid bottom line } T_2 \text{).} \\
 \text{Diagram 2: A rectangle with a dashed top line labeled } W \text{ and a solid bottom line labeled } T_2. \text{ Arrows on the vertical lines indicate a clockwise loop, with an additional diagonal line connecting the top and bottom vertices.}
 \end{array}$$

$$E_{\text{MP2}} = \left\langle 0 \left| \left[W, T_2^{(1)} \right] \right| 0 \right\rangle = \sum_{iajb} (2(ia|jb) - (ib|ja)) T_{ab}^{ij}.$$


The double amplitudes T_{ab}^{ij} are calculated from the first order amplitude equations



$$\langle \mu_2 | W + [F, T_2^{(1)}] | 0 \rangle = (ai|bj) - \sum_k (f_{ki} T_{ab}^{kj} + f_{kj} T_{ab}^{ik}) + \sum_c (f_{ac} T_{cb}^{ij} + f_{bc} T_{ac}^{ij}) = 0.$$

The CC2 method, proposed by Christiansen and coworkers [21], is the simplest and the most economical CC model appropriate for calculations of excited states dominated by single excitations. The CC2 approach can be regarded as a simplification of the CCSD method. The CC2 energy is calculated (as in MP2) to the second order, but the singles are treated as zeroth-order parameters. The singles amplitude equations remains as in CCSD and the doubles amplitude equations are approximated to be correct at the first order only [21].

The diagrams for the CC2 ground-state energy are the same as for CCSD:



$$\sum_{iajb} (2(ia|jb) - (ib|ja)) (T_{ab}^{ij} + t_a^i t_b^j)$$

The CC2 amplitude equations are explicitly specified in the chapter 2.

1.2 Linear Response theory

1.2.1 Time-dependent formalism

The response theory is one of the approaches used for calculating ground- and excited states properties [20]. The time-dependent Coupled Cluster (TD-CC) wavefunction can be written in the phase isolated form as

$$|CC(t)\rangle = \exp(-iF(t)) \widetilde{|CC(t)\rangle} = \exp(-iF(t)) \exp(T(t)) |0\rangle, \quad (1.6)$$

where F is a function of time. Inserting it into the time-dependent Schrödinger equation

$$H\Psi = i\frac{\partial}{\partial t}\Psi \quad (1.7)$$

and projecting on to the reference wavefunction, yields the time-dependent quasienergy

$$Q(t) = \frac{\partial F(t)}{\partial t} = \left\langle 0 \left| \left(H - i \frac{\partial}{\partial t} \right) \right| \widetilde{CC}(t) \right\rangle, \quad (1.8)$$

which reduces to the usual ground-state CC energy (eq. (1.3)) in the time-independent limit. For variational methods the time-dependent Hellmann-Feynman theorem

$$\frac{dQ}{d\epsilon} = \left\langle \tilde{\Psi}_0 \left| \frac{\partial H}{\partial \epsilon} \right| \tilde{\Psi}_0 \right\rangle - i \frac{\partial}{\partial t} \left\langle \tilde{\Psi}_0 \left| \frac{d\tilde{\Psi}_0}{d\epsilon} \right\rangle \right\rangle \quad (1.9)$$

can be derived from the time-dependent variational principle [20], i.e. properties of the system can be obtained as the quasienergy derivatives. In case of nonvariational CC theory, the time-dependent generalized Hellmann-Feynman theorem should be used, where the TD-CC Lagrangian plays the role of the quasienergy. The constraints in the time-dependent Lagrangian are the TD-CC amplitude equations (cf. eq. (1.4)):

$$\Omega_{\mu_i}(t) = \left\langle \mu_i \left| \exp(-T(t)) \left(H - i \frac{\partial}{\partial t} \right) \exp(T(t)) \right| 0 \right\rangle = 0. \quad (1.10)$$

The TD-CC Lagrangian can be written as

$$L(t) = Q(t) + \sum_{i, \mu_i} \lambda_{\mu_i}(t) \Omega_{\mu_i}(t) = \left\langle \tilde{\Lambda}(t) \left| \left(H - i \frac{\partial}{\partial t} \right) \right| \widetilde{CC}(t) \right\rangle, \quad (1.11)$$

$$\left\langle \tilde{\Lambda}(t) \right| = \left\langle 0 \right| + \sum_{i, \mu_i} \lambda_{\mu_i}(t) \left\langle \mu_i \right| \exp(-T(t)) \right\rangle, \quad (1.12)$$

with the time-dependent Lagrange multipliers $\lambda_{\mu_i}(t)$.

The time-dependent perturbation V^t of the Hamiltonian $H = H_0 + V^t$ can be described as a sum of periodic perturbations, i.e. in terms of the Fourier series,

$$V^t = \sum_X \exp(-i\omega_X t) \epsilon_X(\omega_X) X, \quad (1.13)$$

with the sum over all frequencies ω_X (plus and minus) and perturbations. X denotes the perturbation operators, and ϵ_X are the field strength parameters.

Finally, expanding the expectation value of X in orders of the perturbation leads to

$$\begin{aligned}\langle X \rangle(t) &= \langle \tilde{\Lambda}(t) | X | \widetilde{CC}(t) \rangle = \langle X \rangle_0 \\ &+ \sum_Y \exp(-i\omega_Y t) \langle \langle X; Y \rangle \rangle_{\omega_Y} \epsilon_Y(\omega_Y) \\ &+ \frac{1}{2} \sum_{YZ} \exp(-i(\omega_Y + \omega_Z)t) \langle \langle X; Y, Z \rangle \rangle_{\omega_Y \omega_Z} \epsilon_Y(\omega_Y) \epsilon_Z(\omega_Z) + \dots\end{aligned}\quad (1.14)$$

$\langle \langle X; Y \rangle \rangle$, $\langle \langle X; Y, Z \rangle \rangle$ stand for linear, quadratic (and so on) response functions, respectively, and are the expansion coefficients of the Fourier components.

1.2.2 Time-averaging and response functions

If we assume, that all frequencies in eq. (1.13) are a multiple of a fundamental frequency ω , then the Hamiltonian H is periodic in time with a period $T = 2\pi/\omega$. In this case we can introduce the time average of the Lagrangian (1.11):

$$\{L\}_T = \frac{1}{T} \int_{-\frac{T}{2}}^{\frac{T}{2}} L(t) dt. \quad (1.15)$$

If the fundamental frequency do not exist, T can be chosen as a very large number, such that this assumption does not cause practical problems.

It can be shown [20], that the time-averaged generalized Hellmann-Feynman theorem has the following form:

$$\frac{d\{L\}_T}{d\epsilon_X(\omega_X)} = \left\{ \langle \tilde{\Lambda}(t) | X | \widetilde{CC}(t) \rangle \exp(-i\omega_X t) \right\}_T. \quad (1.16)$$

Inserting the TD expectation value of X (eq. (1.14)) in to eq. (1.16), we can identify the response functions as different derivatives of the time-

averaged Lagrangian with respect to the field strength parameters:

$$\frac{d\{L\}_T}{d\epsilon_X(\omega_X)} = \langle X \rangle + \sum_Y \langle \langle X; Y \rangle \rangle_{\omega_Y} \epsilon_Y(\omega_Y) \delta(\omega_X + \omega_Y) \quad (1.17)$$

$$+ \frac{1}{2} \sum_{YZ} \langle \langle X; Y, Z \rangle \rangle_{\omega_Y \omega_Z} \epsilon_Y(\omega_Y) \epsilon_Z(\omega_Z) \delta(\omega_X + \omega_Y + \omega_Z) + \dots,$$

$$\langle X \rangle = \frac{d\{L\}_T}{d\epsilon_X(\omega_X)}, \quad \omega_X = 0; \quad (1.18)$$

$$\langle \langle X; Y \rangle \rangle_{\omega_Y} = \frac{d^2\{L\}_T}{d\epsilon_X(\omega_X) d\epsilon_Y(\omega_Y)}, \quad \omega_X = -\omega_Y; \quad (1.19)$$

$$\langle \langle X; Y, Z \rangle \rangle_{\omega_Y \omega_Z} = \frac{d^3\{L\}_T}{d\epsilon_X(\omega_X) d\epsilon_Y(\omega_Y) d\epsilon_Z(\omega_Z)}, \quad \omega_X = -(\omega_Y + \omega_Z). \quad (1.20)$$

The conditions for ω_X apply because of the time-averaging (an integral over the full periode of a function is not zero only if the frequency of the integrand is zero). Thus, for each order of the response, the frequency ω_X of the "measured" response has to be equal to the sum of the frequencies of the "external" perturbations taken with the opposite sign.

We can, in addition, expand the TD-CC Lagrangian and the parameters (CC amplitudes and Lagrange multipliers) in orders of the periodic perturbation,

$$t_{\mu_i}(t) = t_{\mu_i}^{(0)} + t_{\mu_i}^{(1)}(t) + t_{\mu_i}^{(2)}(t) + \dots, \quad (1.21)$$

$$\lambda_{\mu_i}(t) = \lambda_{\mu_i}^{(0)} + \lambda_{\mu_i}^{(1)}(t) + \lambda_{\mu_i}^{(2)}(t) + \dots, \quad (1.22)$$

$$L(t) = L^{(0)} + L^{(1)}(t) + L^{(2)}(t) + \dots \quad (1.23)$$

The time-dependent parameters of higher order can be expanded into frequency and field-strength dependent components $t_{\mu_i}^{(1)}(\omega_X)$, $t_{\mu_i}^{(2)}(\omega_X, \omega_Y)$ etc. (corresponds to the Fourier transform to frequency domain), or into field-strength independent components $t_{\mu_i}^X(\omega_X)$, $t_{\mu_i}^{XY}(\omega_X, \omega_Y)$ etc.:

$$t_{\mu_i}^{(1)}(t) = \sum_X \exp(-i\omega_X t) t_{\mu_i}^{(1)}(\omega_X) = \sum_X \exp(-i\omega_X t) \epsilon_X(\omega_X) t_{\mu_i}^X(\omega_X), \quad (1.24)$$

$$t_{\mu_i}^{(2)}(t) = \sum_{XY} \exp(-i(\omega_X + \omega_Y)t) t_{\mu_i}^{(2)}(\omega_X, \omega_Y) \quad (1.25)$$

$$= \frac{1}{2} \sum_{XY} \exp(-i(\omega_X + \omega_Y)t) \epsilon_X(\omega_X) \epsilon_Y(\omega_Y) t_{\mu_i}^{XY}(\omega_X, \omega_Y),$$

and the time-averaged CC Lagrangian can be obtained for each order as

$$\{L^{(0)}\}_T = L^{(0)} \quad (1.26)$$

$$\{L^{(1)}\}_T = \sum_X \epsilon_X(\omega_X) L^X(\omega_X), \quad \omega_X = 0; \quad (1.27)$$

$$\{L^{(2)}\}_T = \frac{1}{2} \sum_{XY} \epsilon_X(\omega_X) \epsilon_Y(\omega_Y) L^{XY}(\omega_X, \omega_Y), \quad \omega_X = -\omega_Y. \quad (1.28)$$

Inserting eq. (1.23) (with eqs.(1.26-1.28)) into eq. (1.17) and comparing the left- and right-hand sides leads to the conclusion, that the response functions are equal to the derivatives of the time-averaged Lagrangian of corresponding order, e.g., for the linear response

$$\langle\langle X; Y \rangle\rangle_{\omega_Y} = L^{XY}(\omega_X, \omega_Y) = \frac{d^2 \{L^{(2)}\}_T}{d\epsilon_X(\omega_X) d\epsilon_Y(\omega_Y)}, \quad \omega_X = -\omega_Y. \quad (1.29)$$

The well known Wigner's $2n+1$ rule from the perturbational theory applies also here: using the amplitudes of the n -th order, one can evaluate response function of the $(2n+1)$ -th order (and with the n -th order multipliers even of the $(2n+2)$ -th order) [20].

With the $2n+1$ rule the time-averaged second-order CC Lagrangian in terms of different commutators becomes

$$\begin{aligned} \{(2n+1)L^{(2)}\}_T &= \sum_X \left(\left\langle \Lambda \left| \left[V^{-\omega_X}, T^{(1)}(\omega_X) \right] + \frac{1}{2} \left[[H_0, T^{(1)}(-\omega_X)], T^{(1)}(\omega_X) \right] \right| \text{CC} \right\rangle \right. \\ &\quad + \sum_{i\mu_i} \lambda_{\mu_i}^{(1)}(-\omega_X) \left(\left\langle \mu_i \left| \exp(-T^{(0)}) (V^{\omega_X} + [H_0, T^{(1)}(\omega_X)]) \right| \text{CC} \right\rangle \right. \\ &\quad \left. \left. - [\omega_X t_{\mu_i}^{(1)}(\omega_X)] \right) \right) \end{aligned} \quad (1.30)$$

1.2.3 Excitation energies

The excitation energies within the response theory are a ground-state property and are non-variational even for variational methods. They are obtained as the poles of the linear response functions.

The linear response function (eq. (1.29)) can be written using $2n+1$ and $2n+2$ rules (defined in the previous section 1.2.2) as

$$\begin{aligned} \langle\langle X; Y \rangle\rangle_{\omega_Y} &= \mathcal{P}(X(\omega_X), Y(\omega_Y)) \\ &\times \left(\frac{\partial^2 \{L^{(2)}\}_T}{\partial \epsilon_X(\omega_X) \partial t^{(1)}(\omega_Y)} + \frac{1}{2} \frac{\partial^2 \{L^{(2)}\}_T}{\partial t^{(1)}(\omega_X) \partial t^{(1)}(\omega_Y)} t^X(\omega_X) \right) t^Y(\omega_Y), \end{aligned} \quad (1.31)$$

where $\mathcal{P}(X(\omega_X), Y(\omega_Y))$ symmetrizes the expression with respect to the interchange of $X(\omega_X)$ and $Y(\omega_Y)$. The expression for the linear response function can be transformed to the representation where the Jacobian

$$A_{\mu_i \nu_j} = \left\langle \mu_i \left| \exp(-T^{(0)}) [H_0, \tau_{\nu_j}] \right| \text{CC} \right\rangle. \quad (1.32)$$

is diagonal. It can be shown [20], that in the diagonal representation the response function has the form

$$\begin{aligned} \langle\langle X; Y \rangle\rangle_{\omega_Y} &= \mathcal{P}(X(\omega_X), Y(\omega_Y)) \\ &\times \left(\sum_k \frac{B_k}{\omega_Y - \omega_k} + \frac{1}{2} \frac{C_{kn}}{(\omega_Y + \omega_k)(\omega_Y - \omega_n)} \right), \end{aligned} \quad (1.33)$$

where the matrices B_k and C_{kn} are some products of the Lagrangian-derivatives with the left and right eigenvectors of the Jacobian matrix, and ω_k are the eigenvalues of the CC Jacobian. From the eq.(1.33) it is evident that the linear response function has poles when ω_Y matches one of ω_k . Thus the excitation energies are identical to the eigenvalues of the CC Jacobian and are equivalent to the energies of the EOM-CC approach.

The residue for the pole gives the transition strength of the excitation:

$$\lim_{\omega_Y \rightarrow \omega_f} (\omega_Y - \omega_f) \langle\langle X; Y \rangle\rangle_{\omega_Y} = S_{XY}^{0f} \quad (1.34)$$

To our knowledge the most efficient implementation of conventional (i.e. nonlocal) CC response theory for excited states has been accomplished by Hättig and coworkers [27, 28] and is included in the TURBOMOLE package [29]. It is based on the CC2 model and uses Density Fitting (DF) to approximate the Electron Repulsion Integrals (ERIs).

1.3 Density fitting approximation

In the density fitting [30–34], the 4-index integrals

$$\begin{aligned} (pq|rs) &= \int d\mathbf{r}_1 d\mathbf{r}_2 \phi_p^*(\mathbf{r}_1) \phi_q(\mathbf{r}_1) r_{12}^{-1} \phi_r^*(\mathbf{r}_2) \phi_s(\mathbf{r}_2) \\ &= \int d\mathbf{r}_1 d\mathbf{r}_2 \rho_{pq}(\mathbf{r}_1) r_{12}^{-1} \rho_{rs}(\mathbf{r}_2) \end{aligned} \quad (1.35)$$

are approximated by a product of two 3-index quantities. For this purpose the one-particle density ρ_{pq} in eq.(1.35) is replaced by an approximated

density $\tilde{\rho}_{pq}$ expanded in a fitting basis set:

$$\phi_p(\mathbf{r})\phi_q(\mathbf{r}) = \rho_{pq}(\mathbf{r}) \approx \tilde{\rho}_{pq}(\mathbf{r}) = \sum_P c_{pq}^P \Xi_P(\mathbf{r}). \quad (1.36)$$

The fitting coefficients c_{pq}^P are usually determined by minimization of the following error functional

$$\begin{aligned} f(c_{pq}^P) &= \int d\mathbf{r}_1 d\mathbf{r}_2 (\rho_{pq}(\mathbf{r}_1) - \tilde{\rho}_{pq}(\mathbf{r}_1)) r_{12}^{-1} (\rho_{pq}(\mathbf{r}_1) - \tilde{\rho}_{pq}(\mathbf{r}_1)) \\ &= (pq|pq) - 2 \sum_P c_{pq}^P (P|pq) + \sum_{PQ} c_{pq}^P (P|Q) c_{pq}^P \end{aligned} \quad (1.37)$$

with respect to c_{pq}^P . This yields to a linear equation system

$$\sum_Q (P|Q) c_{pq}^Q = (P|pq). \quad (1.38)$$

Thus the 4-index integral (in nonrobust fitting) is approximated as

$$(pq|rs) = \sum_P c_{pq}^P (P|rs) = \sum_{PQ} (pq|P) (P|Q)^{-1} (Q|rs). \quad (1.39)$$

One should emphasize that although the DF approximation allows for considerable reduction of the computational cost, the overall scaling with molecular size N in the canonical MP2 and CC2 methods remains to be $\mathcal{O}(N^5)$, independently whether the DF approximation is employed for the ERIs or not.

1.4 Local methods

An approach, which allows to decrease the computational cost of the correlation methods by reducing the scaling, consists in utilizing the local approximations in the wavefunctions [35–41]. The DF formalism can be used on top of the local approach, leading to even bigger reductions in the computational cost [42, 43]. The essential idea of local correlation consists of replacing the delocalized canonical orbitals spanning the occupied and virtual space by spatially *localized* orbitals, which makes it possible to exploit the short-range nature of the dynamic correlation in nonmetallic systems. In local correlation methods based on the Pulay ansatz [36] the

occupied orbital space is spanned by mutually orthogonal localized molecular orbitals (LMOs), which are obtained by unitary transformation from the canonical occupied orbitals,

$$|\phi_i\rangle = \sum_{\tilde{i}}^{n_{occ}} |\phi_{\tilde{i}}^{\text{can}}\rangle W_{\tilde{i}i} = \sum_{\mu=1}^{N_{AO}} |\chi_{\mu}\rangle L_{\mu i}, \quad (1.40)$$

while the virtual space is spanned directly by atomic orbitals (AOs) projected onto the virtual space (PAOs)

$$|\phi_a\rangle = \left(1 - \sum_i^{n_{occ}} |\phi_i\rangle \langle \phi_i|\right) |\chi_a\rangle = \sum_{\mu=1}^{N_{AO}} |\chi_{\mu}\rangle P_{\mu a} \quad (1.41)$$

with the projector matrix

$$\mathbf{P} = \mathbf{1} - \mathbf{L}\mathbf{L}^{\dagger} \mathbf{S}_{AO}, \quad (1.42)$$

where \mathbf{S}_{AO} is the overlap matrix between the AOs.

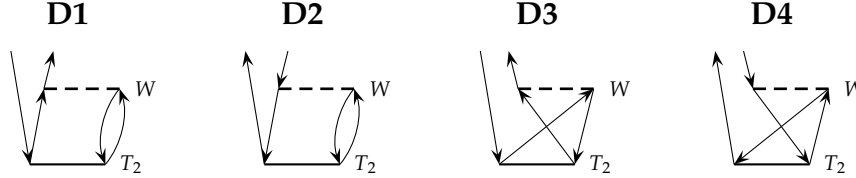
Various approximations to the amplitudes of singly- or doubly- excited configuration functions can then be introduced, based on spatial locality arguments. Hence, restricted pairlists of LMOs and orbital- or pair- specific excitation subspaces of PAOs (domains) are specified and amplitudes outside these lists/domains are *a priori* neglected or treated in a simplified way.

The specification of domains and pair lists for the amplitude response (subject to a frequency dependent perturbation) is less straightforward, as examined for the first time in Ref. 44 in the context of local EOM-CCSD. Excited states may have substantial non-local CT character, hence local approximations based on spatial locality arguments alone are bound to fail. One of the possible ways to determine pair lists and domains for excited states is by analysis of an untruncated wavefunction obtained at a simpler level of theory, e.g., CIS – configuration interaction singles, as described in detail in Ref. 44.

Since the virtual orbitals (PAOs) are nonorthogonal, the diagrammatic rules (Sec. 1.1.2) have to be adapted:

1. each particle line yields a PAO-overlap-matrix $S_{ab} = \langle \phi_a | \phi_b \rangle$;
2. the interaction lines, which come from Fock, fluctuation or perturbation operators, provide a pseudo- (since the PAO-metric is singular) inverse of the PAO-overlap S^+ for each virtual index.

As an example we evaluate now the working expressions for $\langle \mu_1 || [V, T_2] || 0 \rangle$ in the local basis. The diagrams to be considered are



and the corresponding equations are

$$\begin{aligned}
 \langle \mu_1 || [V, T_2] || 0 \rangle \rightarrow v_a^i &= \sum_{jbb'b''cc'c''} S_{aa''}^+ S_{a''a'}^{++} (jb'|a'c') S_{b'b''}^+ S_{c'c''}^+ S_{c''c} S_{b''b} \tilde{T}_{cb}^{ij}(\mathbf{D1}, \mathbf{D3}) \\
 &- \sum_{jka'bb'b''} (jb'|ki) S_{b'b''}^+ S_{aa'} S_{b''b} \tilde{T}_{a'b}^{kj}(\mathbf{D2}, \mathbf{D4}) \\
 &= \sum_{jbc} (jb|ac) \tilde{T}_{cb}^{ij}(\mathbf{D1}, \mathbf{D3}) - \sum_{jkb} (jb|ki) S_{aa'} \tilde{T}_{a'b}^{kj}(\mathbf{D2}, \mathbf{D4}),
 \end{aligned} \tag{1.43}$$

where \tilde{T}_{ab}^{ij} denote the contravariant double amplitudes, $\tilde{T}_{ab}^{ij} = 2T_{ab}^{ij} - T_{ba}^{ij}$. The complications, which arise by, e.g, partitioning of the PAO-metric into two parts (such that the \mathbf{S} -matrix can not compensate the pseudo-inverse \mathbf{S}^+), are an important issue of the Laplace transform in local methods (Chp. 4).

1.5 Laplace transform

In the canonical methods based on the perturbation theory in the Møller-Plesset partitioning, denominators of the type $\Delta_{ij\dots}^{ab\dots} = \epsilon_a + \epsilon_b + \dots - \epsilon_i - \epsilon_j - \dots$ occur, where ϵ_a, ϵ_b , etc are the virtual and ϵ_i, ϵ_j , etc the occupied canonical orbital energies. This denominators can be considered as the real Laplace transform of 1:

$$\frac{1}{\Delta_{ij\dots}^{ab\dots}} = \int_0^\infty \exp(-\Delta_{ij\dots}^{ab\dots} t) * 1 * dt. \tag{1.44}$$

It was applied for the first time by Almlöf [45] in the case of MP2. The integral in eq.(1.44) can be replaced by the numerical quadrature

$$\frac{1}{\Delta_{ij\dots}^{ab\dots}} \approx \sum_q^{n_q} w_q \exp(-\Delta_{ij\dots}^{ab\dots} t_q), \tag{1.45}$$

with w_q and t_q being weights and exponential factors of the quadrature, respectively. As was shown in Ref. 33 only a small number of quadrature

points n_q is needed. Thus an inverse of a sum of the orbital energies is transformed to a sum of products of $\exp(\pm\epsilon_p)$. This allows for non-iterative scheme for solving the MP2 equations in a local basis (where the Fock matrix is not diagonal) [46] (or Chp. 4).

1.6 Structure of the thesis

This thesis is organized as follows. In the next chapter a straight forward implementation of the local formalism to the linear response CC2 model, including DF approximation (DF-LCC2) is presented. In chapter 3 an extension of the DF-LCC2LR to ground- and excited-states properties (like dipole and transition moments) is described. The applicability of Laplace transform to local methods using the example of local MP2 is examined in chapter 4. In chapter 5 we compare two different approaches for evaluating of Laplace transform integration points, since it is a crucial issue for an efficient implementation of Laplace transform methods. The application of the LT formalism of Chp. 4 to local CC2 (LT-DF-LCC2) allows us to improve the previous implementation in many different aspects. The underlying theory for the LT-DF-LCC2 approach is presented in Chp. 6, while the comparison of the two LCC2 schemes is the subject of the last chapter 7.

Chapter 2

Local CC2

2.1 Introduction

There are only few low-scaling local methods reported so far, which are applicable for excited states. Pilot programs for the calculation of excitation energies based on local EOM-CCSD have been developed by Werner and Korona [44] and Crawford and King [47], the latter with rather disappointing results due to the fact, that just the ordinary ground state domains have been used for describing the excited states. It turns out that the determination of appropriate domains for excited states is a non-trivial problem, especially in view of phenomena like charge transfer excitations. In Ref. 44 an initial CIS wave function was analyzed to form the excited state domains and to determine the pair list for the excited state. This approach apparently leads to quite reasonable domains, at least as long as the CIS wave function provides a qualitatively good description of the excited state under study. However, the CCSD method itself and in particular the computation of the Jacobian matrix times trial vector products in the diagonalization procedure become rather expensive when long pair lists are involved. For that reason, only rather strictly truncated pair lists could be used, what hurts the robustness of the method and increases the dependence on the quality of the initial CIS wave function.

In this chapter we present a local method based on a cheaper CC model, namely CC2, allowing for considerably longer pair lists, which is more robust with respect to the local approximation than local EOM-CCSD [44]. Furthermore, we do not present just a local pilot program but an implementation which exploits the local approximations to a full extent in order to save all computational resources. Moreover, the DF approach is rigorously employed to calculate the contributions from individual diagrams.

Hence, with the present code it is possible to treat molecular systems with hundred atoms or more in a basis of polarized double zeta quality. In the next two sections we present working equations for the local CC2 ground-state amplitudes (Sec. 2.2.1) and the matrix times trial vector products used in the diagonalization of the LCC2 Jacobian (Sec. 2.2.2). In order to demonstrate the performance of the new code, the results from test calculations on various molecules are presented in Sec. 2.3, including large molecules comprising 53, 77, and 127 atoms. These molecules, which represent examples for light-induced electron donor-acceptor systems featuring rather long-range charge transfer excitations, was of interest in the Regensburg group in the context of an application project. In the last section we present the summary and conclusions.

2.2 Theory

The review of CC response theory based on a time-averaged quasi-energy Lagrangian and Fourier component variational perturbation theory was outlined in detail by Christiansen and coworkers (see [20] and references therein) and will be not repeated here. We can therefore concentrate on specific features arising from the introduction of local approximations to the CC2 wave function. In this section we also keep the general notation conventions from Ref. 20.

In LR-CC theory excitation energies and transition moments are obtained as poles and residues of the CC linear response (i.e. first-order) function. For the CC Lagrangian the Hellmann-Feynman theorem generalized to CC theory is fulfilled, and therefore the $2n + 1$ rule for amplitudes and $2n + 2$ rule for Lagrangian multipliers apply, e.g. zeroth-order amplitudes and multipliers are required for first-order properties. In a derivation of the first-order property the first-order amplitudes are eliminated by virtue of the stationary conditions for Lagrangian: by differentiating the first-order Lagrangian by the first-order amplitude we obtain conditions for the zeroth-order multipliers. This procedure requires, of course, that the space spanned by zeroth- and first-order amplitudes or multipliers is the same.

Let us see what complications can arise when one uses CC response theory within the local approximations. In local methods zero- and first-order amplitudes and multipliers are restricted to local domains and pair lists (*vide infra*). This alone, however, is not a major problem, since the restriction of the configurational space simply means that $T^{(0)}$, $T^{(1)}$, $\Lambda^{(0)}$

operators etc. are defined within a local space \mathcal{V}_{loc} ,

$$\begin{aligned} T_{\text{loc}}^{(0)} &= \sum_{\mu \in \mathcal{V}_{\text{loc}}} t_{\mu}^{(0)} \tau_{\mu}, \\ T_{\text{loc}}^{(1)} &= \sum_{\mu \in \mathcal{V}_{\text{loc}}} t_{\mu}^{(1)} \tau_{\mu}, \\ \langle \Lambda_{\text{loc}}^{(0)} | &= \langle 0 | + \sum_{\mu \in \mathcal{V}_{\text{loc}}} \bar{t}_{\mu}^{(0)} \langle \mu | \exp(-T_{\text{loc}}^{(0)}), \end{aligned}$$

where τ_{μ} denotes an excited determinant or configurational function having an index μ . The conditions for zeroth-order amplitudes and multipliers are obtained in entire analogy to the canonical case, i.e. from the stationary conditions for the zeroth-order Lagrangian $L^{(0)}$,

$$\begin{aligned} 0 &= \frac{\partial L^{(0)}}{\partial \bar{t}_{\mu}^{(0)}} = \langle \mu | e^{-T_{\text{loc}}^{(0)}} H | \text{CC}_{\text{loc}} \rangle, \\ 0 &= \frac{\partial L^{(0)}}{\partial t_{\mu}^{(0)}} = \left\langle \Lambda_{\text{loc}} \left[[H, \tau_{\mu}] \right] \text{CC}_{\text{loc}} \right\rangle, \quad \mu \in \mathcal{V}_{\text{loc}}, \end{aligned}$$

where H is the unperturbed Hamiltonian and $|\text{CC}_{\text{loc}}\rangle = \exp(T_{\text{loc}}^{(0)})|0\rangle$. This approach (although in a somewhat different formulation) has been already used in a derivation of local gradients [48, 49]. In the local method the result of multiplication of $\exp(-T_{\text{loc}}^{(0)})H\exp(T_{\text{loc}}^{(0)})$ on the Hartree-Fock (HF) wave function is projected on the \mathcal{V}_{loc} space. Only this projected quantity is required to be zero. Note parenthetically that for the gradients in the local case we will have an additional set of Lagrange multipliers, corresponding to the localization conditions, see e.g. [43, 48–50]. Similarly, we define the local Jacobian as the second mixed derivative of the local $L^{(0)}$ (over $\bar{t}_{\mu}^{(0)}$ and $t_{\nu}^{(0)}$, where μ and $\nu \in \mathcal{V}_{\text{loc}}$), and finally use the stationary conditions for the second-order time-averaged Lagrangian to arrive at the equations for the first-order amplitudes. Therefore, the local approach is well-defined, as long as we consequently use amplitudes and Lagrange multipliers corresponding to the same \mathcal{V}_{loc} .

However, in the most convenient local approach domains and pair lists for zeroth- and first-order wave functions do not necessarily coincide, implying that, e.g. not all contributions from first-order terms will be eliminated from the first-order Lagrangian. Of course, by merging the domains and pair lists for zeroth- and first-order wave function parameters this problem can be rigorously circumvented (at the price of a higher computational cost). We will show by performing calculations in merged

(unified) domains and pair lists that we obtain reasonably close results using both approaches: with the same configuration space for zeroth- and first-order (i.e. ground and excited state) wave functions, and for the more practical approach, where the local spaces for zeroth- and first-order wave functions are not identical. We therefore proceed with the assumption that the $2n + 1/2n + 2$ rule is valid also for the local case, which is strictly true only if the domains and pair lists of zeroth- and first-order wave function parameters are merged.

2.2.1 The local CC2 model

The CC2 model has been proposed by Christiansen and coworkers [21] as an approximation to the CCSD model, where the singles are treated as zeroth-order parameters in terms of the fluctuation potential W (W is a difference between the Hamiltonian H and the Fock operator F). The doubles excitations are treated at first order in W (as in MP2). This parametrization was rationalized in Ref. 21 by the fact that singles respond to an external perturbation in zeroth W order. To keep the singles to all orders is crucial for response theory where un-relaxed orbitals are usually used. The orbital-relaxed response approach leads to a pole structure inconsistent with exact theory, as discussed e.g. in Ref. 20. The equations for the ground-state CC2 amplitudes are

$$0 = \langle \tilde{\Psi}_i^a | \hat{H} + [\hat{H}, T_2] | 0 \rangle \doteq \Omega_a^i, \quad (2.1)$$

$$0 = \langle \tilde{\Psi}_{ij}^{ab} | \hat{H} + [F, T_2] | 0 \rangle \doteq \Omega_{ab}^{ij}, \quad (2.2)$$

where $\hat{H} = \exp(-T_1)H\exp(T_1)$ is the Hamiltonian, similarity transformed with the exponent of the singles cluster operator, and $\tilde{\Psi}_i^a$, $\tilde{\Psi}_{ij}^{ab}$ are *contravariant* configuration state functions [51] projecting onto the singles and doubles manifold. The singles and doubles operators are described in terms of usual single and double orbital substitution operators [52],

$$\begin{aligned} T_1 &= \sum_{ia} t_a^i E_i^a, \\ T_2 &= \frac{1}{2} \sum_{ijab} T_{ab}^{ij} E_i^a E_j^b. \end{aligned} \quad (2.3)$$

We denote the occupied orbitals by indices i, j, k, l and the virtual (or PAO) orbitals by a, b, c, d . We have also tested a slightly modified model, where the similarity transformed Fock operator \hat{F} (for a definition of \hat{F} see Ref. 53)

was used also in the commutator of eq. (2.2). We will use in the following the acronym *CC2-b* for this modification of the CC2 model. For CC2-b the doubles-doubles block of the Jacobian is no longer diagonal in a canonical MO basis, what is an essential feature for previous CC2 implementations. On the other hand the doubles-doubles block of the local CC2 Jacobian is non-diagonal anyhow, hence local CC2-b does not involve any additional cost relative to local CC2.

To devise a local CC2 method, orthogonal localized molecular orbitals and mutually non-orthogonal projected atomic orbitals are introduced to span occupied and virtual orbital space, respectively. The former are constructed from the parental occupied canonical Hartree-Fock orbitals by an unitary transformation according to a localization criterion [54,55], the latter by projection of the AOs onto the virtual space. By construction the PAOs can still be assigned to individual atoms. In the spirit of the original CC2 idea no local restrictions are applied for the singles, whereas double excitations from LMOs i and j are restricted to pair-specific subspaces (domains) $[ij]$ of the virtual space. These pair domains contain only PAOs belonging to a certain subset of atoms in the spatial vicinity of the corresponding LMOs and can be determined, e.g. by following a procedure devised by Boughton and Pulay [56]. In addition to the truncation of the virtual space, restrictions on the pair list (based e.g. on a distance criterion between the related LMOs) can be imposed, such that the number of remaining doubles amplitudes scales asymptotically linearly with molecular size.

By employing diagrammatic techniques, working equations for local CC2 in terms of amplitudes and integrals are conveniently obtained from eqs. (2.1,2.2) as

$$(\Omega^i)_a = \left(\hat{\mathbf{f}}^i + \mathbf{S} \sum_k \tilde{\mathbf{T}}^{ik} \hat{\mathbf{f}}^k - \mathbf{S} \sum_{kl} \tilde{\mathbf{T}}^{kl} \hat{\mathbf{f}}^{lki} \right)_a \quad (2.4)$$

$$+ \sum_k \sum_{cd \in [ij]} \tilde{T}_{cd}^{ik} (ac|kd),$$

$$(\Omega^{ij})_{ab} = \left(\hat{\mathbf{K}}^{ij} + \mathbf{S} \mathbf{T}^{ij} \mathbf{F}^\dagger + \mathbf{F} \mathbf{T}^{ij} \mathbf{S} \right. \\ \left. - \mathbf{S} \sum_k \left(f_{ki} \mathbf{T}^{kj} + f_{kj} \mathbf{T}^{ik} \right) \mathbf{S} \right)_{ab}, \quad a, b \in [ij] \quad (2.5)$$

where \mathbf{S} and \mathbf{F} are the PAO overlap and Fock matrices and

$$\tilde{\mathbf{T}}^{ij} = 2\mathbf{T}^{ij} - \mathbf{T}^{ji}. \quad (2.6)$$

Here and in the following we employ the convention to denote matrices and vectors in the virtual space by capital and small bold letters, respectively, and scalars by normal (no-bold) letters [57]. Although not shown explicitly, the summations in eqs. (2.4) and (2.5) involving double amplitudes are restricted to their respective domains and pair lists.

In eqs. (2.4,2.5) modified (dressed) integrals (all objects with a hat) appear due to the similarity transformation of H with the exponent of T_1 . Such dressed integrals are defined as (see, e.g. [53])

$$(pq|\hat{r}s) \doteq \sum_{\mu\nu\rho\sigma} (\mu\nu|\rho\sigma) \Lambda_{\mu p}^p \Lambda_{\nu q}^h \Lambda_{\rho r}^p \Lambda_{\sigma s}^h \quad (2.7)$$

where p, q, \dots and μ, ν, \dots denote general MO (LMO or PAO) and AO indices, respectively. The dressed Fock integrals are defined as

$$\hat{f}_{pq} \doteq \hat{h}_{pq} + \sum_k (2(kk|\hat{p}q) - (kq|\hat{p}k)). \quad (2.8)$$

In eq. (2.7) modified MO coefficient matrices

$$\Lambda^p \doteq \left[\mathbf{L} \parallel (\mathbf{P} - \mathbf{L}^\dagger \mathbf{t}_1^\dagger \mathbf{S}) \right], \quad \Lambda^h \doteq \left[(\mathbf{L} + \mathbf{P} \mathbf{t}_1) \parallel \mathbf{P} \right] \quad (2.9)$$

are used in the integral transformation instead of the usual LMO/PAO coefficient matrices \mathbf{L} and \mathbf{P} (see e.g. [48]). Here the " \parallel " sign means that matrices on the left ($n_{\text{AO}} \times n_{\text{LMO}}$) and on the right ($n_{\text{AO}} \times n_{\text{PAO}}$) are glued together, \mathbf{t}_1 denotes the $n_{\text{PAO}} \times n_{\text{LMO}}$ matrix of the singles amplitudes, where n_{LMO} is the number of occupied and $n_{\text{PAO}} = n_{\text{AO}} -$ the number of projected atomic orbitals. The \mathbf{L} matrix is the rectangular matrix of LMO transformation coefficients, while the \mathbf{P} matrix is the projection matrix from the AO to PAO basis. Therefore, the Λ^p and Λ^h matrices are rectangular with the dimensions $n_{\text{AO}} \times (n_{\text{LMO}} + n_{\text{PAO}})$. Due to the structure of the integral transformation in eq. (2.7) the permutational symmetry between orbitals related to the same electron is lost. In a diagrammatical context, the first and the second orbital index of an electron correspond to an *outgoing* and an *incoming* line, respectively, relative to the interaction vertex. Thus, in eq. (2.7) the indices p, r correspond to outgoing, and q, s to incoming lines. Taking into account the structure of the modified MO coefficient matrices, eq. (2.9), it is immediately clear, that only quasi-particle creation lines, i.e., lines connecting the interaction vertices with the bra side, are effectively dressed. Therefore, the last term of eq. (2.4) involving dressed 3-external integrals can be conveniently rewritten in terms of bare (undressed) inte-

grals,

$$\begin{aligned} \sum_k \sum_{cd \in [ik]} \tilde{T}_{cd}^{ik}(ac|\hat{k}d) &= \sum_k \sum_{cd \in [ik]} \tilde{T}_{cd}^{ik}(ac|kd) \\ &- \sum_{kl} \sum_{cd \in [ik]} t_a^l \tilde{T}_{cd}^{ik}(lc|kd). \end{aligned} \quad (2.10)$$

The only remaining dressed integrals occurring in eqs. (2.4,2.5) are

$$\begin{aligned} (\hat{\mathbf{f}}^i)_a &\doteq \hat{f}_{ai} = \sum_k (2(a\hat{i}|kk) - (ak|\hat{k}i)), \\ (\hat{\mathbf{K}}^{ij})_{ab} &\doteq \hat{K}_{ab}^{ij} = (a\hat{i}|bj), \text{ and } (\hat{\mathbf{k}}^{ijk})_a \doteq \hat{k}_a^{ijk} = (ia|\hat{j}k). \end{aligned} \quad (2.11)$$

The computational cost for obtaining the singles and doubles residuals in eqs. (2.4,2.5) can be significantly reduced by invoking the DF approximation for the ERI integrals [32],

$$\begin{aligned} (pq|\hat{r}s) &= \sum_P (pq|\hat{P}) \hat{c}_{rs}^P, \quad \text{with} \\ \hat{c}_{rs}^P &\doteq \sum_Q (J^{-1})_{PQ} (Q|\hat{r}s). \end{aligned} \quad (2.12)$$

Here, indices P, Q denote auxiliary fitting functions, $J = (P|Q)$ and $(Q|\hat{r}s)$ are 2-index and dressed 3-index ERIs, and \hat{c}_{rs}^P the corresponding (dressed) fitting coefficients. With the definition

$$V_{ia}^P \doteq \sum_k \sum_{c \in [ik]} \tilde{T}_{ac}^{ik} c_{kc}^P, \quad a \in [ik], \quad (2.13)$$

eq. (2.4) can be rewritten in the form

$$\begin{aligned} (\boldsymbol{\Omega}^i)_a &= \left(\hat{\mathbf{f}}^i + \mathbf{S} \sum_k \tilde{\mathbf{T}}^{ik} \hat{\mathbf{f}}^k \right)_a - \sum_{a'} S_{aa'} \sum_{kP} V_{ka'}^P (P|\hat{k}i) \\ &+ \sum_P \sum_{c \in [i]_U} V_{ic}^P \left((P|ac) - \sum_k (P|kc) t_a^k \right). \end{aligned} \quad (2.14)$$

Note that the summation over the PAO index c in the last term of eq. (2.14) is restricted to the united pair domain $[i]_U = \cup[ik], \forall(ik)$, i.e., the union of all pair domains with a fixed LMO i . The quantity V_{ia}^P is identical to the important intermediate in DF-LMP2 gradient calculations, defined in

eq. (51) of Ref. 43 and involves only bare fitting coefficients. The virtual-occupied part of the dressed Fock matrix defined in eq. (2.11) is calculated as

$$\begin{aligned} \hat{f}_{\mu\nu} &= 2 \sum_P \hat{c}_P(P|\mu\nu) - \sum_{kP} (\mu k|P) c_{kv}^P, \quad \text{with} \\ \hat{c}_P &\doteq \sum_{kv} c_{kv}^P \Lambda_{vk}^h. \end{aligned} \quad (2.15)$$

The doubles amplitude equations (2.5) are virtually identical to the local MP2 equations with the sole difference that dressed rather than bare exchange integrals \hat{K}_{ab}^{ij} appear. The latter are obtained according to eq. (2.12) in the usual way [58]. For CC2-b, in addition, also the Fock matrix elements are replaced by their dressed counterparts.

The DF-LCC2 amplitude equations (2.14,2.5) are solved iteratively using DIIS convergence acceleration [59]. Redundancies in the PAO basis are eliminated at the stage of forming the amplitude updates from the residual vectors $\mathbf{\Omega}^i, \mathbf{\Omega}^{ij}$, as described elsewhere [37, 40]. As it is evident from eqs. (2.14,2.15), only dressed 3-index integrals with at least one index transformed to the LMO basis do occur. In particular the bare 2-external integrals $(P|ab)$ can be generated *outside* the CC2 iterations. The use of this integral set could be entirely avoided at the price of back-transforming the PAO index of V_{ia}^P to the AO basis, carrying out the contraction with the integrals (the last term of eq. (2.14)) entirely in the AO basis, and transforming the result again to the PAO basis in each iteration. Assuming 15 iterations until convergence the break even point for this alternative algorithm with respect to the CPU time would be arrived at a basis set size with a ratio $n_{\text{AO}}/n_{\text{LMO}} \approx 30$, which corresponds roughly to the aug-cc-pVTZ basis. As a further disadvantage, the domain restriction in the contraction step is lost in the AO basis.

The formally most expensive step is the formation of the V_{ia}^P intermediate according to eq. (2.13) with a nominal scaling of $\propto n_P n_{\text{AO}}^2 n_{\text{FIT}} = \mathcal{O}(\mathcal{N}^5)$ (n_P : number of pairs, n_{FIT} : number of fitting functions), yet by virtue of the local approximation this scaling reduces to $\propto n_P L^2 n_{\text{FIT}} = \mathcal{O}(\mathcal{N}^3)$ (L is the average size of a pair domain). Restrictions in the pair list reduces the scaling further to $\mathcal{O}(\mathcal{N}^2)$, and linear scaling can be achieved by introducing local fit domains [42].

2.2.2 Local CC2 excitation energies

The CC2 excitation energies are identical to the eigenvalues of the CC2 Jacobian, which is given by the following formula [21],

$$A_{\mu_i \nu_j} = \begin{pmatrix} \left\langle \tilde{\mu}_1 \left| [\hat{H}, \tau_{\nu_1}] + [[\hat{H}, \tau_{\nu_1}], T_2] \right| 0 \right\rangle & \left\langle \tilde{\mu}_1 \left| [\hat{H}, \tau_{\nu_2}] \right| 0 \right\rangle \\ \left\langle \tilde{\mu}_2 \left| [\hat{H}, \tau_{\nu_1}] \right| 0 \right\rangle & \left\langle \tilde{\mu}_2 \left| [F, \tau_{\nu_2}] \right| 0 \right\rangle \end{pmatrix} \quad (2.16)$$

where τ_{ν_x} is the covariant excitation operator, $\tilde{\mu}_x$ is the contravariant configuration function, and x denotes the order of excitation. For the modified CC2 method (CC2-b) the Fock operator occurring in the doubles-doubles block $A_{\mu_2 \nu_2}$ is replaced by \hat{F} . The right-hand eigenvalue problem,

$$\mathbf{A}U^f = \omega^f U^f \quad (2.17)$$

is solved iteratively using a Davidson method [60] generalized to non-symmetric matrices [61]. The right eigenvector U^f is constructed from the singles and doubles amplitudes u_a^i and U_{ab}^{ij} (from now on we drop the index f , denoting the number of the excited state). The corresponding linear wave operator $U = U_1 + U_2$ in its spin-adapted form is defined analogically to the T operator, i.e.

$$\begin{aligned} U_1 &= \sum_{ia} u_a^i E_i^a, \\ U_2 &= \frac{1}{2} \sum_{ijab} U_{ab}^{ij} E_i^a E_j^b. \end{aligned} \quad (2.18)$$

In each iteration the product of the Jacobian with an approximate vector u , $v \doteq \mathbf{A}u$ is required, in order to compute the residual vector as

$$\begin{aligned} 0 &= \sum_{x, \nu_x} A_{iav_x} u_{\nu_x} - \omega (\mathbf{S}u^i)_a \doteq r_a^i, \\ 0 &= \sum_{x, \nu_x} A_{ijabv_x} u_{\nu_x} - \omega (\mathbf{S}u^{ij}\mathbf{S})_{ab} \doteq R_{ab}^{ij}, \end{aligned} \quad (2.19)$$

where ω is an approximate value of the CC2 excitation energy in a given iteration. Having the residual vector R , the next expansion vector of the small Davidson subspace is computed by first-order perturbation theory, as described in Ref. 44.

Working expressions for the vector $\mathbf{v} \doteq \mathbf{A}u$ are again conveniently derived from eq. (2.16) by virtue of diagrammatic techniques. After invoking the DF approximation one obtains for the singles part of \mathbf{v} ,

$$\begin{aligned} v_a^i &= \hat{f}_{ac} u_c^i + S_{aa'} \left(\tilde{U}_{a'c}^{ik} \hat{f}_{kc} - u_{a'}^k \hat{f}_{ki} \right) - \hat{c}_{ki}^P \hat{Y}_P^{ak} \\ &+ 2(\hat{c}_{ai}^P + V_{ia'}^P S_{a'a}) b_P + W_{ic}^P (ac|P) - S_{aa'} W_{ka'}^P (ki|P) \\ &- S_{aa'} \left(u_{a'}^k V_{ic}^P (kc|P) + V_{ka'}^P Y_P^{ki} + \tilde{T}_{a'c}^{ik} x_{kc} \right) \end{aligned} \quad (2.20)$$

and for the doubles part,

$$\begin{aligned} \mathfrak{B}_{ab}^{ij} &= G_{ab}^{ij} + G_{ba}^{ji} + S_{aa'} U_{a'c}^{ij} f_{bc} + f_{ac} U_{cb'}^{ij} S_{b'b} \\ &- S_{aa'} \left(U_{a'b'}^{ik} f_{kj} + U_{a'b'}^{kj} f_{ki} \right) S_{b'b}, \end{aligned} \quad (2.21)$$

with the new intermediates

$$\begin{aligned} Y_P^{ij} &\doteq (P|ic) u_c^j, \quad \hat{Y}_P^{ai} \doteq (P|ac) u_c^i, \quad b_P \doteq (P|kc) u_c^k, \\ x_{ia} &\doteq c_P^{ka} Y_P^{ik}, \\ W_{ia}^P &\doteq \tilde{U}_{ac}^{ik} c_P^{kc}, \\ G_{ab}^{ij} &\doteq \left(\hat{Y}_P^{ai} - S_{aa'} u_{a'}^k (ki|P) \right) \hat{c}_P^{bj}, \end{aligned} \quad (2.22)$$

and \tilde{U}_{ab}^{ij} being defined according to eq. (2.6). The summation over repeated indices (Einstein convention) is assumed in eqs. (2.20-2.22) to improve the visibility of the formulas. The intermediate V_{ia}^P has already been defined in eq. (2.13). For CC2-b the elements of the Fock matrix in eq. (2.21) again are replaced by their dressed counterparts.

Similarly as for the ground state we introduce local restrictions only on the double part of the excitation space, by allowing double excitations only to pair-specific domains. The determination of such ‘excited state’ domains is a non-trivial task. For example, for a charge-transfer eigenstate the relevant virtual space for a given LMO pair is not necessarily located in the spatial vicinity of these LMOs, but may in fact lie far from them. In this work we follow the approach proposed in Ref. 44: a set of ‘important’ LMOs is determined by an analysis of the CIS wave function. All LMOs are ordered according to decreasing values of their weight

$$w_i \doteq \sum_a |c_a^i|^2 \quad (2.23)$$

in the CIS wave function (c_a^i denotes the CIS coefficients). Going sequentially through this ordered list and adding up their weights all LMOs are

considered as important until a certain threshold κ_e is reached. When κ_e is set to 1, all LMOs are considered as important, due to the normalization of the CIS wave function. For each important LMO ϕ_i its ‘excited state’ orbital domain $[i]^*$ is constructed as the union of the original ‘ground state’ orbital domain $[i]$ and an additional domain obtained by employing the Boughton-Pulay procedure [56] to the orbital ϕ_i^* defined as

$$\phi_i^* \doteq \sum_a c_a^i \phi_a, \quad (2.24)$$

which describes for a given excited state the whole excitation from the LMO i . ‘Excited state’ orbital domains for unimportant orbitals, on the other hand, just comprise the related ‘ground state’ orbital domain, i.e., $[i]^* = [i]$. From these ‘excited state’ orbital domains the ‘excited state’ pair domains $[ij]^*$ then are formed as the unions of the corresponding orbital domains, in an entire analogy to the ‘ground state’ pair domains $[ij]$. Finally, restrictions on the ‘excited state’ pair list based on the classification into important and unimportant orbitals can be imposed. For example, the ‘excited state’ pair list may be restricted such that it includes all pairs between important orbitals, but only pairs up to a certain inter-domain distance if at least one unimportant orbital is involved. It should be noted that the inter-domain distance is defined as a minimum distance between atoms contributing to an ‘excited state’ orbital domain. It is usually different (smaller) from the inter-orbital distance, used for the ground-state calculations. The latter is defined as a minimum distance between atoms belonging to LMOs. Domains and restricted pair lists are the cornerstone of all computational savings in local methods. Different ways to restrict the ‘excited state’ pair list and their effect on accuracy and efficiency of the method are discussed in the next section.

At this stage we performed only single-point calculations. However, it should be mentioned here that local methods have also been applied successfully to potential energy surface (PES) calculations [62,63]. In order to avoid PES discontinuities the same domains and pair lists are used along the whole reaction coordinate. These domains and pair lists are usually somewhat enlarged in comparison to a corresponding single-point calculation and include all configurations, which become important along the reaction coordinate. The very same approach can easily be adopted to the DF-LCC2 method and excited state surfaces.

Once the configuration space is selected, we look for the eigenvector, which is the most similar to the CIS wave function (in a sense that the overlap of LCC2 and CIS vectors is the largest), using the root-homing

procedure built in our Davidson algorithm. This assures that the calculation always converges to the correct vector (i.e. having the largest overlap with the CIS vector), independent on possible order changes in CIS and CC2 spectra (root-switching). If the CIS vector appears to be inadequate, e.g., by comparison with the un-truncated CC2 singles vector at a certain iteration, it is of course also possible to re-specify the domains based on the actual CC2 singles vector. We should emphasize here that our approach is state-specific, i.e. in order to obtain the CC2 spectrum we repeat the whole procedure (i.e. a domain selection and looking for the eigenvector) for every CIS vector. Alternatively one could merge domains and pair lists obtained from several CIS vectors and calculate the corresponding CC2 energies simultaneously. This approach will lead, however, to an increased cost of the calculation per state, since each state will be calculated in a larger configuration space than in the state-specific case.

The analysis of eqs. (2.20,2.21) shows that the most expensive steps of the product formation of the Jacobian with an approximate vector are the evaluations of the intermediates W_{ia}^P and G_{ab}^{ij} in eq. (2.22). The cost of calculation of those quantities has a nominal scaling of $\propto n_P n_{AO}^2 n_{FIT} = O(N^5)$, the same as the ground state intermediate V_{ia}^P defined in eq. (2.13). Also here, the local approximation reduces this scaling to $O(N^2)$, and with the local fitting even to $O(N)$. Of course, without any truncations of the singles vector the overall nominal scaling with respect to molecular size remains $O(N^4)$. In contrast to canonical methods with de-localized orbitals, pre-screening may reduce this scaling to some extent. In any case, for the calculations presented here the singles part are not yet dominating the overall cost of the calculation.

2.3 Test Calculations

The CC2 and CC2-b models and the related linear response programs for the calculation of excitation energies have been implemented in the MOLPRO package (development version) [64]. The DF approximation was employed throughout in the correlated calculations. In order to have an efficient program for generating ‘excited state’ domains (cf. section 2.2.2) and starting vectors for the Davidson diagonalization also a DF-CIS program was implemented. The algorithm for the CC2 ground state amplitudes has been outlined already in section 2.2.1. Particularly, the bare 3-index 2-external ERIs used in eq. (2.14) are precomputed and stored on disk. After the ground-state calculation has converged, these integrals are dressed for use in the formation of the right-hand product of the Jacobian with

an approximate vector, eqs. (2.20,2.22). The set of 3-index 2-external ERIs is the largest data object kept on disk, the disk space requirements thus scale as $\propto n_{\text{AO}}^2 n_{\text{FIT}} = O(N^3)$ with molecular size. In order to minimize I/O the computation of the right product is organized such that precomputed 3-index objects like 3-index ERIs and fitting coefficients (and in particular the 3-index 2-external ERIs) are just touched once in each iteration. Furthermore, in order to achieve a compromise between economical use of memory and computational efficiency, just one instance of a vector of the size of a trial vector is kept in memory. Since the individual contraction steps of integrals with amplitudes in the formation of the Jacobian times trial vector product are carried out block-wise, this vector determines the memory requirements for the whole calculation. Formally, its size scales quadratically with molecular size (since the singles are un-truncated), yet the doubles part (in spite of the fact that its size is scaling linearly with molecular size by construction) is still much larger and dominates the overall size of the trial vector for all systems investigated so far. The sizes of the trial vectors for some individual excitation energy calculations on extended molecular systems are compiled in Table 2.6. Evidently, they strongly depend on the character, i.e., the locality of the individual excitations (*vide infra*).

Basis		cc-pVDZ			cc-pVTZ			aug-cc-pVDZ		
Molecule	$n_p(\text{tot})^a$	n_{AO}^b	n_p^c	L^d	n_{AO}^b	n_p^c	L^d	n_{AO}^b	n_p^c	L^d
N-acetyl glycine	276	147	270	43	338	270	93	247	270	71
Propanamide	120	105	120	38	248	120	85	178	120	64
"Dipeptide"	351	176	321	44	410	321	98	297	321	75
" β -dipeptide"	435	200	370	44	468	373	100			
"Tripeptide"	703	247	528	46	572	528	101			
<i>trans</i> -urocanic acid	351	170	323	50	384	323	112	284	325	95
Guanine	406	179	400	56	400	400	122	298	400	102
1-phenylpyrrole	378	199	363	58	456	363	126	334	366	112
DMABN	406	204	372	52	470	373	118			
<i>p</i> -cresol	231	152	222	48	352	225	107			
HPA	528	218	434	48	500	440	107			
Tyrosine	630	237	558	49	544	564	108			
Phenylalanine	528	223	497	49	514	497	107			
DA1	3741	593	1942	64						
DA2	6105	785	2516	61						
Triad	17205	1314	4644	64						

a) Total number of LMO pairs

b) Total number of AOs

c) Number of pairs treated in the LCC2 'ground state' calculation

d) Average pair domain size in the CC2 'ground state' calculation

Table 2.1: Total number of LMO pairs and number of AOs for the individual test molecules. The number of pairs included in the local CC2 calculation and the average pair domain size (which both determine the number of non-zero ground state doubles amplitudes) are also given.

In the following we present test calculations which demonstrate accuracy and efficiency of the new local CC2 method for excitation energies. As AO basis sets the cc-pVDZ, cc-pVTZ, and aug-cc-pVDZ sets [65,66] together with their related fitting basis sets optimized for DF-MP2 [67,68] were employed. In all calculations the LMOs were obtained by using Pipek-Mezey localization [55]. As discussed in section 2.2.2, the LMOs are discriminated into a class of important and unimportant orbitals by analyzing an initial CIS wave function of the state of interest. Suitable pair lists for that particular state can then be specified by taking advantage of this classification. For example, all pairs not including at least one important LMO may be dropped in case of an inter-domain distance exceeding a certain threshold of $R_{ID}=10$ bohr. Denoting important orbitals by i, j , unimportant ones by m, n such a list is specified in the following as $\forall(ij), \forall(im), (mn) \leq 10$. An alternative type of a pair list can be constructed by keeping all important LMO pairs but dropping all other pairs with an inter-domain distance bigger than the threshold R_{ID} , regardless, if one important LMO is involved or not. For such a pair list we use the specification $\forall(ij), (im) \leq R_{ID}, (mn) \leq R_{ID}$. In individual test calculations the threshold R_{ID} was set to 3, 5, and 10 bohrs, respectively. The criterion for selecting important orbitals was set to $\kappa_e = 0.995$ for most calculations, which appears to be a safe choice. The pair list for the ground-state amplitudes was restricted for all calculations to LMO pairs with an inter-orbital distance R_{IO} not exceeding 10 bohr. Test calculations have shown that longer pair lists for ground-state amplitudes (i.e. for $R_{IO} > 10$ bohr) have no significant impact on the excitation energies. The Boughton-Pulay criterion for domain specification was set to 0.98 (0.985) for formation of both the ground- and excited-state amplitude pair domains for the cc-pVDZ (aug-cc-pVDZ, cc-pVTZ) basis sets.

Key quantities of the local calculation relevant to achieve low scaling in the computational cost, such as the length of the pair list, the average pair domain sizes, etc., are compiled in Tables 2.1-2.3 for the unperturbed ‘ground state’ amplitudes and their first-order response, i.e., the ‘excited state’ amplitudes, respectively. These quantities are shown for different parameters used for the selection of important orbitals and for several types of pair lists, which have been tested in the present work. As can be seen from these tables, most computational savings for the smaller molecules are due to the domain restrictions of the double excitations. The average size of a pair domain (in the cc-pVDZ basis) varies only between 38 and 64 for the ground state and between 52 and 239 for the individual excited states (pairlist (2) from Table 2.2 is used for this comparison), while the number of basis functions increases by a factor of 13 between the smallest

Basis Molecule	state	cc-pVDZ									cc-pVTZ		
		$n_p^*(1)$	$L^*(1)$	$r_D(1)$	$n_p^*(2)$	$L^*(2)$	$r_D(2)$	$n_p^*(3)$	$L^*(3)$	$r_D(3)$	$n_p^*(2)$	$L^*(2)$	$r_D(2)$
N-acetyl- glycine	S ₁	274	63	33%	232	63	29%	177	60	19%	254	158	28%
	S ₂	273	62	33%	214	63	27%	173	63	22%	214	126	15%
	S ₃	270	89	66%	249	93	65%	235	93	62%	249	206	46%
Propanamide	S ₁	120	60	54%	117	61	54%	107	62	51%	114	125	31%
	S ₄	120	74	82%	120	74	82%	120	74	82%	120	181	66%
"Dipeptide"	S ₁	340	70	28%	267	70	22%	211	70	18%	289	168	19%
	S ₂	330	71	28%	261	72	23%	216	72	19%	261	176	19%
"β-dipeptide"	S ₁	387	71	20%	282	70	15%	236	69	12%	289	167	12%
	S ₂	393	60	14%	271	57	9%	206	55	6%	310	155	11%
	S ₃	381	82	28%	324	87	26%	273	89	23%	315	186	17%
"Tripeptide"	S ₁	562	64	10%	391	64	7%	291	63	5%	410	151	6%
	S ₂	549	74	13%	391	73	9%	311	74	8%	407	178	8%
<i>trans</i> -uro- canic acid	S ₁	334	85	46%	287	90	43%	261	93	42%	290	202	33%
	S ₂	336	108	69%	315	111	68%	293	113	65%	315	251	52%
	S ₃	342	82	42%	280	84	36%	231	85	30%	274	189	27%
	S ₄	333	102	62%	306	105	60%	279	106	56%	246	150	17%
	S ₅	349	102	64%	323	104	61%	298	104	56%	303	233	44%
Guanine	S ₁	403	107	68%	362	114	66%	333	118	64%	362	253	50%
	S ₂	404	97	55%	370	101	54%	323	104	49%	378	221	39%
	S ₃	406	109	69%	377	113	68%	342	117	65%	375	253	51%
1-phenyl- pyrrole	S ₁	363	92	39%	305	99	36%	265	103	34%	311	235	31%
	S ₂	369	127	67%	351	129	66%	329	133	64%	351	294	50%
	S ₃	373	106	50%	341	108	48%	289	113	43%	332	237	34%
DMABN	S ₄	363	95	44%	309	103	43%	267	110	41%	292	188	22%
	S ₁	393	87	32%	345	92	31%	288	97	28%	346	222	27%
	S ₂	399	121	59%	371	125	57%	353	128	57%	373	293	46%
<i>p</i> -cresol	S ₁	229	76	44%	212	78	43%	181	83	41%	213	189	37%
	S ₂	470	85	26%	363	89	22%	295	91	18%	370	212	18%
	S ₃	460	66	15%	321	63	10%	246	66	8%	325	136	7%
HPA	S ₁	490	97	33%	395	98	28%	326	98	23%	390	217	19%
	S ₂	581	85	23%	431	90	19%	327	92	15%	433	211	15%
	S ₃	580	93	28%	448	97	24%	354	102	21%	447	210	16%
Tyrosine	S ₁	595	111	38%	489	115	33%	406	120	30%	491	247	23%
	S ₂	497	74	21%	367	81	18%	276	84	14%	370	195	16%
	S ₃	515	90	31%	404	95	27%	324	100	23%	407	208	18%
Phenyl- alanine	S ₄	519	101	37%	424	105	33%	338	111	29%	420	226	22%
	S ₁	2462	194	15%	1871	212	13%	1598	224	12%			
	S ₂	2254	163	10%	1671	181	9.0%	1353	190	7.8%			
DA1	S ₃	3017	232	24%	2240	249	20%	1991	257	19%			
	S ₁	2915	153	4.2%	2040	172	3.5%						
	S ₂	2674	111	2.0%	1780	127	1.6%						
Triad	S ₃	4071	217	9.7%	2652	227	6.9%						
	S ₁				4805	239	1.9%						
	S ₂				2847	112	0.3%						
	S ₄				3861	199	1.1%						
	S ₅				2473	82	0.1%						

Table 2.2: Number of pairs n_p^* and average sizes of ‘excited state’ domains L^* (related to the ‘excited state’ doubles amplitudes) as used in the local CC2 linear response calculations with the cc-pVDZ and cc-pVTZ basis sets. The ratio r_D of the overall number of doubles amplitudes treated in the local calculation relative to the total number of doubles amplitudes treated in the corresponding canonical calculation is also included. These quantities are given for all test molecules and states considered, for several specifications of the ‘excited state’ pair list.

- 1) pair list specified as $\forall(ij), (im) \leq 10, (mn) \leq 10$, cc-pVDZ basis
- 2) pair list specified as $\forall(ij), (im) \leq 5, (mn) \leq 5$, cc-pVDZ basis
- 3) pair list specified as $\forall(ij), (im) \leq 3, (mn) \leq 3$, cc-pVDZ basis

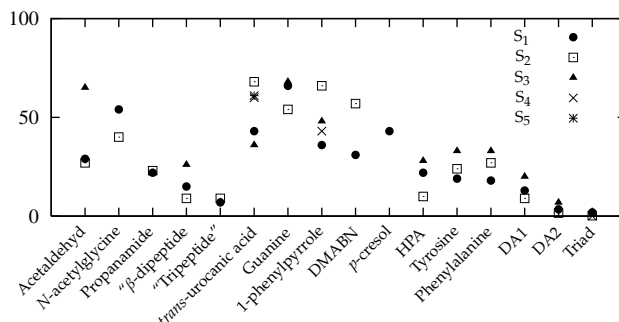


Figure 2.1: The ratio of the number of doubles amplitudes included in the local CC2 calculations relative to the total number of doubles amplitudes for the case 2 of Table 2.2.

and the largest molecule included in the test set. The savings due to the smaller number of pairs of LMOs are less pronounced (e.g. about half of all pairs is used in LCC2 for the DA1 molecule in the ground state), but they become substantial for the largest molecule considered here (only about a quarter of all pairs enters the local CC2 treatment). A similar pattern can be seen for the ‘excited state’ amplitudes with the length of the pair lists depending significantly on the local (or non-local) character of the excited state involved. In Table 2.2 the percentage of local vs. canonical doubles amplitudes is also reported, which shows the combined savings from restricting excitations to domains and pair lists. The percentage of local amplitudes is also depicted in Fig. 2.1. An examination of Table 2.2 and Fig. 2.1 clearly shows that the expected savings relative to the canonical calculation grow with molecular size and for the largest molecule only a few percent (for local excitations merely a few tenths of a percent) of all double amplitudes are needed in the local calculation. Interestingly, on going from the cc-pVDZ to the cc-pVTZ or aug-cc-pVDZ basis the percentage appears to decrease, even though the criterion for the pair list specification is identical and the Boughton-Pulay criterion is even somewhat tighter for the bigger basis. Apparently, if more functions are available per center, less centers per domain are required in a local calculation to describe the excited-state amplitudes.

Tables 2.4 and 2.5 collect the excitation energies of the lowest few states of the same set of test molecules as investigated in Ref. 44. Deviations of the LCC2 excitation energies from the corresponding canonical reference values (i.e. $\Delta\omega = \omega_{\text{loc}} - \omega_{\text{can}}$) are given for different specifications of the pair list for the excited-state amplitudes. The differences between canonical EOM-CCSD (taken from Ref. 44) and CC2 methods are also given. Evidently, the errors in the excitation energies due to the local approxi-

mation do not exceed 0.06 eV for the cc-pVDZ basis, with the exception of one state. For that particular state (the charge transfer excited state of 1-phenylpyrrole) also the deviation between canonical CCSD and CC2 is un-typically large (0.472 eV) and the local CC2 value lies closer to CCSD than canonical CC2 does. Interestingly, the deviation of local CCSD from canonical CCSD in Ref. 44 was smaller (0.057 eV) than here, even though the domain criteria were identical and the pair lists much smaller than in the present work.

Molecule	state	n_p^*	L^*	r_D	n_p^{uni}	L^{uni}	r_D^{uni}
N-acetylglutamine	S ₁	249	126	35%	274	122	36%
	S ₂	226	112	25%	270	112	29%
	S ₃	234	131	37%	274	123	39%
Propanamide	S ₁	118	103	45%	120	103	45%
	S ₂	114	89	34%	120	88	35%
"Dipeptide"	S ₁	274	129	22%	325	124	24%
	S ₂	292	156	33%	330	145	32%
	S ₃	253	117	17%	324	114	21%
<i>trans</i> -urocanic acid	S ₁	348	173	53%	348	173	53%
	S ₂	327	193	61%	333	186	58%
	S ₃	255	119	21%	328	116	25%
	S ₄	325	175	52%	343	172	53%
Guanine	S ₁	342	139	30%	400	130	31%
	S ₂	388	209	67%	402	204	67%
	S ₃	342	135	28%	400	127	30%
	S ₄	375	183	52%	400	178	53%
	S ₅	390	208	67%	404	203	67%
1-phenylpyrrole	S ₆	344	154	37%	400	144	39%
	S ₁	320	180	37%	366	172	39%
	S ₂	351	218	55%	366	215	56%
	S ₃	329	187	41%	366	179	43%
	S ₄	347	210	51%	366	206	52%
	S ₅	327	179	37%	366	171	39%

Table 2.3: Number of pairs n_p^* and average sizes of ‘excited state’ domains L^* (related to the ‘excited state’ doubles amplitudes) in the aug-cc-pVDZ basis, as used in the local CC2 linear response calculations. The ratio r_D of the overall number of doubles amplitudes treated in the local calculation relative to the total number of doubles amplitudes treated in the corresponding canonical calculation is also included. The pair list was specified as $\forall(ij), (im) \leq 5, (mn) \leq 5$. Corresponding values for unified pair lists and domains ($n_p^{\text{uni}}, L^{\text{uni}}$) are also given.

For the lower-lying valence states the errors are smaller than 0.04 eV. This conclusion applies also to the shortest pair list considered in Table 2.4, i.e., the $\forall(ij), (im) \leq 3, (mn) \leq 3$ pair list. The errors of some higher states calculated in the cc-pVTZ basis are somewhat larger, but they do not exceed 0.1 eV with the exception of the same charge transfer state mentioned above and a Rydberg state of *trans*-urocanic acid, which is shifted to lower energy when the cc-pVTZ basis is used (The $S_5 \leftarrow S_0$ excitation in the cc-pVTZ basis corresponds to the $S_4 \leftarrow S_0$ excitation in the cc-pVDZ basis). Generally,

the larger discrepancies for some excitations to higher states are most probably due to the fact that states which have (partly) diffuse character are poorly described by AO basis sets without Gaussians having very low exponents. As a consequence, many AOs are involved to mimic this diffuse behavior and truncations to orbital domains will lead to bigger deviations from the canonical result than for ordinary valence states. If this is true then increasing the number of diffuse Gaussians should make the local vs. canonical error smaller. To this end we repeated the calculations in the aug-cc-pVDZ basis for some molecules, including the troublesome charge transfer state of 1-phenylpyrrole. As is evident from Table 2.5, the error due to the local approximation for this state vanishes almost entirely in the aug-cc-pVDZ basis. Since we are interested in determining *a priori*, which states may cause similar problems, we checked the CIS energies corresponding to this state and the other states of 1-phenylpyrrole in both the cc-pVDZ and aug-cc-pVDZ basis. It turns out that the CIS energy decreases by 1.66 eV for the charge transfer excitation on going from cc-pVDZ to the diffuse basis, while for other excitations in the table the corresponding differences in the CIS energies are smaller than 0.5 eV. We can therefore propose a quick check of “suspicious” states, based on a DF-CIS calculation: if the CIS energies of a given state differ in diffuse and non-diffuse basis sets by more than 1 eV, the smaller basis is completely inappropriate for this state and therefore large errors in the local approximations are expected.

To summarize, Tables 2.4 and 2.5 clearly show that the excitation energies involving the energetically lower-lying excited states are all well reproduced in the cc-pVTZ and aug-cc-pVDZ basis by the local CC2 method, similarly to the results obtained in the smaller cc-pVDZ basis. Considering an expected accuracy of about 0.3 eV for the CC2 method itself, the discrepancies observed can be considered as fair. One should also keep in mind that effects like the basis set superposition error, which are virtually absent in local methods [69], do play a role here. Furthermore, in contrast to the local EOM-CCSD method reported in Ref. 44 it appears that the accuracy of the local CC2 excitation energies do not depend so strongly on the quality of the CIS wave function. For example, the $S_3 \leftarrow S_0$ and $S_4 \leftarrow S_0$ excitation energies of *trans*-urocanic acid are obtained with a local error of about 0.03 eV (≈ 0.06 eV for the shortest pair list), while errors bigger than 0.1 eV were observed for local EOM-CCSD in Ref. 44 and attributed to a poor description of these states by the related CIS wave functions. The reason for the more robust behavior of LCC2 can be most probably ascribed to the fact that (i) single excitations are treated without any local approximation, and (ii) longer pair lists are affordable in LCC2.

We also performed calculations on the set of test molecules employing

Basis Molecule	state	character	cc-pVDZ										cc-pVTZ	
			ω_{CCSD}^a	ω_{CC2}^b	$\Delta\omega_{can}^c$	$\Delta\omega_1^d$	$\Delta\omega_2^d$	$\Delta\omega_3^d$	$\Delta\omega_4^d$	$\Delta\omega_5^d$	$\Delta\omega_6^d$	$\Delta\omega_7^d$	ω_{CC2}^b	$\Delta\omega_3^d$
N-acetylglycine	S ₁	$n \rightarrow \pi^*$	5.810	5.862	0.052	-0.015	-0.015	-0.013	-0.001	0.017	0.012	0.002	5.777	-0.006
	S ₂	$n \rightarrow \pi^*$	6.162	6.252	0.090	0.010	0.010	0.013	0.023	0.032	0.020	0.024	6.148	0.032
	S ₃	$\pi \rightarrow \pi^*$	7.584	7.373	-0.211	0.004	0.004	0.005	0.005	0.046	0.034	-0.001	7.195	0.076
Propanamide	S ₁	$n \rightarrow \pi^*$	5.861	5.926	0.065	0.001	0.001	0.001	0.003	0.031	0.028	0.018	5.804	0.025
	S ₄	$\pi \rightarrow \pi^*$	7.886	7.962	0.076	0.022	0.022	0.022	0.022	0.054	0.045	0.031	7.638	0.037
"Dipeptide"	S ₁	$n \rightarrow \pi^*$	5.828	5.871	0.043	-0.021	-0.021	-0.019	-0.010	0.012	0.008	-0.004	5.790	-0.011
	S ₂	$n \rightarrow \pi^*$	6.067	6.106	0.039	-0.005	-0.005	-0.000	0.010	0.027	0.014	0.012	6.009	-0.000
"β-dipeptide"	S ₁	$n \rightarrow \pi^*$	4.881	4.861	-0.020	-0.035	-0.035	-0.030	-0.023	0.019	0.017	-0.015	4.783	-0.013
	S ₂	$n \rightarrow \pi^*$	5.773	5.825	0.052	-0.016	-0.016	-0.012	-0.003	0.011	0.012	0.002	5.732	-0.003
	S ₃	$\pi \rightarrow \text{Rydb.}$	7.039	6.908	-0.131	0.032	0.032	0.033	0.043	0.077	0.040	0.035	6.501	0.079
"Tripeptide"	S ₁	$n \rightarrow \pi^*$	5.824	5.868	0.044	-0.022	-0.021	-0.019	-0.011	0.012	0.008	-0.004	5.786	-0.011
	S ₂	$n \rightarrow \pi^*$	6.066	6.091	0.025	0.003	0.004	0.010	0.021	0.041	0.028	0.022	5.999	0.014
trans-urocanic acid	S ₁	$n \rightarrow \pi^*$	5.187	4.987	-0.200	-0.021	-0.021	0.010	0.021	0.038	0.014	0.039	4.906	0.023
	S ₂	$\pi \rightarrow \pi^*$	5.384	5.207	-0.177	-0.024	-0.024	-0.024	-0.023	0.036	0.014	-0.026	5.022	-0.004
	S ₃	$\pi \rightarrow \pi^*$	6.415	6.269	-0.146	0.031	0.031	0.033	0.059	0.066	0.028	0.031	6.093	0.040
	S ₄	$\pi \rightarrow \pi^*$	6.708	6.877	0.169	0.027	0.027	0.027	0.028	0.063	0.034	0.026	6.562	0.115
Guanine	S ₅	$\pi \rightarrow \text{Rydb.}$	7.062	7.054	-0.008	-0.062	-0.062	-0.061	-0.060	0.001	0.000	-0.062	6.636	0.045
	S ₁	$\pi \rightarrow \pi^*$	5.404	5.316	-0.088	0.002	0.002	0.002	0.002	0.058	0.020	0.005	5.155	0.027
	S ₂	$n \rightarrow \pi^*$	5.712	5.660	-0.052	-0.023	-0.023	-0.022	-0.013	0.015	0.012	0.004	5.537	-0.008
	S ₃	$\pi \rightarrow \pi^*$	6.052	5.820	-0.232	-0.002	-0.002	-0.002	-0.001	0.042	0.020	-0.006	5.599	0.021
1-phenylpyrrole	S ₁	$\pi \rightarrow \pi^*$	5.060	5.072	0.012	0.007	0.011	0.012	0.019	0.053	0.017	0.010	4.963	0.025
	S ₂	$\pi \rightarrow \pi^*$	5.736	5.555	-0.181	-0.002	-0.002	-0.002	-0.001	0.049	0.019	-0.003	5.422	0.021
	S ₃	$\pi \rightarrow \pi^*$	6.117	5.771	-0.346	0.014	0.014	0.014	0.015	0.055	0.030	0.011	5.609	0.033
	S ₄	CT (py→ph)	6.563	6.091	-0.472	0.135	0.135	0.135	0.140	0.166	0.123	0.132	5.879	0.186
DMABN	S ₁	$\pi \rightarrow \pi^*$	4.650	4.525	-0.125	0.038	0.038	0.038	0.050	0.091	0.026	0.041	4.405	0.057
	S ₂	$\pi \rightarrow \pi^*$	5.130	4.891	-0.239	-0.064	-0.064	-0.064	0.023	0.012	-0.059	0.012	4.780	-0.028
p-cresol	S ₁	$\pi \rightarrow \pi^*$	4.979	4.981	0.002	0.011	0.011	0.011	0.013	0.061	0.020	0.013	4.867	0.025
HPA	S ₁	$\pi \rightarrow \pi^*$	4.987	4.984	-0.003	0.008	0.009	0.013	0.023	0.064	0.025	0.010	4.875	0.030
	S ₂	$n \rightarrow \pi^*$	6.052	6.148	0.096	0.005	0.009	0.011	0.014	0.034	0.028	0.019	6.038	0.024
	S ₃	$\pi \rightarrow \pi^*$	6.436	6.285	-0.151	-0.014	-0.013	-0.024	-0.000	0.047	0.024	-0.027	6.132	0.011
Tyrosine	S ₁	$\pi \rightarrow \pi^*$	4.997	4.995	-0.002	0.011	0.011	0.022	0.038	0.064	0.029	0.013	4.891	0.043
	S ₂	$n \rightarrow \pi^*$	5.757	5.824	0.067	-0.002	-0.004	-0.001	0.009	0.041	0.033	0.009	5.739	0.022
	S ₃	$\pi \rightarrow \pi^*$	6.370	6.205	-0.165	-0.019	-0.019	-0.003	0.016	0.054	0.030	-0.014	6.054	0.013
Phenylalanine	S ₁	$\pi \rightarrow \pi^*$	5.189	5.260	0.071	0.021	0.021	0.029	0.046	0.064	0.012	0.022	5.165	0.045
	S ₂	$n \rightarrow \pi^*$	5.758	5.827	0.069	-0.002	-0.000	0.002	0.013	0.042	0.033	0.013	5.744	0.017
	S ₃	$\pi \rightarrow \pi^*$	6.655	6.574	-0.081	-0.011	-0.011	-0.005	0.019	0.046	0.032	-0.011	6.391	0.020

a) canonical EOM-CCSD excitation energies from Ref. 44 (when available)

b) canonical CC2 excitation energies calculated with TURBOMOLE v. 5.7, Ref. 27,29

c) deviation canonical CC2 vs. canonical EOM-CCSD

d) deviation local CC2 vs. canonical CC2

Table 2.4: Excitation energies for various test molecules. Values (all in eV) are given for canonical EOM-CCSD, CC2, local CC2 and local CC2-b. The Boughton-Pulay criterion for domain specification was set to 0.98 and 0.985, respectively, for the calculations employing the cc-pVDZ and the cc-pVTZ basis. The pair list for the ground-state amplitudes was truncated for inter-orbital distances beyond 10 bohr. For the excited-state amplitudes the pair list was truncated in various ways, as specified below. The criterion to determine important orbitals was set to $\kappa_e = 0.995$ (cf. text). The 1s orbitals for the C, N, and O atoms were frozen in all correlated calculations.

- 1) pair list specified as $\forall(ij), \forall(im), (mn) \leq 10$
- 2) pair list specified as $\forall(ij), (im) \leq 10, (mn) \leq 10$
- 3) pair list specified as $\forall(ij), (im) \leq 5, (mn) \leq 5$
- 4) pair list specified as $\forall(ij), (im) \leq 3, (mn) \leq 3$
- 5) pair list specified as $\forall(ij), (im) \leq 5, (mn) \leq 5$, unified domains/pair list
- 6) pair list specified as $\forall(ij), (im) \leq 5, (mn) \leq 5$, unified domains/pair list, extended domains (3 bohr)
- 7) pair list specified as $\forall(ij), (im) \leq 5, (mn) \leq 5$, CC2-b

a lower criterion of $\kappa_e = 0.99$ for the selection of important LMOs (not included in Table 2.4). This criterion leads in some cases to substantially bigger local errors, e.g. -0.117 rather than -0.033 eV for the $S_3 \leftarrow S_0$ excitation of β -dipeptide, and must be regarded as less safe. Finally, a further dataset, generated by using the CC2-b rather than the CC2 method, is included in Table 2.4. As expected, the deviations between CC2-b and CC2 turn out to be very small. Based on the presented data we propose as a safe domain/pair list specification the pair list defined as $\forall(ij), (im) \leq 5, (mn) \leq 5$ together with the criterion for the important-orbital selection set to $\kappa_e = 0.995$.

Molecule	state	character	ω_{CCSD}^a	ω_{CC2}^b	$\Delta\omega^c$	$\Delta\omega_l^d$	$\Delta\omega_l^{de}$
N-acetylglycine	S_1	$n \rightarrow \pi^*$	5.767	5.732	-0.035	-0.023	0.011
	S_2	$n \rightarrow \pi^*$	6.073	6.089	0.016	0.000	0.026
	S_3	$\pi \rightarrow \text{Rydb.}$	6.552	6.275	-0.277	0.021	0.050
Propanamide	S_1	$n \rightarrow \pi^*$	5.703	5.657	-0.046	0.010	0.038
	S_2	$\pi \rightarrow \text{Rydb.}$	6.483	6.267	-0.216	0.034	0.050
"Dipeptide"	S_1	$n \rightarrow \pi^*$	5.791	5.743	-0.048	-0.012	0.021
	S_2	$\pi \rightarrow \text{Rydb.}$	6.205	5.926	-0.279	0.018	0.053
	S_3	$n \rightarrow \pi^*$	6.003	5.953	-0.050	0.026	0.038
<i>trans</i> -urocanic acid	S_1	$n \rightarrow \pi^*$	5.134	4.863	-0.271	-0.029	0.009
	S_2	$\pi \rightarrow \pi^*$	5.108	4.931	-0.177	-0.019	0.021
	S_3	$\pi \rightarrow \text{Rydb.}$		5.285		0.058	0.069
Guanine	S_4	$\pi \rightarrow \text{Rydb.}$	6.093	6.009	-0.084	0.025	0.043
	S_1	$\pi \rightarrow \text{Rydb.}$	4.946	4.743	-0.203	0.076	0.097
	S_2	$\pi \rightarrow \pi^*$	5.138	5.022	-0.116	-0.020	0.021
	S_3	$\pi \rightarrow \text{Rydb.}$		5.137		0.073	0.091
	S_4	$\pi \rightarrow \pi^*$		5.409		0.009	0.044
	S_5	$n \rightarrow \pi^*$		5.461		-0.023	0.016
1-phenylpyrrole	S_6	$\pi \rightarrow \text{Rydb.}$	5.639	5.669	0.030	0.080	0.106
	S_1	$\pi \rightarrow \pi^*$	4.938	4.921	-0.017	0.023	0.052
	S_2	$\pi \rightarrow \pi^*$	5.488	5.309		0.011	0.054
	S_3	$\pi \rightarrow \text{Rydb.}$		5.434		0.008	0.032
	S_4	CT (py \rightarrow ph)		5.489		-0.004	0.034
	S_5	$\pi \rightarrow \text{Rydb.}$	5.721	5.493	-0.228	0.052	0.074

a) canonical EOM-CCSD excitation energies from Ref. 44 (when available)

b) canonical CC2 excitation energies calculated with TURBOMOLE v. 5.7, Ref. 27,29

c) deviation canonical CC2 vs. canonical EOM-CCSD

d) deviation local CC2 vs. canonical CC2

e) unified pair lists and domains

Table 2.5: Excitation energies for various test molecules. Values (all in eV) are given for canonical EOM-CCSD, CC2, local CC2. The aug-cc-pVDZ basis was used. The pair list was specified as $\forall(ij), (im) \leq 5, (mn) \leq 5$ and results for unified pair lists and domains are also given. The Boughton-Pulay criterion for domain construction and the criterion κ_e to determine important orbitals were set to 0.985 and 0.9975, respectively.

For these particular settings additional calculations employing unified pair lists and domains were performed. For that purpose, the pair lists and domains of unperturbed (ground state) and perturbed (excited state) amplitudes are merged *a posteriori* to a common pair list and common do-

mains. In the process of this unification the configuration space for the ground state becomes significantly larger, while the configuration space for the excited state is hardly affected, which leads to some imbalance in the descriptions of ground and excited state, respectively, such that the resulting excitation energies for unified pair lists and domains are always blue-shifted relative to the canonical or the ordinary local value. This imbalance is most notable in the cc-pVDZ basis and decreases on going to a bigger basis set or on extending the domains. For calculations using the aug-cc-pVDZ basis or the cc-pVDZ basis with extended domains (domains extended by centers ≤ 3 bohrs away from the core Boughton-Pulay domains are sufficiently large) the deviations between unified domain/pair list and ordinary local calculations become quite small (typically something like 0.03 eV). Based on these observations we conclude (i) that the main difference between ordinary local excitation energies and excitation energies computed with unified pair list and domains is primarily due to the imbalance in the local approximation for ground- and the excited states, and (ii) that the error introduced by employing non-identical spaces for zeroth- and first-order amplitudes therefore is small. Although the diagonalization of the LCC2 Jacobian in a calculation with unified pair lists and domains is not dramatically more expensive than in the ordinary local calculation, the ground state calculation is more expensive and needs to be re-computed for each excited state. Therefore, ordinary local calculations with different domains for ground- and excited state are more convenient and appear to be preferable for most cases.

In order to study the accuracy of the new local CC2 method in describing charge transfer excited states we performed calculations on the two phenothiazine-isoalloxazine (flavin) dyads depicted in Fig. 2.2. These dyads are of interest in the context of modeling light processes of blue-light photo-receptors [70]. DA2 corresponds to compound 5 of Ref. 70. DA1 is a simplified version of DA2 insofar that the side chain on the phenothiazine and the methyl group on the flavin ring system are omitted, such that a canonical reference calculation still is possible within an acceptable amount of time (the canonical calculation takes about 60–70 CPU minutes per state and per Davidson iteration). DA2 comprises 220 active electrons and 77 atoms, DA1 – 172 active electrons and 53 atoms. These dyads feature a rather long-range charge transfer $S_3 \leftarrow S_0$ excitation where phenothiazine acts as an electron donor and isoalloxazine as an acceptor (the role of the intermediate phenyl ring is that of a spacer). TD-DFT fails spectacularly here with deviations from the CC2 excitation energy as large as 2.55 (BP86) and 1.69 eV (B3-LYP) for the DA1 case (all TD-DFT calculations were performed with TURBOMOLE v. 5.7 [71] by using the SVP

DA1, 53 atoms, 172 electrons							
pair list	state	ω	Memory ^a	$t(W_{ia}^P)^b$	$t(v_a^i)^c$	$t(\mathfrak{S}_{ab}^{ij})^d$	$t(\text{Iter})^e$
$\forall(ij), \forall(im), (mn) \leq 10$	S ₁	3.159 (-0.031)	1061	1050(1103)	1258(1580)	867(895)	2449(2896)
	S ₂	3.373 (-0.039)	843	1217(1290)	1464(1837)	815(854)	2564(3115)
	S ₃	3.549 (0.036)	1558	1590(1666)	1805(2148)	1111(1159)	3424(4072)
$\forall(ij), (im) \leq 10, (mn) \leq 10$	S ₁	3.160 (-0.031)	945	953(1017)	1155(1490)	650(677)	2102(2643)
	S ₂	3.374 (-0.038)	642	621(688)	814(1165)	478(505)	1496(1979)
	S ₃	3.550 (0.036)	1474	1360(1429)	1578(1930)	1056(1098)	3127(3749)
$\forall(ij), (im) \leq 5, (mn) \leq 5$	S ₁	3.166 (-0.024)	813	957(1017)	1157(1474)	615(642)	2031(2466)
	S ₂	3.380 (-0.032)	557	644(707)	841(1173)	457(479)	1481(1904)
	S ₃	3.557 (0.044)	1221	1489(1553)	1704(2029)	957(990)	3092(3627)
$\forall(ij), (im) \leq 3, (mn) \leq 3$	S ₁	3.183 (-0.007)	753	910(959)	1128(1421)	561(582)	1945(2351)
	S ₂	3.412 (-0.000)	485	590(645)	793(1109)	407(428)	1373(1766)
	S ₃	3.565 (0.052)	1139	1043(1093)	1255(1557)	771(800)	2408(2836)
DA2, 77 atoms, 220 electrons							
pair list	state	ω	Memory ^a	$t(W_{ia}^P)^b$	$t(v_a^i)^c$	$t(\mathfrak{S}_{ab}^{ij})^d$	$t(\text{Iter})^e$
$\forall(ij), (im) \leq 10, (mn) \leq 10$	S ₁	3.142	771	946(1031)	1422(2016)	723(766)	2381(3124)
	S ₂	3.348	357	420(469)	839(1380)	328(351)	1240(1837)
	S ₃	3.686	1739	2062(2186)	2571(3204)	1563(1640)	4660(5700)
$\forall(ij), (im) \leq 5, (mn) \leq 5$	S ₁	3.148	638	780(840)	1239(1787)	581(617)	2019(2669)
	S ₂	3.355	294	336(363)	738(1220)	258(279)	1058(1595)
	S ₃	3.707	1232	1450(1544)	1933(2515)	1119(1173)	3437(4262)
triad, 127 atoms, 370 electrons							
pair list	state	ω	Memory ^a	$t(W_{ia}^P)^b$	$t(v_a^i)^c$	$t(\mathfrak{S}_{ab}^{ij})^d$	$t(\text{Iter})^e$
$\forall(ij), (im) \leq 5, (mn) \leq 5$	S ₁	3.038	2713	5121(5736)	10769(14404)	1854(1939)	13571(18000)
	S ₃	3.354	391	680(888)	4233(6907)	364(400)	4678(7460)
	S ₄	3.529	1562	2811(3114)	7469(10436)	1111(1173)	9059(12488)
	S ₅	3.716	202	359(468)	4280(6678)	231(262)	4554(7008)

a) Memory (in MBytes) for trial vector

b) CPU(elapsed) time for calculation of W_{ia}^P , eq. (2.22)c) overall CPU(elapsed) time for calculation of v_a^i , eq. (2.20)d) overall CPU(elapsed) time for calculation of \mathfrak{S}_{ab}^{ij} , eq. (2.21)

e) total CPU(elapsed) time for one Davidson iteration

Table 2.6: LCC2 excitation energies and used computational resources for the three lowest excited states of two phenothiazine-isoalloxazine dyads and four low-lying excited states of the phenothiazine-isoalloxazine-pyrene triad, as displayed in Fig. 2.2. All energy values are given in eV, deviations from the related canonical values are given in parenthesis. The corresponding memory requirements for one trial vector and the CPU (in parenthesis: elapsed) times in seconds on a dedicated node for different key steps of the calculation are also given. The details of calculations are the same as in Table 2.4. The cc-pVDZ basis was used for all calculations. The pair list for the ground-state amplitudes was truncated for inter-orbital distances beyond 10 bohr. The Boughton-Pulay criterion for domain construction and the criterion κ_e to determine important orbitals were set to 0.985 and 0.995, respectively. The 1s orbitals for the C, N, and O atoms and 1s, 2s, and 2p orbitals for the S atom were frozen in all correlated calculations.

basis set [72]). Table 2.6 compiles the LCC2 excitation energies and the deviations from the canonical reference calculation in the case of DA1 for the lowest three states of these dyads. $S_1 \leftarrow S_0$ and $S_2 \leftarrow S_0$ both are excitations primarily located within the isoalloxazine subunit. For the local calculations again different specifications for the excited-state amplitude pair list were employed. The observed local errors (including the ones of the charge transfer excitation) are again smaller than 0.04 eV (for the shortest pair list the local error connected to the charge transfer excitation rises to about 0.05 eV). The addition of the methyl group and the side chain to DA1 primarily affects the $S_3 \leftarrow S_0$ charge transfer excitation, shifting it by 0.138 (LCC2) and 0.113 eV (TD-DFT/B3-LYP) to the blue, while the two lower excitations are hardly affected (redshifts by ≈ 0.02 eV predicted by both LCC2 and TD-DFT/B3-LYP). TD-DFT appears to pick up these shifts rather well, even though the absolute value of the excitation energy is spectacularly wrong.

When studying the CT states with CC2 (conventional or local), one should keep in mind that in principle the CC2 method (and even the more accurate EOM-CCSD) does not fulfill the so-called generalized size-extensivity (see Ref. 73) for this type of excitations. This property requires that for the case of a charge transfer from one non-interacting subsystem to another the energy is the sum of the IP and EA energies of the respective subsystems. As explained by Dreuw and Head-Gordon [74], the origin of the large errors for CT states for the TD-DFT method is due to the inherent self-interaction error caused by exchange-correlation functionals lacking exact exchange. For valence states the self-interaction error cancels to a large extent, what explains successes of TD-DFT in describing this kind of excited states. Yet if the number of electrons is different in individual subsystems, no cancellation occurs anymore. The generalized size-extensivity error for EOM-CCSD or CC2, on the other hand, is expected to be much smaller. As analyzed in the work of Meissner and Bartlett for the EOM-CCSD case, the generalized size-extensivity is violated by terms of third Møller-Plesset order in the EOM-CCSD amplitude equations [75]. The available numerical experience is mostly based on smaller molecules and shows that the expected errors of CC2 are much smaller than those of TD-DFT. For instance, good agreement between experiment and CC2 (errors < 0.1 eV) was reported [76] for two CT states of *cis*-azobenzene, while the TD-DFT results deviate by more than 1 eV from the experiment. Very recently Barbarella *et al.* [77] measured and calculated the excitation energy of several larger molecules, among them the excitation energy of one CT state of the amide-bound bithiophene molecule. In this case the agreement of CC2 and experiment was not so good (an error of 0.4 eV was reported),

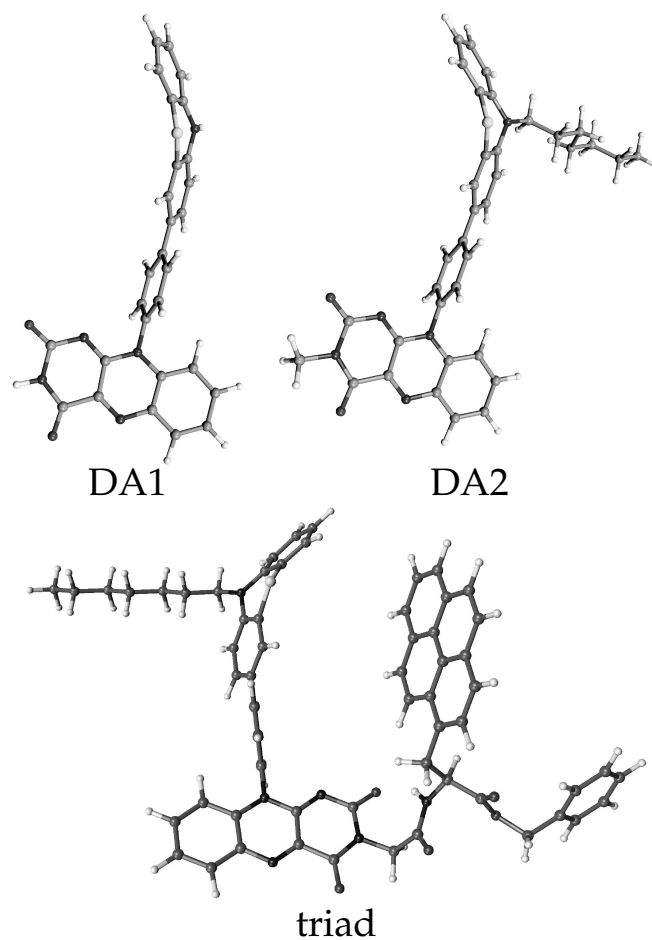


Figure 2.2: Structures of the phenothiazine-isoalloxazine (flavin) electron donor-acceptor dye-dyads and the related triad involving pyrene in addition, as synthesized and characterized in Ref. 70. All structures were optimized at the DFT/BP86 level by using the SVP basis set [72]. DA2: compound 5 of Ref. 70. DA1: compound 5 without the methyl group on the flavin – and without the side chain on the phenothiazine subsystem. Triad: compound 6 of Ref. 70.

but it should be noted that the authors of Ref. 77 did not use diffuse functions in their calculations, while it is known that these functions usually lower the excitation energy of such states by few tenths of eV. Nevertheless, it cannot definitely be ruled out at the present stage, that long-range charge transfer states in extended molecules will be hampered by a non-negligible size-extensivity error. Possibly, STEOM theory [78,79], which apparently fulfills generalized size-extensivity, might constitute a rigorous and viable platform to devise a local method for excited states in extended molecular systems.

Apart from two dye-dyads also the excitation energies of four low-lying excited states of a dye-triad (compound 6 of Ref. 70) were computed. In this triad DA2 is augmented by a pyrene system acting as an antenna and energy transfer from the pyrene to the flavin subunit subsequent to a local excitation of the pyrene system is postulated [70]. The triad system comprises 127 atoms and 370 correlated electrons and the purpose of the test calculations on this system at the present stage is to show that such calculations are possible, i.e., to demonstrate the computational efficiency of the new program. A detailed study of the photophysical behavior of the dyads DA1, DA2 and the triad can be found in Ref. 11. Table 2.6 compiles CPU times for individual key steps of the calculation, all measured on AMD 252 OPTERONS in a dedicated node. The individually most expensive step is the calculation of the W_{ia}^P intermediate, followed by the assembly of G_{ab}^{ij} in eq. (2.22), which both together dominate the calculation of v_a^i . The cost for computing \mathfrak{B}_{ab}^{ij} , on the other hand, is rather small. Evidently, the computational cost depends heavily on the type of excitation and can change significantly for different excited states of the same molecule. The $S_3 \leftarrow S_0$ charge transfer states of the dyads, which naturally involve more important LMOs and hence bigger domains and longer pair lists, are more than twice as expensive as the corresponding more local $S_2 \leftarrow S_0$ excitations. On going from the DA1 to the bigger DA2 molecule the computational cost for the canonical method are expected to increase by about a factor of 3.4 (based on its $O(N^5)$ scaling). For the local method, on the other hand, factors of 1.1, 0.9, and 1.4 are observed for the three excitations, respectively, the $S_2 \leftarrow S_0$ excitation becomes even cheaper for DA2, since the additional methyl group on the isoalloxazine moiety apparently increases the locality of this excitation. The $S_1 \leftarrow S_0$ excitation of the triad is a (de-localized) superposition of the two local excitations within pyrene and isoalloxazine, respectively, hence leading to comparatively large pair domains. Nevertheless, as Table 2.2 clearly shows, still less than 2% of the number of first-order (i.e. excited state) doubles in the canonical CC2

response calculation need to be considered, with one Davidson iteration within the local scheme taking about 4 CPU hours. The $S_3 \leftarrow S_0$ and $S_5 \leftarrow S_0$ excitations on the other hand both are localized within the isoalloxazine and the pyrene subunits, respectively, with the former corresponding to the $S_2 \leftarrow S_0$ excitation of DA1 or DA2. Naturally, for these excitations the required domains and pair lists are smaller and the calculation is less expensive, taking between 1 and 1.5 CPU hours per Davidson iteration. Here, the CPU time for calculating the W_{ia}^P intermediate already becomes comparatively small and the diagrams involving the un-truncated singles vectors start to dominate the computational cost. The $S_4 \leftarrow S_0$ excitation of the triad finally represents the charge transfer excitation corresponding to $S_3 \leftarrow S_0$ of the dyads. Presumably, the triad system represents the largest system so far, for which electronic excitation energies have been treated at a level beyond TD-DFT.

2.4 Conclusions

A new *ab initio* approach for the calculation of excitation energies in extended molecular systems is presented. The new method is based on the CC2 model introduced by Christiansen and coworkers [21], which was modified by introducing the local approximations to the doubles amplitudes. Quite in the spirit of the original CC2 ansatz, the singles in our approach are treated non-locally. Uniform selection criteria, leading to small errors in excitation energies have been proposed. Pair list and domains for the perturbed amplitudes are generated by analysis of an initial CIS wave function, as proposed before in Ref. 44 in the context of local EOM-CCSD. However, in contrast to the former method, considerably longer pair lists are affordable here, making the new method more robust with respect to the quality of the initial CIS description of the excitation. A modified LCC2-b model, where the single excitations are rigorously kept to all orders also in the doubles equations, has also been tested. As expected, the deviations in excitation energies relative to the original CC2 model turn out to be small for all cases considered so far. The deviations of the LCC2 excitation energies from the canonical reference values do not exceed 0.05 eV for states (also charge transfer) which are not too high in energy (and for which the CC2 description is still meaningful anyhow). The obtained results should be considered as an excellent justification of the new method, since (i) the anticipated error of the CC2 method itself is about 0.3 eV for such states, and (ii) that effects like the basis set superposition error (virtually absent in local methods [69]) also play a role.

The LCC2 method could also be used in the context of a hybrid scheme together with LCCSD or CC3, with very short pair lists of only the most important pairs for the latter, in analogy to related hybrid schemes like LCCSD(T)|LMP2 for local ground state calculations.

For reasons of efficiency the Density-Fitting approximation was employed for all ERIs in our program, which leads to very efficient algorithms, especially in combination with local methods. With the present code it is certainly possible to compute excitation energies for molecular systems well beyond 100 atoms in a basis set of polarized double zeta quality, i.e., systems only accessible for TD-DFT so far.

Chapter 3

Properties of excited states

3.1 Introduction

In this chapter we present a method for calculating transition strengths and first-order properties of excited states in the framework of local CC2 linear response theory. With the new program it is possible to compute these quantities for molecular systems of the size of 150 atoms or more. As in the implementation of DF-LCC2 for calculating of excitation energies (Chp. 2, [10]), the DF approximation for ERIs, instrumental for an efficient program, is rigorously employed. In the next section we briefly discuss the underlying theory and present the resulting working equations. Accuracy and efficiency of the new method are demonstrated in section 3.3, where the results of calculations for a series of different molecules, excited states, basis sets, and various settings specifying pair lists and domains are discussed. A summary of the presented work and concluding remarks are provided in section 3.4.

3.2 Theory

In this section we will derive working expressions for transition strengths and first-order properties of excited states for local CC2 theory based on density fitting (DF-LCC2). The underlying general Coupled Cluster response theory based on a time-averaged quasi-energy Lagrangian and Fourier component variational perturbation theory has been extensively discussed by Christiansen *et al.* in Ref. 20 and is not repeated here. We will just give the few general equations which form a starting point of our derivation of the local formalism. We preserve the naming conventions for auxiliary quantities, since it is used extensively in the CC response pa-

pers. (Note parenthetically that one should be careful not to mix various quantities, denoted in those papers by the same letters.) The first-order responses of the cluster amplitudes $t^X(\omega_X)$ and related Lagrange multipliers $\lambda^X(\omega_X)$ subject to the periodic perturbation $\epsilon_X(\omega_X) \exp(-i\omega_X t)X$ (X symbolizes a time-independent perturbing operator and $\epsilon_X(\omega_X)$ – its strength at frequency ω_X) are determined by the equations

$$0 = (\mathbf{A} - \omega_X \mathbf{M}) t^X(\omega_X) + \xi^X, \quad (3.1)$$

$$0 = \lambda^X(\omega_X) (\mathbf{A} + \omega_X \mathbf{M}) + \eta^X + \mathbf{F} t^X(\omega_X), \quad (3.2)$$

where \mathbf{M} is the appropriate metric and the quantities \mathbf{A} , ξ^X , η^X , \mathbf{F} are mixed derivatives of the time-averaged second-order Lagrangian $\{L^{(2)}\}_T$ with respect to first-order amplitudes, multipliers, and perturbation strengths, taken at zero field strength, i.e.,

$$(\mathbf{A} - \omega_X \mathbf{M})_{\mu_i \nu_j} = \frac{\partial^2 \{L^{(2)}\}_T}{\partial \lambda_{\mu_i}^{(1)}(-\omega_X) \partial t_{\nu_j}^{(1)}(\omega_X)}, \quad (3.3)$$

$$\xi_{\mu_i}^X = \frac{\partial^2 \{L^{(2)}\}_T}{\partial \lambda_{\mu_i}^{(1)}(-\omega_X) \partial \epsilon_X(\omega_X)}, \quad (3.4)$$

$$\eta_{\mu_i}^X = \frac{\partial^2 \{L^{(2)}\}_T}{\partial t_{\mu_i}^{(1)}(-\omega_X) \partial \epsilon_X(\omega_X)}, \quad (3.5)$$

$$(\mathbf{F})_{\mu_i \nu_j} = \frac{\partial^2 \{L^{(2)}\}_T}{\partial t_{\mu_i}^{(1)}(-\omega_X) \partial t_{\nu_j}^{(1)}(\omega_X)}. \quad (3.6)$$

For the CC2 Lagrangian $\{L^{(2)}\}_T$ one obtains for these vectors and matrices

$$\mathbf{A} = \begin{pmatrix} \langle \tilde{\mu}_1 | [\hat{H}, \tau_{v_1}] + [[\hat{H}, \tau_{v_1}], T_2] | 0 \rangle & \langle \tilde{\mu}_1 | [\hat{H}, \tau_{v_2}] | 0 \rangle \\ \langle \tilde{\mu}_2 | [\hat{H}, \tau_{v_1}] + [[\hat{V}, \tau_{v_1}], T_2] | 0 \rangle & \langle \tilde{\mu}_2 | [F + \hat{V}, \tau_{v_2}] | 0 \rangle \end{pmatrix}, \quad (3.7)$$

$$\xi^X = \begin{pmatrix} \langle \tilde{\mu}_1 | \hat{X} + [\hat{X}, T_2] | 0 \rangle \\ \langle \tilde{\mu}_2 | \hat{X} + [\hat{X}, T_2] | 0 \rangle \end{pmatrix}, \quad (3.8)$$

$$\eta^X = \left(\begin{array}{c} \langle 0 | [\hat{X}, \tau_{\mu_1}] | 0 \rangle + \sum_{iv_1} \lambda_{v_1} \langle \tilde{v}_1 | [\hat{X}, \tau_{\mu_1}] | 0 \rangle + \sum_{v_2} \lambda_{v_2} \langle \tilde{v}_2 | [[\hat{X}, \tau_{\mu_1}], T_2] | 0 \rangle \\ \sum_{iv_1} \lambda_{v_1} \langle \tilde{v}_1 | [\hat{X}, \tau_{\mu_2}] | 0 \rangle \end{array} \right), \quad (3.9)$$

$$\mathbf{F} = \left(\begin{array}{cc} \left(\langle 0 | + \sum_{i\rho_i} \lambda_{\rho_i} \langle \tilde{\rho}_i | \right) [[\hat{H}, \tau_{\mu_1}], \tau_{v_1}] | 0 \rangle & \sum_{i\rho_i} \lambda_{\rho_i} \langle \tilde{\rho}_i | [[\hat{H}\delta_{i1} + \hat{V}\delta_{i2}, \tau_{\mu_1}], \tau_{v_2}] | 0 \rangle \\ \sum_{i\rho_i} \lambda_{\rho_i} \langle \tilde{\rho}_i | [[\hat{H}\delta_{i1} + \hat{V}\delta_{i2}, \tau_{\mu_2}], \tau_{v_1}] | 0 \rangle & 0 \end{array} \right), \quad (3.10)$$

where τ_{μ_i} is the covariant excitation operator, $\tilde{\mu}_i$ are the contravariant configuration functions, λ_{μ_i} are the zeroth-order multipliers, and i is the related excitation class ($i = 1$ or 2 for CC2). T_2 is the usual doubles cluster operator and V a frequency-independent external perturbation operator already included in H . Operators H, F, V , and X decorated with a hat are similarity-transformed with $\exp(T_1)$ (for a definition of \hat{F} see Ref. 80). For all integrals in this paper (*vide infra*) we use the convention that the first (second) index refers to the outgoing (incoming) line relative to the interaction vertex, implying that the first index corresponds either to an annihilator of a hole or a creator of a particle state. Note that only quasiparticle creators are dressed [10].

Whenever the frequency $\pm\omega_X$ of the frequency-dependent external perturbation approaches the electronic excitation energy ω^f of an excited state (numbered f), the linear response described by eqs. (3.1,3.2) exhibits a pole. This immediately leads to the eigenvalue equations for the electronic excitation energies and the related left and right excited state amplitudes

$$\mathbf{A}\mathbf{R}^f = \omega^f \mathbf{M}\mathbf{R}^f, \quad L^f \mathbf{A} = \omega^f L^f \mathbf{M}, \quad (3.11)$$

involving the non-symmetric Jacobian \mathbf{A} . Working equations for solving the right eigenvalue problem in the context of DF-LCC2 have been presented in the previous chapter 2 [10]. In order to compute transition strengths and properties of excited states the left eigenvector is needed, too. Explicit expressions for the vector $v \doteq u\mathbf{A}$ (the left transform of the Jacobian) in terms of integrals and amplitudes are readily obtained from eq. (3.7) by virtue of diagrammatic techniques. The DF approximation is invoked for all ERIs in order to reduce the computational cost, i.e. all ERIs are represented as,

$$(pq|\hat{r}s) = (pq|\hat{P})\hat{c}_{rs}^P, \quad \text{with} \quad \hat{c}_{rs}^Q(Q|P) = (P|\hat{r}s), \quad (3.12)$$

where $(P|Q)$ and $(P|\hat{P}s)$ denote the two-index and dressed three-index ERIs, respectively. Summation over repeated indices (Einstein convention) is used here and throughout this chapter.

The working equations for the left transform of the Jacobian are then obtained as

$$\begin{aligned}
 v_a^i = & \tilde{u}_c^i \hat{f}_{ca} - S_{aa'} \tilde{u}_{a'}^k \hat{f}_{ik} - \hat{B}_P^{ka} \hat{c}_{ik}^P + 2c_{ia}^P \hat{b}_P - \\
 & - (P|ka) c_{id}^P \tilde{u}_{c'}^l S_{c'c} \tilde{T}_{cd}^{lk} + \\
 & + \left((2(P|ia) \tilde{u}_{c'}^k - (P|ka) \tilde{u}_{c'}^i) S_{c'c} - S_{aa'} \tilde{u}_{a'}^k (P|ic) \right) V_{kc}^P + \\
 & + 2(P|ca) \hat{W}_{ic}^P - 2S_{aa'} \hat{W}_{ka'}^P (P|ik)
 \end{aligned} \tag{3.13}$$

for the singles, and

$$\begin{aligned}
 \mathfrak{B}_{ab}^{ij} = & \hat{G}_{ab}^{ij} + \hat{G}_{ba}^{ji} - \frac{1}{2} (\hat{G}_{ba}^{ij} + \hat{G}_{ab}^{ji}) + \\
 & + S_{aa'} (\tilde{u}_{a'}^i \hat{f}_{jb} - \frac{1}{2} \tilde{u}_{a'}^j \hat{f}_{ib}) + (\hat{f}_{ia} \tilde{u}_{b'}^j - \frac{1}{2} \hat{f}_{ja} \tilde{u}_{b'}^i) S_{b'b} + \\
 & + f_{ca} \tilde{U}_{cb'}^{ij} S_{b'b} + S_{aa'} \tilde{U}_{a'c}^{ij} f_{cb} - \\
 & - S_{aa'} (\tilde{U}_{a'b'}^{ik} f_{jk} + f_{ik} \tilde{U}_{a'b'}^{kj}) S_{b'b}
 \end{aligned} \tag{3.14}$$

for the doubles part of the v vector. In eqs. (3.13,3.14) the intermediates

$$\begin{aligned}
 \hat{B}_P^{ia} & \doteq (P|ca) \tilde{u}_c^i, \quad \hat{b}_P = (P|ck) \tilde{u}_c^k, \\
 V_{ia}^P & \doteq \tilde{T}_{ac}^{ik} c_{kc}^P, \quad \hat{W}_{ia}^P \doteq \tilde{U}_{ac}^{ik} \hat{c}_{ck}^P, \\
 \hat{G}_{ab}^{ij} & \doteq (\tilde{u}_c^i (P|ca) - \tilde{u}_{a'}^k S_{a'a} (P|ik)) c_{jb}^P,
 \end{aligned} \tag{3.15}$$

were used. The symbols t_a^i , T_{ab}^{ij} and u_a^i , U_{ab}^{ij} denote the LCC2 ground state and trial vector amplitudes, respectively. All “contravariant” amplitudes [40] are denoted by a tilde, i.e.,

$$\tilde{t}_a^i \doteq 2t_{a'}^i, \quad \tilde{T}_{ab}^{ij} \doteq 2T_{ab}^{ij} - T_{ab}^{ji}. \tag{3.16}$$

Dressed integrals and quantities containing dressed integrals are decorated by a hat. Furthermore, we denote occupied orbitals by indices i, j, k, \dots , virtual orbitals (in our case: PAOs) by a, b, c, \dots , general orbitals by p, q, \dots , and auxiliary fitting functions by P, Q . S is the usual PAO overlap matrix. Note that the dressed Fock matrix is formed from dressed ERIs as a consequence of the similarity transform [81], i.e.,

$$\hat{f}_{pq} = \hat{h}_{pq} + 2(kk|pq) - (pk|kq), \tag{3.17}$$

hence \hat{f}_{ia} is non-zero even though both indices refer to quasiparticle annihilators.

As described in the previous chapter 2 [10], the doubles parts of the left and right eigenvectors L^f and R^f are restricted to excited state domains determined by analysis of an initial CIS wavefunction, while the doubles parts of the CC2 ground state amplitudes T_{ab}^{ij} (and multipliers Λ_{ab}^{ij} , *vide infra*) are restricted to the usual domains employed in local correlation methods for electronic ground states. In the context of this work we implemented an optional extension of the Boughton-Pulay orbital domains [56], where the basic building blocks of ground- and excited-state domains rest upon the solutions of the Coupled Perturbed Localization (CPL) and Coupled Perturbed Hartree-Fock (CPHF) equations. It turns out that the use of these extended domains leads to improved results for properties. This issue is discussed in detail in section 3.2.3. The singles parts of all vectors remain untruncated.

3.2.1 Transition strengths

The transition strength of an electronic one-photon excitation $f \leftarrow 0$ is obtained in the context of CC response theory as the related residual of the linear response function. As discussed in Ref. 20, one obtains for the transition strength (where X and Y are perturbing operators, e.g. dipole field operators),

$$S_{XY}^{0f} = \frac{1}{2} \left(M_X^{0f} M_Y^{f0} + (M_Y^{0f} M_X^{f0})^* \right), \quad (3.18)$$

with the left and right transition moments given as

$$M_X^{0f} = \eta^X R^f + \bar{M}^f(\omega_f) \xi^X, \quad M_X^{f0} = L^f \xi^X, \quad (3.19)$$

where ξ^X and η^X are defined in eqs. (3.4,3.8) and (3.5,3.9), respectively, and the multipliers $\bar{M}^f(\omega_f)$ are obtained by solving the system of linear equations,

$$0 = \bar{M}^f(\omega_f) (\mathbf{A} + \omega_f \mathbf{M}) + \mathbf{F} R^f. \quad (3.20)$$

In order to solve eq. (3.20) the left transform of the Jacobian is needed, hence the explicit eqs. (3.13,3.14) can be reused. The doubles part of the $\bar{M}^f(\omega_f)$ vector is restricted to the same excited state domains as R^f and L^f . The right-hand side (rhs) of eq. (3.20) involves the right transform of the matrix \mathbf{F} defined in eqs. (3.6,3.10) with the right eigenvector R^f of the Jacobian. Note that the vector $\mathbf{F} R^f$ is covariant.

A further ingredient occurring in the vector η^X and matrix \mathbf{F} are the (contravariant) ground state multipliers λ . These are obtained by solving the system of linear equations,

$$0 = \lambda \mathbf{A} + \eta, \quad (3.21)$$

with the rhs η being defined as

$$\eta_{\mu_i} = \left(\begin{array}{c} \langle 0 | [\hat{H}, \tau_{\mu_1}] | 0 \rangle \\ \langle 0 | [\hat{H}, \tau_{\mu_2}] | 0 \rangle \end{array} \right) = \left(\begin{array}{c} 2\hat{f}_{ia} \\ 2K_{ab}^{ij} - K_{ab}^{ji} \end{array} \right), \quad (3.22)$$

where $K_{ab}^{ij} = (ia|jb)$ denote the usual bare exchange ERIs, obtained in the DF context according to eq. (3.12). Again the left transform of the Jacobian, thus eqs. (3.13,3.14), are needed for solving eq. (3.21), although this time λ_{μ_2} , η_{μ_2} and $\mathbf{A}_{\mu_2\nu_i}$, $\mathbf{A}_{\mu_i\nu_2}$ are restricted to the *ground state domains*.

Working equations for the right product \mathbf{FR}^f in eq. (3.20) are obtained from eq. (3.10) again by applying diagrammatic techniques, yielding

$$\begin{aligned} (\mathbf{FR})_a^i &= 4\check{c}_P(P|ia) - 2\check{C}_P^{ik}(ka|P) - (\check{y}_{ik}\hat{f}_{ka} + \hat{f}_{ic}R_c^k\tilde{\lambda}_{a'}^k S_{a'a}) - \\ &\quad - S_{aa'}\tilde{\lambda}_{a'}^k (2(ik|\hat{P})\check{c}_P - (lk|\hat{P})\check{C}_P^{il}) + \\ &\quad + 2R_d^k\hat{B}_P^{kd}c_{ia}^P - \hat{B}_P^{ka}\check{C}_P^{ik} + 2\hat{B}_P^{ia}\check{c}_P - R_c^k\hat{B}_P^{ic}c_{ka}^P - \\ &\quad - 2(\hat{V}_{ic}^P S_{c'c}(ka|P) + S_{aa'}\hat{V}_{ka'}^P(ic|P))R_c^k - 2S_{aa'}\hat{W}_{ka'}^P(ik|\hat{P}) + 2\hat{W}_{ic}^P(ca|\hat{P}) + \\ &\quad + \check{x}_c^k(2c_{kc}^P(P|ia) - c_{ka}^P(P|ic)) - \check{y}_{kl}(2\hat{c}_{lk}^P(ia|P) - \hat{c}_{ik}^P(la|P)) \\ &\quad - \check{V}_{kc}^P(S_{cc'}\tilde{\lambda}_{c'}^i(P|ka) + S_{aa'}\tilde{\lambda}_{a'}^k(P|ic)), \end{aligned} \quad (3.23)$$

$$(\mathbf{FR})_{ab}^{ij} = \frac{1}{2}(\tilde{X}_{ab}^{ij} + \tilde{X}_{ba}^{ji} + \tilde{Y}_{ab}^{ij} + \tilde{Y}_{ba}^{ji}), \quad (3.24)$$

where we have introduced the following intermediates

$$\begin{aligned} \check{C}_P^{ij} &\doteq c_{ic}^P R_c^j, \quad \check{c}_P \doteq c_{kc}^P R_c^k, \\ \hat{B}_P^{ia} &\doteq \tilde{\lambda}_c^i(ca|\hat{P}), \\ \hat{V}_{ia}^P &\doteq \tilde{\Lambda}_{ac}^{ik}\hat{c}_{ck}^P, \quad \check{V}_{ia}^P \doteq \tilde{R}_{ac}^{ik}c_{kc}^P, \\ \hat{W}_{ia}^P &\doteq \tilde{\Lambda}_{ac}^{ik}(\hat{c}_{cd}^P R_d^k - S_{cc'}R_{c'}^l\hat{c}_{lk}^P), \\ \check{x}_a^i &\doteq \tilde{\lambda}_c^k S_{cc'}\tilde{R}_{ac}^{ik}, \quad \check{y}_{ij} \doteq \tilde{\lambda}_c^i S_{cc'}R_{c'}^j, \\ X_{ab}^{ij} &\doteq -(ka|P)(\check{y}_{ik}\hat{c}_{jb}^P + \check{C}_P^{ik}\tilde{\lambda}_{b'}^j S_{b'b}), \\ Y_{ab}^{ij} &\doteq (ia|P)(2\check{c}_P\tilde{\lambda}_{b'}^j - \check{C}_P^{jk}\tilde{\lambda}_{b'}^k)S_{b'b}. \end{aligned} \quad (3.25)$$

In eqs. (3.23–3.25) we have dropped the index f enumerating individual excited states. Quantities involving the right eigenvector R and the ground-state multipliers λ are decorated by a breve and a bar, respectively. For quantities decorated by a tilde eq. (3.16) applies. Note that the quantity \hat{c}_{ab}^P occurring in the definition of \hat{W}_{ia}^P is never constructed explicitly. Instead, the equation for the fitting coefficients is solved for a modified rhs of $(ab|\hat{P})R_b^i - (ki|\hat{P})S_{aa'}R_{a'}^k$.

An alternative way to compute the right product \mathbf{FR}^f is via introduction of the trial-vector transformed Hamiltonian $\hat{H}' = [\hat{H}, R_{\mu_1}]$, which leads to equations very similar to those of the left transform of the Jacobian with the ground-state multipliers λ , yet with modified integrals [28,81,82]. This has the important advantage that the routines for the left transform of the Jacobian could be reused by just feeding them with these modified integrals. However, since the modified ERIs are formed as the sum of four differently transformed sets of ERIs [81], the DF approximation in eq. (3.12) cannot be applied straightforwardly to the modified ERIs themselves. Moreover, a second set of modified two-external three-index integrals, which occur in eqs. (3.13–3.15), has to be generated. Therefore we decided to implement the diagrams of the \mathbf{FR}^f product *directly*, i.e., without introducing \hat{H}' as in previous implementations, thus avoiding these disadvantages at the price of additional coding.

After the eigenvectors L^f , R^f and multipliers $\bar{M}^f(\omega_f)$ are constructed, the three one-particle density matrices: $\mathcal{D}^\xi(L)$,

$$\begin{aligned}\mathcal{D}_{ij}^\xi(L) &\doteq -2\tilde{L}_{cd}^{ik}S_{d'd}T_{d'c'}^{kj}S_{c'c}, \\ \mathcal{D}_{ia}^\xi(L) &\doteq \tilde{L}_a^i, \\ \mathcal{D}_{ai}^\xi(L) &\doteq \tilde{T}_{ac}^{ik}S_{c'c}\tilde{L}_c^k, \\ \mathcal{D}_{ab}^\xi(L) &\doteq 2T_{ac'}^{kl}S_{c'c}\tilde{L}_{c'b}^{lk},\end{aligned}\tag{3.26}$$

$\mathcal{D}^\xi(\bar{M})$ (analogously defined), and $\mathcal{D}^\eta(\lambda, R)$,

$$\begin{aligned}\mathcal{D}_{ij}^\eta(\lambda, R) &\doteq -\tilde{\lambda}_{c'}^iS_{c'c}R_c^j - 2S_{cc'}\tilde{\Lambda}_{c'd'}^{ik}S_{d'd}R_{dc'}^{kj}, \\ \mathcal{D}_{ia}^\eta(\lambda, R) &\doteq 0, \\ \mathcal{D}_{ai}^\eta(\lambda, R) &\doteq 2R_a^i + \tilde{R}_{ac'}^{ik}S_{c'c}\tilde{\lambda}_c^k - \\ &\quad - 2\left(T_{ac}^{kl}R_d^i + R_a^lT_{cd}^{ik}\right)S_{cc'}\tilde{\Lambda}_{c'd'}^{lk}S_{d'd}, \\ \mathcal{D}_{ab}^\eta(\lambda, R) &\doteq R_a^k\tilde{\lambda}_b^k + 2R_{ac'}^{kl}S_{c'c}\tilde{T}_{cb}^{lk},\end{aligned}\tag{3.27}$$

can be formed. Note that the vectors L_{μ_2} , R_{μ_2} , \bar{M}_{μ_2} occurring in eqs. (3.26,3.27) are restricted to excited state domains and pair lists, while ground state

restrictions apply for amplitudes T_{μ_2} and multipliers Λ_{μ_2} . Therefore the overlap matrices are in general rectangular and not quadratic.

The trace of these density matrices, back-transformed (with the dressed coefficient matrices [10]) to the AO basis, with the appropriate dipole integrals yields the left and right transition moments and finally the transition strength according to eqs. (3.18,3.19).

3.2.2 First-order properties

In the context of this work we have implemented orbital-unrelaxed first-order properties for ground- and excited states. The formalism can be derived by differentiation [83] of the corresponding orbital-unrelaxed Lagrangian with respect to the strength ϵ_Y of an external perturbation. The orbital-unrelaxed ground-state time-independent Lagrangian can be written as

$$\mathcal{L}(t, \lambda) = E(t) + \lambda_{\mu_i} \Omega_{\mu_i}(t), \quad (3.28)$$

where $E(t)$ and $\Omega_{\mu_i}(t)$ represent the ground-state coupled cluster energy and amplitude equations, and t denotes symbolically the ground-state amplitudes. The Lagrangian $\mathcal{L}(t, \lambda)$ is required to be fully variational, and differentiating it with respect to t yields the equations for the ground-state multipliers λ (see eq. (3.21)). The derivative of $\mathcal{L}(t, \lambda)$ with respect to the field strength represents the first-order property of CC2

$$\begin{aligned} \langle Y \rangle &= \frac{d\mathcal{L}}{d\epsilon_Y} = \frac{\partial E}{\partial \epsilon_Y} + \lambda_{\mu_i} \frac{\partial \Omega_{\mu_i}}{\partial \epsilon_Y} = \\ &= \langle 0|Y \exp(T_1 + T_2)|0 \rangle + \lambda \xi^Y, \end{aligned} \quad (3.29)$$

where Y is the related perturbation operator, and $|0\rangle$ is the reference determinant. The orbital-unrelaxed first-order properties hence are obtained from the density matrix

$$\mathcal{D}_{pq} = 2 \left(\delta_{pi} \delta_{qj} + \delta_{pa} \delta_{qi} t_a^i \right) + \mathcal{D}_{pq}^\xi(\lambda), \quad (3.30)$$

where $\mathcal{D}^\xi(\lambda)$ is defined in accordance to eq. (3.26), with the left eigenvector of the Jacobian replaced by the ground-state multipliers.

The orbital-unrelaxed Lagrangian for excited states, on the other hand, takes the form

$$\begin{aligned} \mathcal{L}_f(t, \lambda^{f'}, L^f, R^f, \alpha) &= E(t) + L_{\mu_i}^f A_{\mu_i v_j}(t) R_{v_j}^f + \\ &+ \lambda_{\mu_i}^{f'} \Omega_{\mu_i}(t) + \alpha (L_{\mu_i}^f M_{\mu_i v_j} R_{v_j}^f - 1) \end{aligned} \quad (3.31)$$

and differentiation with respect to the ground-state amplitudes t yields the equations for the excited state multipliers $\lambda^{f'}$. In combination with eq. (3.21) one obtains

$$0 = L_{\mu_i}^f B_{\mu_i, \nu_j, \rho_k} R_{\rho_k}^f + \lambda_{\mu_i}^f A_{\mu_i, \nu_j}, \quad (3.32)$$

where $\lambda^f \doteq \lambda^{f'} - \lambda$ and

$$B_{\mu_i, \nu_j, \rho_k} \doteq \frac{\partial A_{\mu_i, \rho_k}}{\partial t_{\nu_j}}. \quad (3.33)$$

In order to solve eq. (3.32) for the multipliers λ^f , the left transform of the Jacobian is required with the λ^f amplitudes restricted to ground-state pair lists and domains. The matrix $L^f \mathbf{B}$ is almost identical to the matrix \mathbf{F} given in eq. (3.10). The sole difference consists of replacing the ground-state multipliers λ by the left eigenvector L^f and omitting the first term in the $F_{\mu_1 \nu_1}$ block (which involves the bra reference state). Therefore, eqs. (3.23, 3.24) can be reused for the calculation of the rhs $L^f \mathbf{B} R^f$ in eq. (3.32). For the first-order properties of the excited states one obtains

$$\begin{aligned} \langle Y \rangle_f &= \frac{d\mathcal{L}_f}{d\epsilon_Y} = \frac{d\mathcal{L}}{d\epsilon_Y} + L_{\mu_i}^f \frac{\partial A_{\mu_i, \nu_j}(t)}{\partial \epsilon_Y} R_{\nu_j}^f + \lambda_{\mu_i}^f \frac{\partial \Omega_{\mu_i}(t)}{\partial \epsilon_Y} = \\ &= \langle Y \rangle + L^f \mathbf{A}^Y R^f + \lambda^f \xi^Y. \end{aligned} \quad (3.34)$$

The vector $L^f \mathbf{A}^Y$ is almost identical to η^Y , as defined in eq. (3.9). As above, the differences consist of replacing the ground-state multipliers λ by the left eigenvector L^f and dropping the first term of $\eta_{\mu_1}^Y$ (which involves the bra reference state). Therefore, the orbital-unrelaxed first-order properties of excited states can be computed from the density matrix

$$\mathcal{D}_{pq}^f = \mathcal{D}_{pq} + \mathcal{D}_{pq}^\eta(L, R) - 2\delta_{pa}\delta_{qi}R_a^i + \mathcal{D}_{pq}^\xi(\lambda^f), \quad (3.35)$$

where the density matrices \mathcal{D} , $\mathcal{D}^\eta(L, R)$ and $\mathcal{D}^\xi(\lambda^f)$ are defined according to eqs. (3.30), (3.27) and (3.26), respectively.

3.2.3 CP domains for property calculations

The most common way to determine the orbital domains (out of which the pair domains are formed by union of the corresponding orbital domains) uses the Boughton-Pulay (BP) procedure [56]. It is essentially based on a required maximum least-square deviation between a given LMO ϕ_i and

an approximated LMO ϕ'_i spanned in the AO subspace of a certain subset A of the centers of the molecule,

$$\begin{aligned} f(\mathbf{L}') &= \min(\langle \phi_i - \phi'_i | \phi_i - \phi'_i \rangle) = \\ &= \min(L_{\mu i} \tilde{S}_{\mu\nu} L_{\nu i} - L_{\mu i} \tilde{S}_{\mu\nu A} L'_{\nu A i} - \\ &\quad - L'_{\mu A i} \tilde{S}_{\mu A \nu} L_{\nu i} + L'_{\mu A i} \tilde{S}_{\mu A \nu A} L'_{\nu A i}) \leq 1 - \tau, \end{aligned} \quad (3.36)$$

where \mathbf{L} and \mathbf{L}' are the coefficients of the given and the approximated LMOs ϕ_i and ϕ'_i , respectively, \tilde{S} is the AO overlap matrix, τ an appropriate threshold, and indices μ_A run over the AO subspace A only. The subspace A is extended by further centers according to a priority list until the inequality (eq. (3.36)) is satisfied, with the priority list set up in advance either according to a Mulliken, or preferably Löwdin population analysis of ϕ_i . The PAOs assigned to the final set of centers representing the subspace A form the orbital domain $[i]$ of LMO ϕ_i . The presence of an external field influences the LMOs and a preferable way of augmenting the original domains by additional centers should be indicated by this LMO modification. The first derivatives of the LMO and the canonical virtual MO coefficients with respect to the strength ϵ_Y of an external field perturbation are

$$\begin{aligned} \frac{\partial L_{\mu i}}{\partial \epsilon_Y} &\doteq L_{\mu i}^Y = C_{\mu a} U_{a i}^Y + L_{\mu k} V_{k i}^Y, \quad \text{and} \\ \frac{\partial C_{\mu a}}{\partial \epsilon_Y} &\doteq C_{\mu a}^Y = -L_{\mu i} U_{a i}^Y, \end{aligned} \quad (3.37)$$

where \mathbf{U}^Y represents the solutions of the Coupled-Perturbed Hartree-Fock (CPHF) equations in mixed canonical virtual/localized occupied basis, and \mathbf{V}^Y – the solutions of the Coupled-Perturbed Localization (CPL) equations. We propose to extend the original BP ground-state domains with additional centers by using the coefficients $L'_{\mu i} \doteq L_{\mu i} \pm \alpha L_{\mu i}^Y$ instead of $L_{\mu i}$ in eq. (3.36) for the three external field perturbations in x-, y-, and z-direction, where α is a small scaling factor. Analogously, we can extend the original excited-state domains [10, 44] of the important orbitals by using

$$C_{\mu i}^{*'} \doteq t_a^i (C_{\mu a} \pm \alpha C_{\mu a}^Y) \pm t_a^k V_{k i}^Y C_{\mu a} \quad (3.38)$$

instead of $C_{\mu i}^* \doteq t_a^i C_{\mu a}$ in the related BP procedure. Here, the t_a^i coefficients denote the coupled cluster singles (CCS) or CIS amplitudes in mixed canonical virtual/localized occupied basis, as used for the construction of excited-state pair list and domains. For further reference we use the term *CP domains* for these augmented domains.

Solving the CPHF equations for the three perturbations is by far the most time consuming step in the construction of these CP domains. In order to speed-up the formation of the electron interaction matrix used in each CPHF iteration we employ DF according to eqs. (61-63) in Ref. 43. Fortunately, rather slack thresholds can be used in this case. For Pipek-Mezey [55] orbital localization the CPL equations in the context of an external field perturbation can be written as [84]

$$0 = \mathcal{B}_{ijk} U_{ak}^Y + \mathcal{C}_{ijkl} V_{kl}^Y, \quad (3.39)$$

with

$$\begin{aligned} \mathcal{B}_{ijk} &\doteq (1 - \mathcal{P}_{ij}) (2S_{ja}^A W_{kj} S_{ij}^A + \\ &\quad + S_{jj}^A (S_{ia}^A W_{kj} + S_{ja}^A W_{ki})), \\ \mathcal{C}_{ijkl} &\doteq (1 - \mathcal{P}_{ij})(1 - \mathcal{P}_{kl}) \delta_{jl} (2S_{ij}^A S_{kl}^A + \\ &\quad + \frac{1}{2} S_{ki}^A (S_{ll}^A + S_{jj}^A - S_{ii}^A - S_{kk}^A)), \\ S_{ij}^A &\doteq L_{\mu_A i} \tilde{S}_{\mu_A \nu} L_{\nu j} + L_{\mu_A j} \tilde{S}_{\mu_A \nu} L_{\nu i}, \\ S_{ia}^A &\doteq L_{\mu_A i} \tilde{S}_{\mu_A \nu} C_{\nu a} + C_{\mu_A a} \tilde{S}_{\mu_A \nu} L_{\nu i}, \end{aligned} \quad (3.40)$$

where \mathbf{W} is the localization matrix transforming from canonical occupied orbitals to LMOs, \mathbf{C} – the canonical MO coefficient matrix, and \mathcal{P}_{ij} – a permutation operator interchanging labels i and j . As it is evident from eq. (3.39), the solutions of the CPHF equations are also needed for the rhs of the CPL equations. Solving the CPL equations takes a negligible amount of time in comparison to the CPHF ones.

3.3 Test Calculations

The formalism outlined in section 3.2 for calculating transition strengths and orbital-unrelaxed first-order properties for ground- and excited states, along with the new option for constructing extended CP domains, has been implemented in the MOLPRO package (development version) [64] on top of the already existing local CC2 program for excitation energies [10]. Apart from the quite simple routines for forming the individual density matrices in eqs. (3.26), (3.27), (3.30), and (3.35), basically two new major modules were coded. The first module is the left transform of the Jacobian according to eqs. (3.13), (3.14) needed for the left eigenvector L^f , the ground- and excited state multipliers λ and λ^f , as well as for the multiplier $\bar{M}^f(\omega_f)$

occurring in the expression for the left transition moment. The left transform of the Jacobian is rather similar to the right transform, hence a very similar algorithm as described in Ref. 10 for the latter can be implemented straightforwardly. The computational cost for the left- and right transform thus are, as expected, virtually identical. The second module is the right transform of the matrix F according to eqs. (3.23), (3.24) occurring as the rhs of eqs. (3.20), and, in a slightly modified form, as the rhs of eq. (3.32). Three different objects involving two-index contractions of doubles amplitudes with fitting coefficients do occur here, i.e., the intermediates \hat{V}_{ia}^P , \check{V}_{ia}^P , and \hat{W}_{ia}^P defined in eq. (3.25). The latter involves three-index two-external ERIs. The quantity $(cd|P)R_d^k - S_{cc'}R_{c'}^l(lk|P)$ is calculated simultaneously with \hat{B}_p^{ia} , subsequently multiplied with the Coulomb metric and then contracted with the contravariant ground state doubles multipliers $\tilde{\Lambda}_{ab}^{ij}$ to form \hat{W}_{ia}^P . \hat{W}_{ia}^P itself also has to be contracted with two-external ERIs, as indicated in eq. (3.23). Therefore, in overall two passes through the list of three-index two-external ERIs are required for the formation of the right transform of F . In total, its computational cost is somewhat higher than a single left/right transform of the Jacobian, yet it only occurs as the rhs of two equations and is not needed in the iterative part of the program, and therefore is entirely insignificant.

Basis		cc-pVDZ						aug-cc-pVDZ					
Molecule	n_p^{tot}	n_{AO}	n_p^{BP}	L^{BP}	$L^{r=3}$	$L^{\alpha=0.1}$	$L^{\alpha=0.2}$	n_{AO}	n_p^{BP}	L^{BP}	$L^{\alpha=0.1}$	$L^{\alpha=0.2}$	
N-acetylglycine	276	147	270	43	85	64	79	247	270	69	89	121	
Propanamide	120	105	120	38	73	57	66	178	120	64	78	95	
"Dipeptide"	351	176	321	44	91	67	89	297	321	70	96	131	
" β -dipeptide"	435	200	370	44	93	73	94	338	367	73	109	138	
trans-urocanic acid	351	170	323	50	98	82	103	284	323	91	139	167	
1-phenylpyrrole	378	199	363	58	113	92	119	334	366	112	169	210	
DMABN	406	204	372	52	106	89	117	343	396	142	181	212	
p-cresol	231	152	222	48	96	80	94	256	225	104	148	164	
HPA	528	218	434	48	103	87	106	366	466	111	161	184	
Tyrosine	630	237	558	49	105	87	109	398	571	109	162	190	
BDP-Flv(a)	3828	579	2132	65		132	170	963	2256	126			
BDP-Flv(b)	6555	795	3108	66		144	189						

Table 3.1: Total number of LMO pairs and AOs entering the canonical calculation, compared to the length of the pair list n_p^{BP} and the average pair domain sizes for the ground state amplitudes entering the local CC2 calculation, for the individual test molecules and basis sets. Ordinary Boughton-Pulay domains (criterion set to 0.98) with the average pair domain size denoted as L^{BP} , as well as domains extended according to a distance criterion of 3 bohr ($L^{r=3}$), and extended CP domains (cf. section II C) with α set to 0.1 ($L^{\alpha=0.1}$) or 0.2 ($L^{\alpha=0.2}$) were used in our test calculations.

In order to test the correctness of the new local program results of local calculations with untruncated pair lists and full domains were verified against the corresponding canonical reference calculations carried out with

Basis		cc-pVDZ								aug-cc-pVDZ					
Molecule	st	n_p^{sBP}	L^{sBP}	$n_p^{sF=3}$	$L^{sF=3}$	$n_p^{s\alpha=0.1}$	$L^{s\alpha=0.1}$	$n_p^{s\alpha=0.2}$	$L^{s\alpha=0.2}$	n_p^{sBP}	L^{sBP}	$n_p^{s\alpha=0.1}$	$L^{s\alpha=0.1}$	$n_p^{s\alpha=0.2}$	$L^{s\alpha=0.2}$
N-acetyl-glycine	S ₁	232	63	273	94	258	83	265	92	246	125	257	137	264	153
	S ₂	214	63	268	93	241	80	250	90	226	111	251	125	264	149
Propanamide	S ₃	249	93	267	105	255	107	261	114	234	131	240	143	256	163
	S ₄	117	61	120	79	120	72	120	75	118	101	118	106	120	116
"Dipeptide"	S ₁	111	56	120	78	120	67	120	74	117	97	120	107	120	120
	S ₂	267	70	327	102	328	89	337	104	273	131	306	158	327	175
"β-dipeptide"	S ₁	261	72	326	103	303	91	324	104	279	144	307	161	335	182
	S ₂	282	70	356	106	326	91	374	111	310	144	356	178	408	202
<i>trans</i> -urocanic acid	S ₁	271	57	364	100	361	87	385	105	320	129	343	152	364	179
	S ₃	324	87	369	112	352	101	388	116	315	124	347	148	362	167
1-phenyl-pyrrole	S ₁	287	90	328	116	322	116	323	126	342	173	349	206	348	223
	S ₂	315	111	330	124	326	123	329	130	322	190	327	211	335	223
DMABN	S ₃	280	84	321	110	317	107	324	118	251	116	287	158	318	184
	S ₅	265	79	324	113	302	102	314	119	325	174	332	207	335	222
<i>p</i> -cresol	S ₁	305	99	359	131	327	121	359	136	336	202	361	242	375	260
	S ₂	351	129	365	147	355	144	369	151	365	235	370	270	375	282
HPA	S ₃	341	108	363	135	353	131	371	144	336	205	352	246	366	266
	S ₄	309	103			327	126	359	134	357	221	364	254	374	276
Tyrosine	S ₁	347	94	391	124	379	115	396	130	377	202	385	235	397	259
	S ₂	371	125	393	138	392	140	400	149	377	194	385	230	397	253
BDP-Flv(a)	S ₁	212	78	229	105	227	97	229	106	223	150	228	176	229	192
	S ₂	363	89	446	120	419	111	445	128	432	197	459	239	475	260
BDP-Flv(b)	S ₁	321	63	437	110	417	99	453	117	424	198	448	243	453	257
	S ₃	395	98	451	120	434	118	457	130						
	S ₁	431	90	529	121	510	114	540	132	493	191	551	235	580	260
	S ₂	448	97	544	126	549	117	572	135	504	224	560	258	585	281
	S ₃	489	115	542	130	537	130	558	142						
	S ₁	1595	142			2279	202	2580	231	1885	286				
	S ₂	1721	186			2075	239	2583	262	2044	359				
	S ₁	2857	195			3635	247	4093	274						
	S ₂	2230	172			3296	219	3973	255						

Table 3.2: Lengths of individual pair lists and average pair domain sizes for the excited-state amplitudes entering the local CC2 response calculation, for the individual test molecules, excited states, and basis sets. Domains and pair lists were constructed as described in Ref. [10] by analysis of an initial CIS wavefunction. The Boughton-Pulay criterion and the criterion for determining important orbitals κ_e were set to 0.985 and 0.9975, respectively. Extended domains based either on a distance criterion of 3 bohr or CP domains (cf. section II C) with α set to 0.1 or 0.2 were also used.

the TURBOMOLE CC2 response code [28]. In this section we report results of test calculations performed with our new program for a set of different molecules and excited states. As AO basis sets the cc-pVDZ and aug-cc-pVDZ sets [65,66] together with the related fitting basis sets optimized for DF-MP2 [67] were used. All LMOs were obtained via Pipek-Mezey localization [55]. For the aug-cc-pVDZ set the most diffuse function of each angular momentum type for each atom was deleted in the Pipek-Mezey localization procedure, yielding improved localization with diffuse basis sets. The pair lists for the ground-state, i.e., zeroth-order amplitudes and multipliers were restricted to pairs of LMOs with an inter-orbital distance of 10 bohr or less (the inter-orbital distance between two LMOs is defined as the smallest distance between any pair of centers within the related orbital domains). For the specification of the pair lists and domains for the excited states, i.e., the first-order response of amplitudes and multipliers, the initial CIS wave functions of the states of interest were analyzed, as de-

scribed in Ref. 10: Important and unimportant orbitals were distinguished based on the criterion κ_e set to 0.9975. The pair list was truncated such that all pairs (regardless of the inter-orbital distance) between two important LMOs and other pairs up to an inter-orbital distance of 5 bohr were included, corresponding to the notation $\forall(ij), (im) \leq 5, (mn) \leq 5$, where i, j and m, n denote important and unimportant LMOs, respectively. This applies to all results of calculations reported here. The pair domains were constructed according to the Boughton-Pulay (BP) [56] criterion of 0.98 (cc-pVDZ) and 0.985 (aug-cc-pVDZ) for both the ground- and excited state amplitudes and multipliers. Extended domains were formed by applying either a distance criterion of 3 bohr (augmenting the BP domains by further centers within a distance 3 bohr or less from those centers already included within the BP domains), or by employing the new CP domain construction scheme outlined in section 3.2.3 with scaling factors of $\alpha = 0.1$ and $\alpha = 0.2$, respectively. Tables 3.1 and 3.2 collect information about key quantities of the individual test molecules like the number of basis functions, the number of LMO pairs, and the average domain sizes for ground- and excited states, respectively. (For the definitions of the small molecules and the original references to their geometries see Ref. 44.) The average pair domain sizes for *extended* ground- and excited-state domains are appreciably larger than for the original BP domains. For extended domains based on a distance criterion of 3 bohr the sizes lie somewhere in between those of the CP domains with $\alpha = 0.1$ and $\alpha = 0.2$.

Table 3.3 compiles the norms of the transition strength vectors $|\vec{S}^{0f}|$ (\vec{S}^{0f} contains the diagonal elements of matrix \mathbf{S}^{0f} defined in eq. (3.18)) for various test molecules and excited states. The deviations between canonical and local results (for different specifications of the domains) are given as the norm of the related difference vector $|\delta\vec{S}^{0f}| = |\vec{S}^{0f}(\text{loc.}) - \vec{S}^{0f}(\text{can.})|$. Evidently, these deviations are rather small, especially for the extended domains. The biggest absolute error occurs for the S_2 state of DMABN, 0.26 a.u. (5%) for the original BP domains, which reduce to 0.07 a.u. for the extended CP ($\alpha = 0.2$) domains. Another sizeable deviation occurs for the S_3 state of HPA, 0.12 a.u. (11%) for BP domains, which again reduce to 0.04 a.u. for the extended CP ($\alpha = 0.2$) domains. Generally, a significant improvement is observed when going from the original BP to extended domains. Furthermore, domain extensions based on the CP scheme appear to be somewhat more robust compared to a pure distance criterion, as can be seen e.g. for the S_3 state of N-acetyl-glycine: here, the CP ($\alpha = 0.1$) domains, in contrast to the extended domains constructed for a distance criterion of 3 bohr, lead to a significant improvement over the original BP

Basis		cc-pVDZ								aug-cc-pVDZ					
		char.	ω_{CC2}	$ \vec{S}^{0f} $		$ \delta S^{0f} $			char.	ω_{CC2}	$ \vec{S}^{0f} $		$ \delta S^{0f} $		
Molecule	st			can.	loc.,BP	$r=3$	$\alpha=0.1$	$\alpha=0.2$			can.	loc.,BP	$\alpha=0.1$	$\alpha=0.2$	
N-acetyl-glycine	S ₁	$n \rightarrow \pi^*$	5.862	0.0112	0.0003	0.0003	0.0001	0.0002	$n \rightarrow \pi^*$	5.732	0.0084	0.0003	0.0002	0.0001	
	S ₂	$n \rightarrow \pi^*$	6.252	0.0044	0.0002	0.0001	0.0000	0.0000	$n \rightarrow \pi^*$	6.089	0.0000	0.0001	0.0000	0.0000	
	S ₃	$\pi \rightarrow \pi^*$	7.373	0.2627	0.1001	0.0792	0.0022	0.0011	$\pi \rightarrow \text{Rydb}$	6.275	0.0013	0.0003	0.0001	0.0001	
Propanamide	S ₁	$n \rightarrow \pi^*$	5.926	0.0066	0.0010	0.0011	0.0000	0.0000	$n \rightarrow \pi^*$	5.657	0.1931	0.0001	0.0000	0.0000	
	S ₂	$\pi \rightarrow \pi^*$	7.962	0.0363	0.0007	0.0005	0.0002	0.0005	$\pi \rightarrow \text{Rydb}$	6.267	0.1217	0.0037	0.0036	0.0030	
"Dipeptide"	S ₁	$n \rightarrow \pi^*$	5.871	0.0104	0.0005	0.0005	0.0003	0.0003	$n \rightarrow \pi^*$	5.743	0.0092	0.0006	0.0004	0.0003	
	S ₂	$n \rightarrow \pi^*$	6.106	0.0068	0.0002	0.0002	0.0002	0.0001	$n \rightarrow \pi^*$	5.953	0.0015	0.0001	0.0001	0.0002	
"β-dipeptide"	S ₁	$n \rightarrow \pi^*$	4.861	0.0041	0.0002	0.0000	0.0001	0.0000	$n \rightarrow \pi^*$	4.715	0.0001	0.0001	0.0000	0.0000	
	S ₂	$n \rightarrow \pi^*$	5.825	0.0114	0.0000	0.0001	0.0002	0.0001	$\pi \rightarrow \text{Rydb}$	5.635	0.1046	0.0106	0.0091	0.0072	
	S ₃	$\pi \rightarrow \text{Rydb}$	6.908	0.0964	0.0089	0.0063	0.0070	0.0039	$n \rightarrow \pi^*$	5.665	0.0180	0.0113	0.0138	0.0155	
trans-urocanic acid	S ₁	$n \rightarrow \pi^*$	4.987	0.0008	0.0001	0.0000	0.0001	0.0000	$n \rightarrow \pi^*$	4.863	0.0000	0.0000	0.0000	0.0000	
	S ₂	$\pi \rightarrow \pi^*$	5.207	5.2365	0.0724	0.0074	0.0140	0.0098	$\pi \rightarrow \pi^*$	4.931	5.5697	0.0462	0.0114	0.0015	
	S ₃	$\pi \rightarrow \pi^*$	6.269	0.5199	0.0029	0.0262	0.0183	0.0028	$\pi \rightarrow \text{Rydb}$	5.285	0.0029	0.0004	0.0003	0.0003	
1-phenyl-pyrrole	S ₅	$\pi \rightarrow \text{Rydb}$	7.054	0.0016	0.0002	0.0003	0.0003	0.0003	$\pi \rightarrow \text{Rydb}$	6.009	0.0305	0.0052	0.0058	0.0052	
	S ₁	$\pi \rightarrow \pi^*$	5.072	0.0235	0.0007	0.0013	0.0015	0.0013	$\pi \rightarrow \pi^*$	4.921	0.0359	0.0026	0.0023	0.0024	
	S ₂	$\pi \rightarrow \pi^*$	5.555	2.2771	0.0524	0.0047	0.0047	0.0063	$\pi \rightarrow \pi^*$	5.309	2.1535	0.0449	0.0080	0.0017	
DMABN	S ₃	$\pi \rightarrow \pi^*$	5.771	0.0848	0.0191	0.0037	0.0033	0.0024	$\pi \rightarrow \text{Rydb}$	5.434	0.0003	0.0055	0.0003	0.0001	
	S ₄	CT	6.091	0.0103	0.0017	0.0015	0.0006	0.0013	CT	5.489	0.1302	0.0276	0.0105	0.0089	
	S ₁	$\pi \rightarrow \pi^*$	4.525	0.3043	0.0226	0.0084	0.0230	0.0083	$\pi \rightarrow \text{Rydb}$	4.495	0.2130	0.0052	0.0045	0.0033	
p-cresol	S ₂	$\pi \rightarrow \pi^*$	4.891	5.3951	0.2645	0.0766	0.0842	0.0707	$\pi \rightarrow \text{Rydb}$	5.085	0.0000	0.0000	0.0000	0.0000	
	S ₁	$\pi \rightarrow \pi^*$	4.981	0.2036	0.0076	0.0024	0.0035	0.0027	$\pi \rightarrow \text{Rydb}$	5.145	0.0001	0.0001	0.0000	0.0000	
	S ₁	$\pi \rightarrow \pi^*$	4.984	0.1903	0.0052	0.0031	0.0035	0.0025	$\pi \rightarrow \pi^*$	4.816	0.1842	0.0038	0.0017	0.0011	
HPA	S ₂	$n \rightarrow \pi^*$	6.148	0.0023	0.0009	0.0007	0.0004	0.0003	$\pi \rightarrow \text{Rydb}$	5.216	0.0015	0.0006	0.0004	0.0003	
	S ₃	$\pi \rightarrow \pi^*$	6.285	1.1457	0.1238	0.0401	0.0681	0.0442	$\pi \rightarrow \text{Rydb}$	5.726	0.0990				
	S ₃	$\pi \rightarrow \pi^*$	4.995	0.1654	0.0033	0.0044	0.0044	0.0039	$\pi \rightarrow \pi^*$	4.834	0.1540	0.0045	0.0022	0.0013	
Tyrosine	S ₂	$n \rightarrow \pi^*$	5.824	0.0513	0.0242	0.0116	0.0120	0.0089	$\pi \rightarrow \text{Rydb}$	5.292	0.0111	0.0044	0.0029	0.0025	
	S ₃	$\pi \rightarrow \pi^*$	6.205	1.5584	0.1178	0.0347	0.0677	0.0373	$\pi \rightarrow \text{Rydb}$	5.488	0.1516				

- a) $|\vec{S}^{0f}| = \left((S_{XX}^{0f})^2 + (S_{YY}^{0f})^2 + (S_{ZZ}^{0f})^2 \right)^{\frac{1}{2}}$
b) $|\delta\vec{S}^{0f}| = |\vec{S}^{0f}(\text{loc.}) - \vec{S}^{0f}(\text{can.})|$

Table 3.3: Norms (in a.u.) of the transition strength vectors $|\vec{S}^{0f}|^a$ for the individual test molecules, excited states, and basis sets. The results for the different local calculations are given as the norm of the related difference vector $|\delta\vec{S}^{0f}|^b$ (canonical minus local vector). Local results for ordinary Boughton-Pulay domains, as well as for extended domains based either on a distance criterion of 3 bohr or CP domains (cf. section 3.2.3) with α set to 0.1 or 0.2 are given. The canonical excitation energies (in eV) are provided for easier identification of the individual states.

domains.

In Table 3.4 the norms of the dipole vectors $|\vec{\mu}| = |\vec{\mu}^{00}|$ of the ground states along with the norms of the dipole difference vectors $|\vec{\mu}^{0f}|$ of the excited states relative to the related ground states are shown for the same set of test molecules and excited states as above. The deviations between the local and the canonical results are given as the ratios $|\delta\vec{\mu}^{0f}| / |\vec{\mu}^{0f}|$ of the norms of the related difference vectors (canonical minus local vector) relative to the canonical reference values. They are all quite small for the ground state dipoles, i.e., less than 10% for BP domains and less than 3% for extended domains. The excited state dipole difference vectors $|\vec{\mu}^{0f}|$, on the other hand, are more delicate. Here, especially for the diffuse basis set, several cases are observed with deviations of more than 10% even for the extended CP domains. One of the worst cases is the S₃

Basis		cc-pVDZ						aug-cc-pVDZ					
			$ \vec{\mu}^{0f} $	$ \delta\vec{\mu}^{0f} / \vec{\mu}^{0f} $				$ \vec{\mu}^{0f} $	$ \delta\vec{\mu}^{0f} / \vec{\mu}^{0f} $				
Molecule	st	char.	can.	loc.,BP	$r=3$	$\alpha=0.1$	$\alpha=0.2$	char.	can.	loc.,BP	$\alpha=0.1$	$\alpha=0.2$	
N-acetyl-glycine	S ₀		1.0697	1.04	0.12	0.56	0.41		1.0346	1.04	0.64	0.31	
	S ₁	$n \rightarrow \pi^*$	0.7408	3.74	1.68	2.11	1.71	$n \rightarrow \pi^*$	0.9480	0.90	0.79	0.61	
	S ₂	$n \rightarrow \pi^*$	0.5942	3.50	2.06	5.85	4.34	$n \rightarrow \pi^*$	0.5878	13.22	12.46	11.36	
	S ₃	$\pi \rightarrow \pi^*$	1.9856	27.11	21.12	0.21	0.51	$\pi \rightarrow \text{Rydb}$	1.5037	7.18	5.22	3.69	
Propanamide	S ₀		1.3124	1.07	0.20	0.65	0.53		1.3727	0.84	0.55	0.34	
	S ₁	$n \rightarrow \pi^*$	0.7889	5.99	6.15	0.67	0.48	$n \rightarrow \pi^*$	3.7126	11.10	10.59	10.64	
	S ₂	$\pi \rightarrow \pi^*$	2.0787	2.79	2.04	1.93	1.94	$\pi \rightarrow \text{Rydb}$	3.1085	4.08	2.13	2.02	
	S ₀		1.3045	0.20	0.13	0.68	0.15		1.3391	0.48	0.14	0.14	
"Dipeptide"	S ₁	$n \rightarrow \pi^*$	0.7353	5.44	3.08	3.09	2.73	$n \rightarrow \pi^*$	0.9629	1.94	1.70	1.38	
	S ₂	$n \rightarrow \pi^*$	0.7401	5.74	3.29	4.50	3.03	$n \rightarrow \pi^*$	1.0227	16.58	14.64	12.24	
	S ₀		0.4226	4.34	0.77	1.36	1.32		0.4357	1.72	2.43	0.56	
	S ₁	$n \rightarrow \pi^*$	0.3875	1.68	2.50	1.47	1.00	$n \rightarrow \pi^*$	0.3721	7.40	6.49	2.28	
"β-dipeptide"	S ₂	$n \rightarrow \pi^*$	0.7600	6.25	3.73	3.50	3.21	$\pi \rightarrow \text{Rydb}$	2.9470	7.26	3.31	2.17	
	S ₃	$\pi \rightarrow \text{Rydb}$	1.6283	2.86	1.67	1.98	1.40	$n \rightarrow \pi^*$	1.0765	7.54	6.49	6.01	
	S ₀		1.9037	1.82	0.29	0.38	0.19		2.0304	1.70	0.31	0.26	
	S ₁	$n \rightarrow \pi^*$	2.3098	1.12	0.52	1.35	1.38	$n \rightarrow \pi^*$	2.2847	1.49	0.43	0.32	
trans-urocanic acid	S ₂	$\pi \rightarrow \pi^*$	2.2610	2.68	1.06	0.78	0.06	$\pi \rightarrow \pi^*$	2.2021	2.85	1.34	1.18	
	S ₃	$\pi \rightarrow \pi^*$	0.4262	5.97	1.85	5.63	5.63	$\pi \rightarrow \text{Rydb}$	5.7190	2.74	2.33	2.05	
	S ₀		4.6874	4.65	5.25	5.03	5.25	$\pi \rightarrow \text{Rydb}$	3.1825	8.48	5.93	5.02	
	S ₁	$\pi \rightarrow \pi^*$	0.6964	1.21	0.03	1.20	0.22		0.6894	1.36	0.43	0.20	
1-phenyl-pyrrole	S ₁	$\pi \rightarrow \pi^*$	0.8822	4.36	6.45	6.63	6.42	$\pi \rightarrow \pi^*$	1.0998	8.71	7.80	7.27	
	S ₂	$\pi \rightarrow \pi^*$	2.3809	3.74	2.48	3.82	1.96	$\pi \rightarrow \pi^*$	2.2354	4.91	3.54	2.74	
	S ₃	$\pi \rightarrow \pi^*$	4.4506	1.78	1.34	0.20	0.08	$\pi \rightarrow \text{Rydb}$	0.4478	71.74	25.53	20.26	
	S ₄	CT	5.7148	0.65	0.25	0.13	0.20	CT	3.8053	4.14	5.23	5.87	
DMABN	S ₀		2.9042	0.70	0.05	0.57	0.16		3.0388	0.00	0.24	0.16	
	S ₁	$\pi \rightarrow \pi^*$	0.9348	0.34	1.64	3.18	1.70	$\pi \rightarrow \text{Rydb}$	2.8072	0.61	3.45	2.33	
	S ₂	$\pi \rightarrow \pi^*$	2.0718	4.49	0.28	1.14	0.84	$\pi \rightarrow \text{Rydb}$	1.9141	4.21	4.62	2.92	
	S ₀		0.5207	7.29	1.34	2.42	2.22		0.5192	3.82	0.43	0.87	
p-cresol	S ₁	$\pi \rightarrow \pi^*$	0.2562	9.73	8.07	9.51	7.99	$\pi \rightarrow \text{Rydb}$	4.2811	1.78	1.37	0.65	
	S ₀		0.7344	6.71	1.24	1.78	1.42		0.7256	2.92	0.69	0.38	
	S ₁	$\pi \rightarrow \pi^*$	0.2418	8.87	7.95	9.47	6.38	$\pi \rightarrow \pi^*$	0.2030	19.91	12.79	9.47	
	S ₂	$n \rightarrow \pi^*$	0.6240	3.65	3.36	2.47	1.70	$\pi \rightarrow \text{Rydb}$	4.5105	3.36	2.35	1.63	
HPA	S ₃	$\pi \rightarrow \pi^*$	0.8985	3.70	1.16	3.49	1.37	$\pi \rightarrow \text{Rydb}$	1.5189				
	S ₀		1.3198	3.21	0.49	1.60	1.05		1.4086	1.87	1.06	0.74	
	S ₁	$\pi \rightarrow \pi^*$	0.2217	7.31	9.71	8.00	6.59	$\pi \rightarrow \pi^*$	0.1916	6.73	4.53	3.13	
	S ₂	$n \rightarrow \pi^*$	0.5702	7.51	6.85	6.82	5.27	$\pi \rightarrow \text{Rydb}$	4.1572	6.63	4.44	3.34	
Tyrosine	S ₃	$\pi \rightarrow \pi^*$	1.0688	9.84	5.61	6.39	4.76	$\pi \rightarrow \text{Rydb}$	4.4276				

Table 3.4: Norms (in a.u.) of the dipole vectors $|\vec{\mu}| = |\vec{\mu}^{00}|$ (ground state) and the dipole difference vectors $|\vec{\mu}^{0f}|$ (excited states, relative to the ground state) for the individual test molecules, excited states, and basis sets. The results for the different local calculations are given as the ratio (in %) $|\delta\vec{\mu}^{0f}|/|\vec{\mu}^{0f}|$ of the norm of the related difference vector (canonical minus local vector) relative to the canonical reference value. Local results for ordinary Boughton-Pulay domains, as well as for extended domains based either on a distance criterion of 3 bohr or CP domains (cf. section 3.2.3) with α set to 0.1 or 0.2 are given.

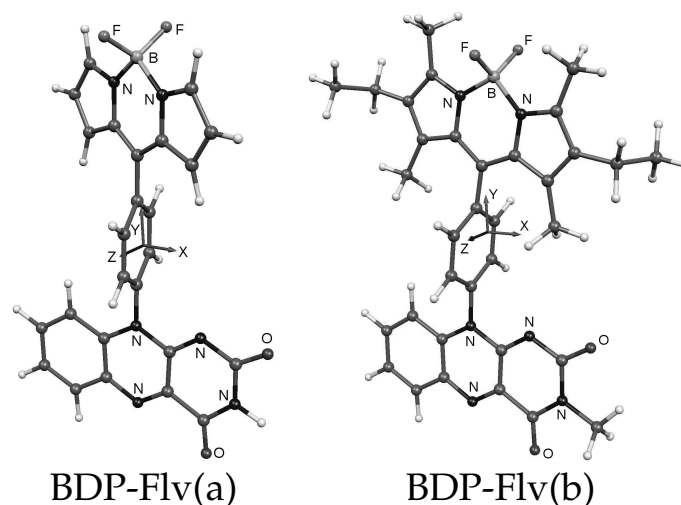


Figure 3.1: Structures of the borondipyrromethene – flavin dyads. BDP-Flv(b): Structure (1) from Ref. 85. BDP-Flv(a): BDP-Flv(b) with side chains of BDP and flavin removed. All structures were optimized at the DFT/BP86 level by using the SVP basis set [72]. The individual coordinate axes are also plotted.

($\pi \rightarrow$ Rydberg) state of 1-phenylpyrrole at 5.434 eV (appearing for the aug-cc-pVDZ basis only) with a deviation of 72% for BP domains, reducing to 20% for extended CP ($\alpha = 0.2$) domains. Moreover, there are cases like the S_2 state of the “dipeptide”, where domain extension leads to hardly any improvement. Some of these cases are expected to improve once the excited state pair lists and domains are no longer based on CIS, but on a more reliable method like semi-local LCC2 response, where we have a full set of the (canonical) excited state amplitudes and a truncated set of the (local) ground-state amplitudes [86]. Furthermore, local and canonical orbital-unrelaxed properties are not entirely comparable. In local MP2 gradient theory additional terms involving the residual in the full PAO basis do occur (cf. eqs. (26) and (27) in Ref. 43), which are vanishing entirely for the canonical or the local case with full domains, but not otherwise. Therefore, it is quite likely that the discrepancies between canonical and local *orbital-relaxed* CC2 dipole moments are again smaller. The importance of the full orbital relaxation is also indicated by the recent finite-field study of the local CCSD dipole moments and static polarizabilities [87]. *Orbital-relaxed* first-order properties for local CC2 are presently under development.

In order to test the new program on more extended molecular systems additional calculations were performed for the borondipyrromethene (BDP) – flavin (Flv) dyads displayed in Fig. 3.1. BDP-Flv(b) corresponds

		cc-pVDZ				aug-cc-pVDZ
		can. ^a	loc.,BP ^b	$\alpha = 0.1^c$	$\alpha = 0.2^d$	loc.,BP ^b
S ₀	μ_X	-2.207	-2.234	-2.233	-2.231	-2.472
	μ_Y	-0.450	-0.496	-0.478	-0.463	-0.433
	μ_Z	0.360	0.366	0.365	0.364	0.398
S ₁	ω	2.820	2.754	2.810	2.813	2.693
	μ_X^{01}	-0.024	-0.046	-0.028	-0.027	-0.039
	μ_Y^{01}	0.656	0.571	0.638	0.645	0.577
	μ_Z^{01}	-0.031	-0.035	-0.032	-0.032	-0.034
	S_{XX}^{01}	5.084	5.372	5.224	5.133	5.309
	S_{YY}^{01}	0.009	0.015	0.011	0.009	0.015
	S_{ZZ}^{01}	0.497	0.484	0.502	0.500	0.492
	$D, \%$	100	5.3	14.0	19.8	7.2
	ω	3.117	3.092	3.139	3.132	2.958
	μ_X^{02}	-0.088	-0.095	-0.089	-0.089	-0.147
S ₂	μ_Y^{02}	1.154	1.166	1.146	1.149	1.140
	μ_Z^{02}	0.040	0.035	0.038	0.039	0.038
	S_{XX}^{02}	2.363	2.959	2.497	2.459	3.611
	S_{YY}^{02}	0.773	0.774	0.764	0.776	0.750
	S_{ZZ}^{02}	0.048	0.026	0.045	0.045	0.010
	$D, \%$	100	10.2	18.7	26.6	12.2

a) canonical CC2

b) local CC2, Boughton-Pulay domains

c) local CC2, CP domains, $\alpha = 0.1$ d) local CC2, CP domains, $\alpha = 0.2$

Table 3.5: Excitation energies ω (in eV), transition strengths \vec{S}^{0f} , and changes $\vec{\mu}^{0f}$ relative to the ground state dipole moment $\vec{\mu}$ (all in a.u.) for the two lowest excited states of the BDP-Flv(a) molecule. Results are given for canonical CC2, as well as for local CC2 with the usual Boughton-Pulay and the extended CP domains ($\alpha = 0.1$ and $\alpha = 0.2$). The ratio D (in %) of the number of excited-state doubles amplitudes entering the calculations (relative to the canonical calculation) are also given.

to structure (1) of Ref. 85 synthesized by Trieflinger *et al.* as an example for a reversible fluorescent switch. In BDP-Flv(a) the ethyl/methyl side chains on the BDP and flavin subunits are omitted such that a canonical reference calculation still could be performed. The results from calculations of the two lowest excited states of these molecules are compiled in Tables 3.5 and 3.6, respectively. As already seen before for the smaller molecules, the deviations between canonical and local results significantly decrease when going from the original BP to the extended CP domains. For instance the transition strength vector \vec{S}^{02} obtained with BP domains deviates from the canonical value by 0.60 a.u. (24%). In this case primarily the x-component is affected. This discrepancy decreases to 0.13 a.u. (5%) and 0.10 a.u. (4%) for the CP ($\alpha = 0.1$) and ($\alpha = 0.2$) domains, respectively. Also the excitation energies generally improve (not shown here for the test set of molecules) and are consistently slightly larger than the corresponding canonical values. The number of doubles amplitudes included in the

		cc-pVDZ		
		loc.,BP ^a	$\alpha = 0.1^b$	$\alpha = 0.2^c$
S ₀	μ_X	-2.131	-2.110	-2.101
	μ_Y	-0.304	-0.271	-0.253
	μ_Z	-0.018	-0.020	-0.016
S ₁	ω	2.574	2.645	2.649
	μ_X^{01}	-0.072	-0.045	-0.041
	μ_Y^{01}	0.423	0.415	0.414
	μ_Z^{01}	-0.012	-0.010	-0.010
	S_{XX}^{01}	7.463	7.277	7.230
	S_{YY}^{01}	0.379	0.362	0.356
	S_{ZZ}^{01}	0.032	0.031	0.031
	$D, \%$	5.0	10.0	13.2
	$t(\text{iter})^d$	51(68)	101(138)	120(156)
S ₂	ω	3.073	3.121	3.114
	μ_X^{02}	-0.060	-0.086	-0.083
	μ_Y^{02}	1.122	1.088	1.085
	μ_Z^{02}	-0.007	-0.006	-0.005
	S_{XX}^{02}	2.875	2.387	2.268
	S_{YY}^{02}	0.688	0.659	0.659
	S_{ZZ}^{02}	0.001	0.000	0.000
	$D, \%$	3.3	7.6	11.7
	$t(\text{iter})^d$	42(56)	60(68)	86(96)

a) Boughton-Pulay domains

b) CP domains, $\alpha = 0.1$ c) CP domains, $\alpha = 0.2$

d) in minutes, on AMD 252 Opteron

Table 3.6: Excitation energies ω (in eV), transition strengths \vec{S}^{0f} , and changes $\vec{\mu}^{0f}$ relative to the ground state dipole moment $\vec{\mu}$ (all in a.u.) for the two lowest excited states of the BDP-Flv(b) molecule. Results are given for local CC2 with the usual Boughton-Pulay and the extended CP domains ($\alpha = 0.1$ and $\alpha = 0.2$). The ratio D (in %) of the number of excited-state doubles amplitudes entering the calculations (relative to the canonical calculation) and the CPU (elapsed) times in minutes for a left transform of the Jacobian are also given.

calculation increases by a factor of 2–3 on going from the BP domains to the extended CP domains and depends on the nature of the excited state. For the BDP-Flv(b) dyad about 10% of the excited-state doubles amplitudes of the canonical calculation are needed in a local calculation using extended domains. This fraction of course decreases with increasing size of the molecular system under study.

3.4 Conclusions

In this chapter we presented an *ab initio* method for calculating transition strengths and orbital-unrelaxed first-order properties of ground- and excited states of extended molecular systems. The method is based on Cou-

pled Cluster response theory and employs the CC2 model proposed by Christiansen *et al.* [21]. Local approximations were introduced for the doubles amplitudes only, restricting both the ground- and excited-state, i.e., the zeroth- and first-order amplitudes with respect to a time-dependent perturbation to *a priori* determined domains. The Density Fitting approximation was used for all electron repulsion integrals. As a consequence, all diagrams are exclusively computed from three-index objects, the only four-index objects which do occur at all, are doubles amplitudes, which (i) are quite compact by virtue of the local approximation and (ii) are immediately contracted to a three-index object, as well. The new program is an extension of our previous local CC2 implementation for calculating excitation energies [10]. However, the computation of transition strengths and first-order properties is considerably more demanding from the programming point of view, requiring – apart from the right eigenvector – also the left eigenvector of the local CC2 Jacobian plus the solutions of several linear equation systems.

The accuracy of the new method was tested for a set of different molecules and excited states by comparing the results of the local method with canonical reference values. It turned out that transition strengths and in particular properties of excited states are much more demanding than excitation energies; the original Boughton-Pulay domains turned out to be insufficient in several cases and leading to rather poor results. A considerable improvement could be achieved by extending the domains according to a new scheme involving the solutions of the CPL and the CPHF equations. When such extended domains are used, the discrepancies between local and canonical results usually reduce to about 5% or less. Severe problems occur in the cases when the initial CIS wavefunction, used for the specification of the domains for the excited-state amplitudes (cf. Ref. 10) is a rather bad approximation. One can circumvent this problem by substituting the CIS wavefunction by a semi-local CC2 wavefunction for excited-state domain construction [86].

In order to demonstrate the capabilities of the new implementation we also report results from calculations on a possible target system, i.e., a borondipyrromethene – flavin dyad which was recently studied experimentally in Regensburg. This system comprises 78 atoms, 228 active electrons, and 795 basis functions in the cc-pVDZ basis set. Transition strength and property calculations on systems of this size or bigger on a single processor appear to be readily possible with the new code. Yet the main motivation of the new developments reported here is not the possibility to compute transition strengths and properties *per se*, but to make a further step towards efficient analytic nuclear gradients for excited states,

so that geometry optimizations of extended molecular systems in excited states could be performed at the DF-LCC2 level of theory.

Chapter 4

Laplace Transform in local methods

4.1 Introduction

The local correlation methods [10, 38–43, 88–91] are all based on an orbital invariant formalism of the related underlying electron correlation theory. Such an orbital invariant formalism, e.g. for MP2, is straight-forwardly devised by perturbative analysis of the (orbital invariant) CC equations. Yet, in comparison to the canonical formulation some complication arises. Due to the non-diagonality of the Fock operator in a general (local) orbital basis the first-order amplitudes no longer decouple and a linear equation system has to be solved (usually by an iterative procedure) to get the amplitudes and from those the second-order energy. In a canonical formulation, on the other hand, the second-order energy can be calculated directly. Similar complications w.r. to the canonical formulation occur also for the CC2 model and the related response theory, and for perturbative triples corrections.

An alternative orbital invariant formalism for MP2, pioneered by Almlöf and Häser, is based on the Laplace transform of the denominators in the expression for the canonical MP2 amplitudes [33, 45]. Here, instead of solving a linear equation system a numerical quadrature of the Laplace integral must be performed, the latter requiring only a few quadrature points. So far, the Laplace transform approach has been primarily utilized to devise formulations of MP2 theory in AO basis representation [92–95]. Some studies on the use of the Laplace transform technique in the context of other localized orbitals have also been reported [96, 97]. Recently, Nakajima and Hirao presented an implementation of a Laplace MP2 method

based on localized orbitals and DF [98].

A major disadvantage of the Laplace transform ansatz, present in all these methods, is the requirement of an individual ERI evaluation or transformation for each quadrature point, even though the related transformation matrices, resembling density matrices, are sparse. In the present work we develop a local correlation method for MP2 theory along the lines of the Pulay ansatz based on the Laplace transform of canonical MP2 theory. In contrast to other methods the required ERI sets for the individual quadrature points are generated from an initial compact integral set in local basis by transforming the PAOs *within* the related excitation domains. These transformations are rather inexpensive and no new ERI evaluation in AO basis is needed for the individual quadrature points. DF is also utilized to make the method more economical. Overall, the new Laplace transformed DF-LMP2 (LT-DF-LMP2) method is competitive to DF-LMP2, in particular for extended domains, where the linear equation system in the latter becomes more expensive to solve. A local Laplace transform method for Scaled Opposite-Spin MP2 has been recently presented by Jung *et al.* [99, 100]. In contrast to our method orthogonalized localized orbitals rather than non-orthogonal PAOs were used to span the virtual space, and (ii) locality was exploited entirely based on screening, not on *a priori* specified domains. The main motivation of the present work was not to propose yet another MP2 method for extended systems, but to work out a general methodology on how to use the Laplace transform in the context of local correlation methods based on the Pulay ansatz, i.e., with *a priori* specified domains, which then can easily be adapted to other local methods like CC2, time-dependent CC2, local triples, or periodic local MP2. The theory of Laplace transformed local correlation methods based on pre-defined excitation domains with *lower rank* than the space of the canonical virtuals is less straight-forward than for methods where the rank of the space spanned by the local functions is either larger than or equal to that of the canonical virtuals like in the previous methods. This issue is outlined in the following section.

4.2 Theory

Formalism of Laplace transformed DF-LMP2

As shown by Almlöf [45] the energy denominator $\Delta_{\bar{i}\bar{j}}^{\bar{a}\bar{b}} = \epsilon_{\bar{a}} - \epsilon_{\bar{i}} + \epsilon_{\bar{b}} - \epsilon_{\bar{j}}$ appearing in the energy expression of canonical MP2,

$$\begin{aligned} E^{(2)} &= \sum_{\bar{i}\bar{j}\bar{a}\bar{b}} \tilde{K}_{\bar{a}\bar{b}}^{\bar{i}\bar{j}} T_{\bar{a}\bar{b}}^{\bar{i}\bar{j}}, \quad \tilde{K}_{\bar{a}\bar{b}}^{\bar{i}\bar{j}} = 2(\bar{i}\bar{a}|\bar{j}\bar{b}) - (\bar{i}\bar{b}|\bar{j}\bar{a}), \\ T_{\bar{a}\bar{b}}^{\bar{i}\bar{j}} &= -\frac{(\bar{a}\bar{i}|\bar{b}\bar{j})}{\Delta_{\bar{i}\bar{j}}^{\bar{a}\bar{b}}} \end{aligned} \quad (4.1)$$

is eliminated via the identity $1/x = \int_0^\infty e^{-xt} dt$,

$$T_{\bar{a}\bar{b}}^{\bar{i}\bar{j}} = - \int_0^\infty (\bar{a}\bar{i}|\bar{b}\bar{j}) e^{-\Delta_{\bar{i}\bar{j}}^{\bar{a}\bar{b}} t} dt. \quad (4.2)$$

The barred indices \bar{i}, \bar{j}, \dots and \bar{a}, \bar{b}, \dots refer to canonical occupied and virtual orbitals, respectively. The $\epsilon_{\bar{i}}, \epsilon_{\bar{a}}$ etc. in $\Delta_{\bar{i}\bar{j}}^{\bar{a}\bar{b}}$ denote related orbital energies. The $(\bar{i}\bar{a}|\bar{j}\bar{b})$, finally, represent the usual electron repulsion integrals (ERIs). The Laplace integration in eq. (4.2) can be replaced by a numerical quadrature,

$$\begin{aligned} T_{\bar{a}\bar{b}}^{\bar{i}\bar{j}} &= - \sum_q^{n_q} w_q e^{(\epsilon_{\bar{i}} - \epsilon_F) t_q} e^{(-\epsilon_{\bar{a}} + \epsilon_F) t_q} (\bar{a}\bar{i}|\bar{b}\bar{j}) e^{(\epsilon_{\bar{j}} - \epsilon_F) t_q} e^{(-\epsilon_{\bar{b}} + \epsilon_F) t_q} \\ &= - \sum_q^{n_q} w_q \mathfrak{Z}_{\bar{a}\bar{b}}^{\bar{i}\bar{j}}(q). \end{aligned} \quad (4.3)$$

$\epsilon_F = (\epsilon_{\text{HOMO}} + \epsilon_{\text{LUMO}})/2$ cancels in eq. (4.3) and ensures that the individual exponential factors are always smaller than one. $\mathfrak{Z}_{\bar{a}\bar{b}}^{\bar{i}\bar{j}}(q)$ is implicitly defined in (4.3) and has the meaning of an incremental amplitude w.r. to the Laplace quadrature, rather than that of an ERI. The number of quadrature points n_q required to achieve μH accuracy is rather small (5–7). A short discussion about how to obtain points t_q and weights w_q for the quadrature is given below.

In order to develop a formalism for local correlation methods we introduce the usual transformation matrices connecting LMOs and PAOs with canonical occupied and virtual orbitals. The unitary transformation

matrix \mathbf{W} specified by the chosen localization criterion (Boys [54], Pipek-Mezey [55], *etc.*) transforms canonical occupied orbitals to LMOs,

$$|\phi_i^{\text{LMO}}\rangle = \sum_{\tilde{i}} |\phi_i^{\text{CAN}}\rangle W_{\tilde{i}i}, \quad (4.4)$$

whereas the transformation matrix $\mathbf{Q} = \mathbf{C}^{\text{v}\dagger} \mathbf{S}_{\text{AO}}$ [43] transforms canonical virtuals to PAOs,

$$\langle \phi_a^{\text{PAO}} | = \sum_{\tilde{a}} Q_{a\tilde{a}}^{\dagger} \langle \phi_{\tilde{a}}^{\text{CAN}} |. \quad (4.5)$$

In the definition of \mathbf{Q} the matrix \mathbf{C}^{v} is the virtual block of the (canonical) MO-coefficient matrix and \mathbf{S}_{AO} is the AO overlap matrix. Here and in the following we use indices i, j, \dots and a, b, \dots for LMOs and PAOs, respectively. The matrix product

$$\mathbf{Q}^{\dagger} \mathbf{Q} = \mathbf{S}_{\text{PAO}} \quad (4.6)$$

yields the metric of the PAOs. Using these transformations the relations

$$(ia|jb) = \sum_{\tilde{i}\tilde{j}\tilde{a}\tilde{b}} W_{\tilde{i}i}^{\dagger} W_{\tilde{j}j}^{\dagger} (\tilde{i}\tilde{a}|\tilde{j}\tilde{b}) Q_{\tilde{a}a} Q_{\tilde{b}b} \quad (4.7)$$

$$T_{\tilde{a}\tilde{b}}^{\tilde{i}\tilde{j}} = \sum_{ijab} Q_{\tilde{a}a} Q_{\tilde{b}b} T_{ab}^{ij} W_{\tilde{i}i}^{\dagger} W_{\tilde{j}j}^{\dagger} \quad (4.8)$$

straight-forwardly follow. Eq. (4.8) is obtained from the expression for the local correlation energy,

$$E_{\text{LOC}}^{(2)} = \sum_{ijab} \tilde{K}_{ab}^{ij} T_{ab}^{ij} \quad (4.9)$$

and eq. (4.7). Integrals and amplitudes always transform conversely, as covariant and contravariant objects. The relation (4.7) also holds for the case when the PAO indices a, b are confined to excitation domains, i.e., when the number of PAOs a, b is *smaller* than the number of canonical virtuals. Yet the conversely transforming 'canonical' amplitudes of (4.8) are not identical to the canonical amplitudes of eq. (4.2), but represent a fit to those *within* the specified local basis (*vide infra*), and the local MP2 energy defined in (4.9) deviates from the canonical MP2 energy of eq. (4.1).

The transformation of eq. (4.3) to the local basis, i.e., the inversion of eq. (4.8), is not straight-forward due to two reasons: In contrast to AOs the PAOs form a non-orthogonal redundant set of functions. Furthermore,

the PAOs are usually restricted to excitation domains and are therefore spanning a space with lower dimension than that of the canonical virtuals. In order to investigate this transformation we introduce the new matrix $\bar{\mathbf{Q}} = \mathbf{V}\mathbf{Q}^\dagger$ with property

$$\sum_{a\bar{a}} |\phi_a^{\text{PAO}}\rangle \bar{Q}_{a\bar{a}} Q_{\bar{a}c} = |\phi_c^{\text{PAO}}\rangle, \quad (4.10)$$

with ϕ_a^{PAO} and ϕ_c^{PAO} belonging to the same domain. Multiplying (4.10) with the bra PAO ϕ_d^{PAO} (again of the same domain) and integrating yields

$$\mathbf{S}_{\text{PAO}} \bar{\mathbf{Q}} \mathbf{Q} = \mathbf{S}_{\text{PAO}} \mathbf{V} \mathbf{S}_{\text{PAO}} = \mathbf{S}_{\text{PAO}}, \quad (4.11)$$

defining the unknown matrix \mathbf{V} as a pseudoinverse $\mathbf{S}_{\text{PAO}}^+$ of \mathbf{S}_{PAO} . \mathbf{V} is obtained by (i) diagonalizing \mathbf{S}_{PAO} , (ii) inverting elements of the diagonal matrix so obtained, which are above a given threshold defining redundancies, and zeroing the remaining ones, and (iii) back-transforming of the diagonal matrix. We emphasize at this point, that if PAO domains are introduced, \mathbf{V} is domain specific (even though we omit the explicit dependence on domains at the present stage), while \mathbf{Q} is not. For a transformation involving \mathbf{Q} the columns related to the relevant domain are just extracted from \mathbf{Q} . Now utilizing eq. (4.10) the relations

$$(ia|jb) = \sum_{cd} (ic|jd) (\bar{\mathbf{Q}}\mathbf{Q})_{ca} (\bar{\mathbf{Q}}\mathbf{Q})_{db} \quad (4.12)$$

$$T_{ab}^{ij} = \sum_{cd} (\bar{\mathbf{Q}}\mathbf{Q})_{ac} (\bar{\mathbf{Q}}\mathbf{Q})_{bd} T_{cd}^{ij} \quad (4.13)$$

straight-forwardly follow. Exploiting (4.13) and unitarity of \mathbf{W} , eq. (4.8) can now be transformed with $\bar{\mathbf{Q}}$ and \mathbf{W} yielding

$$T_{ab}^{ij} = \sum_{\bar{i}\bar{j}\bar{a}\bar{b}} \bar{Q}_{a\bar{a}} \bar{Q}_{b\bar{b}} T_{\bar{a}\bar{b}}^{\bar{i}\bar{j}} W_{\bar{i}i} W_{\bar{j}j}. \quad (4.14)$$

Eq. (4.14) is valid for both the true and the fitted canonical amplitudes.

The related ERIs again transform conversely,

$$(\bar{i}\bar{a}|\bar{j}\bar{b}) = \sum_{ijab} W_{\bar{i}i} W_{\bar{j}j} (ia|jb) \bar{Q}_{a\bar{a}} \bar{Q}_{b\bar{b}}. \quad (4.15)$$

Combining eqs. (4.3), (4.14), and (4.15) leads to

$$T_{ab}^{ij} = - \sum_q^{n_q} w_q \mathfrak{T}_{ab}^{ij}(q), \quad \text{with} \quad (4.16)$$

$$\mathfrak{T}_{ab}^{ij}(q) = \sum_{klcd} Y_{ac}^v(q) Y_{bd}^v(q) (ck|dl) X_{ki}^o(q) X_{lj}^o(q),$$

where we have introduced the quadrature point dependent matrices

$$\begin{aligned} X_{ij}^o(q) &= \sum_{\bar{i}} W_{i\bar{i}}^\dagger e^{(\epsilon_{\bar{i}} - \epsilon_F)t_q} W_{\bar{i}j}, \\ X_{ab}^v(q) &= \sum_{\bar{a}} Q_{a\bar{a}}^\dagger e^{(-\epsilon_{\bar{a}} + \epsilon_F)t_q} Q_{\bar{a}b}, \\ Y_{ab}^v(q) &= \sum_{cd} V_{ac} X_{cd}^v V_{db}^\dagger. \end{aligned} \quad (4.17)$$

Eqs. (4.16) and (4.17) show that the compact ERI set ($ck|dl$) in local basis can be re-used at each quadrature point by applying a sequence of rather inexpensive transformations within the local basis. No new AO integral evaluation and (AO to MO or AO to AO) transformation is required for each quadrature point.

In contrast to ordinary local MP2 the local approximation in the amplitudes does not carry over to the ERIs, as is clearly evident from eq. (4.16), i.e., introducing *a priori* a restricted pair list $\{ij\}$ and pair domains $a, b \in [ij]$ for T_{ab}^{ij} does not imply *a priori* restrictions on the pairs $\{kl\}$ and the PAO ranges c, d of the ERIs. This has some important consequences distinguishing the local Laplace approach from ordinary local correlation methods (*vide infra*).

We now proceed by invoking the Density Fitting approximation to the ERIs. We assume that the auxiliary basis set is always identical for all orbital pair densities in the ERIs. If the Coulomb metric is employed for such a case the one-term formula

$$\begin{aligned} (ai|bj) &= \sum_{PQ} (ai|P) J_{PQ}^{-1} (Q|bj) = \sum_P B_P^{ai} B_P^{bj}, \quad \text{with} \\ B_P^{ai} &= \sum_Q (ai|Q) (Q|P)^{-1/2} \end{aligned} \quad (4.18)$$

can be used, while otherwise, *e.g.* in case of local fitting [42, 58], the three term formula has to be utilized. In eq.(4.18) indices P, Q, \dots denote functions of the auxiliary basis set with Coulomb metric $J_{PQ} = (P|Q)$. Inserting (4.18) in (4.16) yields

$$\mathfrak{T}_{ab}^{ij}(q) = \sum_{cd} \sum_P V_{ac} V_{bd} \mathfrak{B}_P^{ci}(q) \mathfrak{B}_P^{dj}(q), \quad \text{with} \quad (4.19)$$

$$\mathfrak{B}_P^{ai}(q) = \sum_{kcd} X_{ac}^v(q) V_{cd}^\dagger B_P^{dk} X_{ki}^o(q). \quad (4.20)$$

If instead of the MP2 the scaled opposite-spin MP2 energy is requested, then the energy of the related quadrature point can be computed with

a nominal scaling of the cost of $O(N^4)$ instead of $O(N^5)$ (cf. Ref. 99 for details).

The whole formalism developed so far is by construction also valid for the case of PAO domains, i.e., if the number of PAOs involved in the transformations is *smaller* than the number of canonical virtuals. At this point we now want to specify our local approximation: As in ordinary local MP2 we impose a restricted pair list and pair domains to confine the amplitudes T_{ab}^{ij} , and accordingly $\mathfrak{T}_{ab}^{ij}(q)$. Then the matrices \mathbf{V} appearing in eq. (4.19) are actually pseudoinverses of the PAO overlap matrices restricted to the $[ij]$ pair domains, which we denote as V_{ab}^{ij} . Eq. (4.19) explicitly written for the specified domains takes the form

$$\mathfrak{T}_{ab}^{ij}(q) = \sum_{cd \in [ij]} \sum_P V_{ac}^{ij} V_{bd}^{ij} \mathfrak{B}_P^{ci}(q) \mathfrak{B}_P^{dj}(q). \quad (4.21)$$

For the ERIs $(ck|P)$ (and hence for the B_P^{ck}), on the other hand, we do not explicitly introduce any restriction on the set of indices. Consequently, the matrix \mathbf{V} of eq. (4.20) is the pseudoinverse of the un-truncated PAO overlap matrix.

In order to achieve higher efficiency in computing the $\mathfrak{B}_P^{ai}(q)$ quantities the sparsity of various matrices can be utilized. For example, since LMOs and PAOs k and c are localized functions the ERIs $(ck|P)$ and therefore the B_P^{ck} for a given k have negligibly small values when ϕ_c^{PAO} is spatially far from ϕ_k^{LMO} . The matrices $X_{ij}^o(q)$ and $X_{ab}^v(q)$ are also sparse. This is due to the fact that these quantities are analogous to the exponentially decaying Hartree-Fock density matrices for the occupied and virtual spaces, but with Laplace-weighted occupation numbers [92, 93]. Yet this sparsity might depend on the quadrature point t_q . This will be explored further for a test case in section 4.3.

The computational cost of calculating the pseudoinverse \mathbf{V} of the un-truncated PAO overlap matrix scales as $O(N^3)$. Another $O(N^3)$ step (with a larger prefactor) is the inversion of the Coulomb metric for density fitting (4.18). In order to reduce the scaling of the latter either attenuated Coulomb fitting ($O(N^2)$, cf. Ref. 100) or local fit domains ($O(N)$, cf. Refs. 42,58) could be introduced. In our present program we have not yet implemented any of these schemes. The $O(N^3)$ scaling of calculating the pseudoinverse \mathbf{V} can be avoided by confining the PAO index c of the ERIs $(ck|P)$ to united pair domains $[U(k)] = \bigcup_{v_l} [kl]$, the union of all pair domains $[kl]$ with common k . These, dictated by the truncated pair list, reflect the r^{-6} decay behavior of the pair energies and safely cover the relevant range of the exponentially decaying ERIs. Then the dimensions of the pseudoinverses are confined

to the related orbital specific united pair domains and the computational cost of their construction decreases to $O(N)$. In our test calculations such a restriction of the integrals to the corresponding united domains had only a negligible effect on the energy.

The MP2 energy finally is obtained as

$$\begin{aligned}
 E_{\text{LOC}}^{(2)} &= - \sum_q w_q \sum_{ij \in [ij]} \sum_{ab \in [ij]} \tilde{L}_{ab}^{ij} \sum_P \mathfrak{B}_P^{ai}(q) \mathfrak{B}_P^{bj}(q), \quad \text{with} \\
 \tilde{L}_{ab}^{ij} &= 2L_{ab}^{ij} - L_{ba}^{ij}, \quad \text{and} \\
 L_{ab}^{ij} &= \sum_{cd \in [ij]} \left(\sum_P B_P^{ci} B_P^{dj} \right)^* V_{ca}^{ij} V_{db}^{ij}.
 \end{aligned} \tag{4.22}$$

The \tilde{L}^{ij} matrices do not depend on the quadrature point and have to be computed just once at the beginning. After that also the \mathbf{V}^{ij} matrices can be discarded. Hence, just one four-indexed quantity in local basis must be kept, in comparison to at least three in ordinary DF-LMP2. Moreover, for a given quadrature point just a single pass through the list of \tilde{L}^{ij} matrices is required, whereas in the original DF-LMP2 multiple passes through the list of amplitude matrices are needed for each iteration to calculate the coupling between amplitudes via the Fock matrix [38] (see also eq. (4.26)).

It can also be seen from eq. (4.22) that even for the case of an unrestricted set of ERIs ($ck|dl$) in eq. (4.16) the PAO index a of the quantity $\mathfrak{B}_P^{ai}(q)$ entering the assembly step still is confined to the pair domain $[ij]$. *A priori* restriction of the ERI set, i.e., restricting index d in eq. (4.20) to $[U(k)]$ helps reducing the cost for computing the $\mathfrak{B}_P^{ai}(q)$ intermediates, and, especially, for getting the related pseudoinverse. On the other hand, the scheme with a completely unrestricted set of the ERI benefits from the possibility to pre-multiply $\mathbf{X}^t \mathbf{V}$ before transforming the three-index object B_P^{dk} .

But independent of all that, the essential point here is that all the assembly steps in our algorithm always go just over pair domains and restricted pair lists, whether the ERI ($ck|dl$) in eq. (4.16) is *a priori* truncated to the united domain, or not, and hence are always computationally inexpensive.

The algorithm as outlined scales nominally cubically (calculation of the inverse of the Coulomb metric for DF which is also independent of the quadrature point), yet $O(N)$ scaling could be achieved by introducing local fit domains [42, 58]. Moreover, the Laplace scheme allows for an easy parallelization of the code by a partitioning of the quantities occurring in the energy expression (4.22), which is lacking any coupling between large objects.

Discrete quadrature of Laplace integral

Following Häser and Almlöf [33] the points t_q and weights w_q for the discrete quadrature of the Laplace integral are obtained from a least-squares fit,

$$\int_{x_{\min}}^{x_{\max}} f(x) \left(\frac{1}{x} - \sum_q^{n_q} w_q e^{-xt_q} \right)^2 = \min. \quad (4.23)$$

x_{\min} and x_{\max} are the minimal and maximal energy denominators of all $\Delta_{ij}^{\bar{a}\bar{b}}$, respectively. $f(x)$ is a distribution function counting the $\Delta_{ij}^{\bar{a}\bar{b}}$ in the vicinity of a certain x . It is constructed by generating a histogram of all $\Delta_i^{\bar{a}} = \epsilon_{\bar{a}} - \epsilon_i$ based on 600 equidistant bins subdividing the interval between the minmax values of $\Delta_i^{\bar{a}}$. The two identical histograms reflecting the distributions of the $\Delta_i^{\bar{a}}$ and the $\Delta_j^{\bar{b}}$ are then added to a new histogram based on 1200 equidistant bins subdividing the interval between x_{\max} and x_{\min} . The final histogram so obtained then corresponds very closely to the desired distribution function $f(x)$, which would be obtained by generating a histogram of the $\Delta_{ij}^{\bar{a}\bar{b}}$ directly. The computational cost of forming $f(x)$ in that way however scales as $O(N^2)$ rather than $O(N^4)$ and in practice takes only a negligible amount of time. In our test calculations the use of an $f(x)$ reflecting the distribution of the $\Delta_{ij}^{\bar{a}\bar{b}}$ as described turned out to be superior to the simpler uniform distribution, i.e., $f(x) = 1$, certainly so for small n_q .

The t_q are obtained by using a Simplex algorithm, the related weights needed in each Simplex step by solving the set of linear equations obtained from (4.23) by differentiation w.r. to w_q (for details see Ref. 33). The necessary numerical integrations are carried out by subdividing the interval of integration defined by x_{\min} and x_{\max} into 1200 subintervals (logarithmic scale). The related $f(x)$ for a certain x was obtained by linear interpolation. For $t_q = 0$ we have $\mathfrak{B}_p^{ai}(0) = B_p^{ai}$ (this immediately follows from eqs. (4.12), (4.17), and (4.19)), thus, the energy contribution for $t_q = 0$ can be computed virtually for free as a by-product of the initial calculation of \tilde{L}_{ab}^{ij} . For that reason, the $t_q = 0$ point is always included and kept fixed in the Simplex minimization.

Laplace transformed vs. original LMP2

The Laplace transformed and the original local MP2 method differ in some interesting aspects. A common basis for both is the equation

$$R_{\bar{a}\bar{b}}^{\bar{i}\bar{j}} = \sum_{ijab} Q_{\bar{a}a} Q_{\bar{b}b} T_{ab}^{ij} W_{ii}^{\dagger} W_{jj}^{\dagger} + \frac{1}{\Delta_{\bar{i}\bar{j}}^{\bar{a}\bar{b}}} \sum_{ijab} \bar{Q}_{\bar{a}a}^{\dagger} \bar{Q}_{\bar{b}b}^{\dagger} (ai|bj) W_{ii}^{\dagger} W_{jj}^{\dagger}. \quad (4.24)$$

Provided that the local ERI set $(ai|bj)$ (but not the local amplitude set T_{ab}^{ij}) is un-truncated, i.e., corresponds to full domains then the second term of eq. (4.24) is identical to the canonical amplitudes and $R_{\bar{a}\bar{b}}^{\bar{i}\bar{j}}$ represents the difference between the genuine canonical amplitudes and the local amplitudes in canonical basis, obtained according to eq. (4.8). Except for full amplitude domains, the $R_{\bar{a}\bar{b}}^{\bar{i}\bar{j}}$ cannot be strictly zero, since the number of the equations exceeds the number of the variables. $\Delta_{\bar{i}\bar{j}}^{\bar{a}\bar{b}} R_{\bar{a}\bar{b}}^{\bar{i}\bar{j}}$ is the canonical MP2 residual (w.r. to the fitted amplitudes obtained from the local ones) entering the canonical Hylleraas functional.

In the Laplace transformed LMP2 method presented here the functional $\sum_{\bar{i}\bar{j}\bar{a}\bar{b}} (R_{\bar{a}\bar{b}}^{\bar{i}\bar{j}})^2$ is minimized w.r. to the local amplitudes,

$$0 = \frac{d \sum_{\bar{i}\bar{j}\bar{a}\bar{b}} (R_{\bar{a}\bar{b}}^{\bar{i}\bar{j}})^2}{d(T_{ab}^{ij})} = 2 \sum_{\bar{i}\bar{j}\bar{a}\bar{b}} W_{ii}^{\dagger} W_{jj}^{\dagger} R_{\bar{a}\bar{b}}^{\bar{i}\bar{j}} Q_{\bar{a}a} Q_{\bar{b}b}. \quad (4.25)$$

Note that the PAO and LMO indices of the transformation matrices are restricted to the space of the local amplitudes. Dividing eq. (4.25) by two, multiplying it from the left and the right with \mathbf{V}^{\dagger} and \mathbf{V} , respectively, inserting $R_{\bar{a}\bar{b}}^{\bar{i}\bar{j}}$ as defined in (4.24), making use of eq. (4.13), and finally Laplace transforming the denominator leads to the LT-LMP2 amplitude equations given in eq. (4.16). The LT-LMP2 therefore corresponds to a least-squares minimization of the canonical MP2 residual, weighted with the inverse of the related denominator. Amplitudes corresponding to a small denominator (i.e. corresponding to the HOMO-LUMO region) hence have a larger weight and are fitted more accurately.

The original LMP2, on the other hand, corresponds to a projection onto the space of the local amplitudes of eq. (4.24) after multiplying it with the denominator. Multiplication with \mathbf{W}^{\dagger} from the left, and \mathbf{Q} from the right

then yields

$$\begin{aligned} \sum_{\bar{i}\bar{j}\bar{a}\bar{b}} W_{\bar{i}\bar{i}}^{\dagger} W_{\bar{j}\bar{j}}^{\dagger} (\Delta_{\bar{i}\bar{j}}^{\bar{a}\bar{b}} R_{\bar{a}\bar{b}}^{\bar{i}\bar{j}}) Q_{\bar{a}\bar{a}} Q_{\bar{b}\bar{b}} &= (a\bar{i}|b\bar{j}) + (\mathbf{fT}^{ij}\mathbf{S})_{ab} \\ &+ (\mathbf{ST}^{ij}\mathbf{f})_{ab} - \sum_k (\mathbf{S}(f_{ik}\mathbf{T}^{kj} + f_{kj}\mathbf{T}^{ik})\mathbf{S})_{ab}. \end{aligned} \quad (4.26)$$

If the local ERIs in the second term of eq. (4.24) are un-truncated then the transformed ERIs correspond to the canonical MO integrals and eq. (4.7) can be utilized to expose the local ERIs in eq. (4.26). The very same equations however are also obtained if these ERIs are restricted to the space of the local amplitudes and eq. (4.12) can be used instead. After projection, the ERIs *outside* the space of the local amplitudes, even if sizeable, cannot influence the local amplitudes. The usual LMP2 amplitude equations are obtained from (4.26) by requiring that the canonical MP2 residual $\Delta_{\bar{i}\bar{j}}^{\bar{a}\bar{b}} R_{\bar{a}\bar{b}}^{\bar{i}\bar{j}}$, projected onto the local space, is zero. Residual elements outside the local space are entirely neglected even though there is no guarantee that they are negligible (in particular for small Boughton-Pulay domains).

The Laplace transformed LMP2 presented here and the original LMP2 therefore are two non-equivalent local methods based on *a priori* restrictions of the wavefunction parameters. The former corresponds to a weighted least-squares fit of the canonical amplitudes, the latter to a projection of the canonical residual onto the specified local space (in order to reduce the number of equations to the number of variables) with the requirement that the projected canonical residual is strictly zero. For the Laplace transformed LMP2 none of the residual elements is strictly zero yet those *outside* the local space are also required to be as small as possible and are not left un-controlled. This corresponds to a better fit of the whole set of the weighted residuals, and, for most basis sets, to an energy slightly closer to that of canonical MP2 than the original local method provides.

LT-LMP2 Lagrangian and the first order properties

As mentioned above, application of the Laplace transformation in the context of the local scheme, i.e. for a truncated set of amplitudes, implies fitting of the latter to the full set of canonical amplitudes. This implies that this method is no longer solely based on perturbation theory (in a reduced local space), but rather is a fit to results of perturbation theory carried out in the un-truncated first-order interacting space. The Hylleraas functional hence is not a proper Lagrangian for the LT-LMP2 energy. The LT-LMP2

Lagrangian can be specified instead as

$$\begin{aligned}
 L[\mathbf{T}, \mathbf{\Lambda}, \mathbf{T}', \mathbf{\Lambda}'] = & \sum_{ijab} \tilde{K}_{ab}^{ij} T_{ab}^{ij} + \Lambda_{\bar{a}\bar{b}}'^{ij} \left(T_{\bar{a}\bar{b}}'^{ij} + \frac{K_{\bar{a}\bar{b}}^{ij}}{\Delta_{ij}^{\bar{a}\bar{b}}} \right) \\
 & + \sum_{ijab} \Lambda_{ab}^{ij} \left(T_{ab}^{ij} - \sum_{\bar{i}\bar{j}\bar{a}\bar{b}} \bar{Q}_{a\bar{a}} \bar{Q}_{b\bar{b}} T_{\bar{a}\bar{b}}'^{ij} W_{\bar{i}\bar{i}} W_{\bar{j}\bar{j}} \right), \quad (4.27)
 \end{aligned}$$

where \mathbf{T}' and \mathbf{T} represent the canonical and fitted MP2 amplitudes, respectively. The first term of the right-hand-side of (4.27) corresponds to the LT-LMP2 energy, the second comprises the conditions for the (canonical) MP2 amplitudes (4.1), while the third term refers to the fit of the canonical amplitudes by the local ones and represents the set of equations (4.25). The multipliers of the second and the last term obviously live in the un-truncated canonical and in the local restricted space, respectively.

Differentiation of $L[\mathbf{T}, \mathbf{\Lambda}, \mathbf{T}', \mathbf{\Lambda}']$ w.r. to the amplitudes \mathbf{T} yields the equations for the multipliers $\mathbf{\Lambda}$ simply as

$$\Lambda_{ab}^{ij} = -\tilde{K}_{ab}^{ij}. \quad (4.28)$$

Note that the multipliers and the contravariant integrals in (4.28) are confined to the restricted local space. Finally, differentiation w.r. to the canonical amplitudes \mathbf{T}' provides a set of equations relating the two sets of multipliers \mathbf{T}' and \mathbf{T} ,

$$\Lambda_{\bar{a}\bar{b}}'^{ij} = \sum_{ijab} W_{\bar{i}\bar{i}} W_{\bar{j}\bar{j}} \Lambda_{ab}^{ij} \bar{Q}_{a\bar{a}} \bar{Q}_{b\bar{b}}, \quad (4.29)$$

which can be used to eliminate the canonical amplitudes and multipliers in the Lagrangian (4.27). This yields (after invoking the Laplace identity)

$$L[\mathbf{T}, \mathbf{\Lambda}] = \sum_{ijab} \tilde{K}_{ab}^{ij} T_{ab}^{ij} + \Lambda_{ab}^{ij} \left(T_{ab}^{ij} + \sum_q^{n_q} w_q \mathfrak{T}_{ab}^{ij}(q) \right). \quad (4.30)$$

and the condition specifying the local amplitudes then is identical to eq. (4.16).

In order to introduce a (one-body) perturbation into the Hamiltonian the condition specifying the canonical amplitudes of $L[\mathbf{T}, \mathbf{\Lambda}, \mathbf{T}', \mathbf{\Lambda}']$ is augmented by the two connected diagrams contracting the perturbation with the canonical amplitudes, which are divided by the energy denominator,

i.e., $[VT']_{\bar{a}\bar{b}}^{\bar{i}\bar{j}} / \Delta_{\bar{i}\bar{j}}^{\bar{a}\bar{b}}$. The derivative of this Lagrangian w.r. to the perturbation strength at zero perturbation strength then leads to an expression for the LT-LMP2 density matrix which contains the *canonical* first-order amplitudes of the unrestricted space T' , i.e.,

$$\begin{aligned} D_{\bar{b}\bar{a}} &= 2 \sum_{\bar{i}\bar{j}\bar{c}} \left(\sum_{ijab} W_{\bar{i}i} W_{\bar{j}j} \tilde{K}_{ab}^{ij} \bar{Q}_{a\bar{a}} \bar{Q}_{b\bar{c}} \right) T'_{\bar{b}\bar{c}}^{\bar{i}\bar{j}}, \\ D_{\bar{j}\bar{i}} &= -2 \sum_{\bar{k}\bar{a}\bar{b}} \left(\sum_{ijab} W_{\bar{i}i} W_{\bar{k}k} \tilde{K}_{ab}^{ij} \bar{Q}_{a\bar{a}} \bar{Q}_{b\bar{b}} \right) T'_{\bar{a}\bar{b}}^{\bar{j}\bar{k}}. \end{aligned} \quad (4.31)$$

Eq. (4.31) therefore is impractical for extended systems.

The occurrence of the canonical amplitudes in eq. (4.31) can be avoided by substituting the genuine canonical amplitudes in the perturbation diagrams by their fit through the local amplitudes in the canonical basis. The structure of the Lagrangian given in eq. (4.27) then is not altered, but the influence of the perturbation on the canonical amplitudes is approximated (note that in the case of the LMP2 method both the perturbation and the amplitudes refer to the restricted local space). As a result of this approximation the genuine canonical amplitudes T' in eq. (4.31) are replaced by the amplitudes T of the local space, transformed to the canonical basis according to eq. (4.8). The resulting LT-LMP2 density matrix, in contrast to MP2 or LMP2, is non-symmetric, as it is generally the case for Coupled Cluster theory. This is a consequence of the two different sets of ERIs (truncated and un-truncated) which appear in the first and second term of the Lagrangian, eq. (4.27), respectively, and implies that two different sets of amplitudes have to be determined. This is of course a severe disadvantage of LT-LMP2 compared to LMP2, yet if the Laplace approach is employed in the context of a method like CC2 then amplitudes and multipliers have to be determined separately anyhow.

Symmetric LT-LMP2 density matrices are obtained if the full set of ERIs appearing in the second term of eq. (4.27) is replaced by its fit through a truncated local set of ERIs, again transformed to the canonical basis according to eq. (4.15). The local space of this ERI set must coincide with that of the local amplitudes. In such a case only one set of amplitudes has to be determined and the resulting LT-LMP2 density matrix is symmetric. On the other hand, when density fitting is employed for the ERIs, it is not convenient to insist on an identical truncation of amplitudes and ERIs since a factorization of the local ERIs as exploited in eq. (4.21) then is not possible (pair domain restrictions cannot be applied for the relevant three-index quantities). As a consequence the quadrature-dependent assembly step of (4.21) has to be replaced by a quadrature-dependent four-index

transformation of the local ERI set. Moreover, the results obtained for the properties are anticipated to be of lower quality if the full set of ERIs is replaced by a set of ERIs truncated in the same severe manner as the amplitudes. Instead, an alternative symmetrical approach is proposed here, where the amplitude set related to the truncated set of ERIs is replaced by that related to the full ERI set. The expression for the density matrix in the local basis then takes the form

$$\begin{aligned} D_{ij} &= -2 \sum_{kabcd} \tilde{T}_{ab}^{jk} S_{ac} T_{cb}^{ik} S_{db}, \\ D_{ab} &= 2 \sum_{ijcd} \tilde{T}_{bd}^{ij} S_{dc} T_{ac}^{ij}, \end{aligned} \quad (4.32)$$

which from its structure is identical to that of the original LMP2 method.

Such a definition of the density matrix is related to multipliers which do not satisfy the stationary conditions for the Lagrangian, hence the first-order properties cannot be strictly regarded as the derivatives of the LT-LMP2 energy w.r. to the corresponding perturbation. This implies that such a strategy cannot be used in the context of nuclear energy gradients used for geometry optimizations. On the other hand, (i) the deviations from the proper derivative of the LT-LMP2 energies are small (especially for extended domains), and (ii) the resulting properties are slightly closer to the corresponding canonical result than either those obtained from LMP2 or from the non-symmetric LT-LMP2 approach (since the unrestricted set of ERIs obviously provides a better fit for the canonical amplitudes than the restricted set). A first illustration of this issue is given in the next section.

4.3 Test Calculations

Sparsity of transformation matrices

For an efficient algorithm the sparsity of the transformation matrices $\mathbf{X}^o(q)$, $\mathbf{X}^v(q)$ as defined in eq. (4.17) and of the matrix product $\mathbf{X}^v(q)\mathbf{V}$ occurring in eq. (4.20) is of a major concern. The $\mathbf{X}^o(q)$ and $\mathbf{X}^v(q)$ matrices are essentially the density matrices of the occupied and virtual space in LMO and PAO basis, respectively, but with exponentially weighted occupation numbers [93]. In order to analyze the sparsity of such matrices in a large molecule a crosslink to solid state theory may be helpful [92]. It has been show by Des Cloizeaux in Ref. 101 that the density matrix in nonmetallic systems decays exponentially and the rate of this decay depends on the width of the band gap. The density matrix for the virtual states should

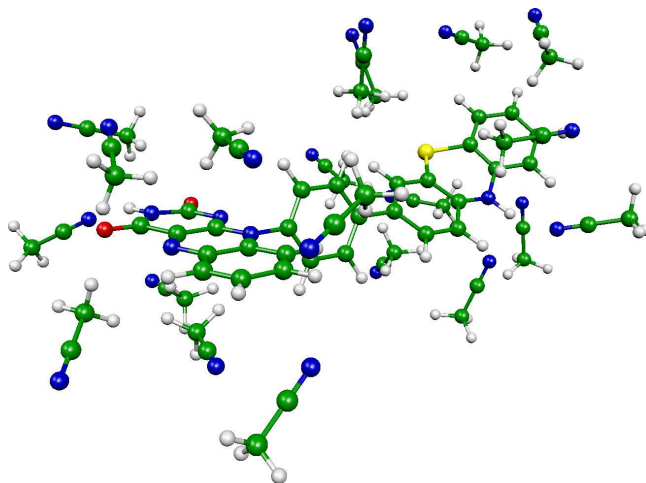


Figure 4.1: A cluster of a phenothiazine-phenyl-isoalloxazine dye dyad solvated by 20 acetonitrile solvent molecules (173 atoms in total).

behave in a similar way due to the finite size of the basis set. The decay rates of $X^o(q)$ and $X^v(q)$ for different t_q points should therefore remain the same, yet the prefactor and therefore the actual sparsity of the matrices may differ. Trivially, for the point $t_q = 0$ these matrices correspond to the identity and the PAO overlap matrix, respectively. For non-zero, but small t_q the prefactor may increase since the Laplace exponentials are cutting out regions with very low (for $X^o(q)$) or very high (for $X^v(q)$) energies. For larger t_q the exponential factor becomes very small and the sparsity of the matrices increases again.

We have investigated the sparsity of the $X^o(q)$, $X^v(q)$ matrices and the $X^v(q)\mathbf{V}$ matrix product in detail for the case of a solvent cluster consisting of a phenothiazine-phenyl-isoalloxazine dye dyad solvated by 20 acetonitrile solvent molecules (cf. Fig. 4.1). This solvated dye dyad has been investigated before in our group in the context of an application project on artificial blue-light photoreceptors [11]. In Fig. 4.2 the mean values of the elements $X_{ij}^o(q)$ and $X_{ab}^v(q)$ as a function of the spatial separation of the functions ϕ_i^{LMO} , ϕ_j^{LMO} , and ϕ_a^{PAO} , ϕ_b^{PAO} , respectively, are plotted.

For all calculations presented here the maximum of the quadrature points $\max(t_q)_{\forall q}$ remains below 10 Hartree⁻¹, hence, for Fig. 4.2, representative t_q values of 0 (0.01 for $X^o(q)$) and 10 Hartree⁻¹ were taken. Evidently,

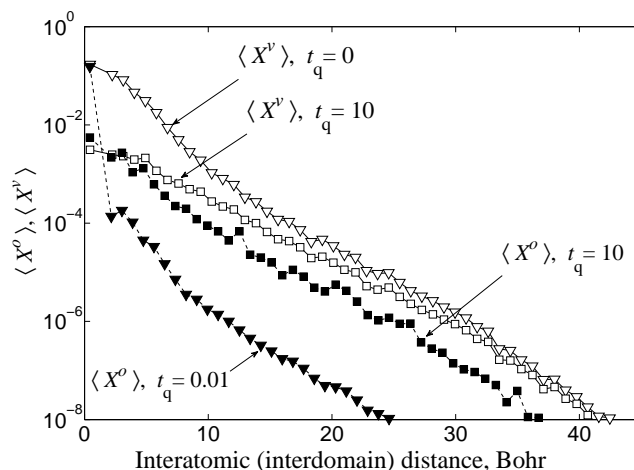


Figure 4.2: Mean absolute values of the $X_{ij}^o(q)$ and $X_{ab}^v(q)$ for the system shown in Fig. 4.1 versus the spatial separation between the i and j domains or a and b atoms. Filled markers correspond to X^o , open ones to X^v . The dependencies are given for small (triangles) and large (squares) values of the Laplace quadrature points t_q .

the transformation matrices $X^o(q)$ and $X^v(q)$ all decay exponentially according to (nearly) the same rate which is governed by the HOMO-LUMO gap. All matrices appear to be reasonably sparse. The sparsity of the matrix $X^v(q)$ for a moderately small t_q is similar to that of the PAO overlap matrix ($t_q = 0$). For $t_q = 10$ Hartree⁻¹ the elements of $X^v(q)$ become small due to the larger exponents in the exponential factors. The sparsity of the $X^o(q)$ matrix is decreasing on going from $t_q = 0.01$ to $t_q = 10$ Hartree⁻¹, but $X^o(q)$ remains more sparse than $X^v(q)$. For the whole relevant range of the t_q the sparsity of both matrices is sufficient to allow for an efficient prescreening in the transformation steps. Test calculations show that the prescreening of transformations involving the $X^v(q)$ matrix is much more important for molecules of the present size range since the transformations with $X^o(q)$ take only a small fraction of the overall computational time.

In Fig. 4.3 an analogous plot of the decay behaviour of the matrix product $X^v(q)V$ is given. V is the pseudoinverse of the PAO overlap matrix S_{PAO} (cf. eq. (4.11)) and hence might destroy the sparsity of the product $X^v(q)V$, regardless that $X^v(q)$ itself is sparse. On the other hand, if there were no redundancies in S_{PAO} the matrix product at point $t_q = 0$, $X^v(0)V$ would be identical to the identity matrix, and one may anticipate that $X^v(q)V$ nevertheless is sparse, also for non-zero t_q , in spite of a subset of

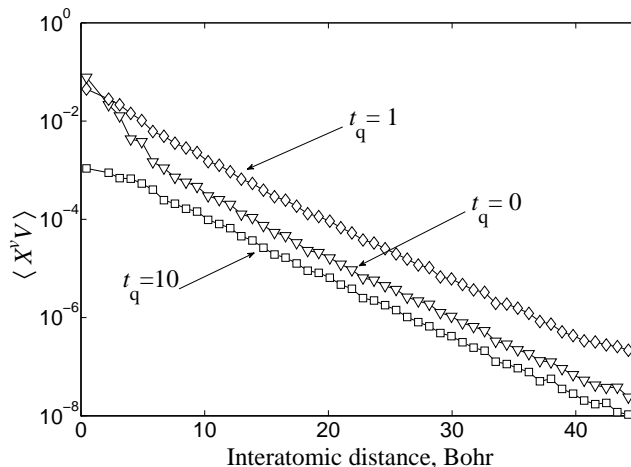


Figure 4.3: Mean absolute values of the matrix product $(X^v \mathbf{V})_{ab}(q)$ for the solvent cluster displayed in Fig. 4.1 versus the distance between the atoms a and b .

redundant PAOs. Fig. 4.3 shows that the decay rate of $X^v(q)\mathbf{V}$ is somewhat lower than that of $X^v(q)$ itself, yet it is still exponential. The exponent of the exponential decay appears to be insensitive to a particular value of t_q , whereas the prefactor is increasing for intermediate values of t_q , and then decreasing again for larger t_q due to the smallness of the exponential factors.

An efficient prescreening, which exploits the sparsity of the $X^0(q)$, $X^v(q)$ matrices, and the $X^v(q)\mathbf{V}$ product therefore can significantly reduce the scaling of the computational cost w.r. to the molecular size N . It ties spatially the LMOs and PAOs related to the ERI of eq. (4.16) to those of the amplitudes, thus, consequently, all functions have to be spatially "close" to ϕ_i^{LMO} .

Accuracy of the discrete Quadrature

The accuracy of the discrete quadrature was investigated for the different distribution functions $f(x) = 1$ (uniform distribution), $f(x) = \Delta_{ij}^{\bar{a}\bar{b}}$ (genuine distribution of the denominators $\Delta_{ij}^{\bar{a}\bar{b}}$), and $f(x) = (\Delta_i^{\bar{a}})^2$ (distribution obtained via the addition theorem from the distribution of the denominators $\Delta_i^{\bar{a}}$). As already pointed out in the previous section the computational costs for generating $f(x) = \Delta_{ij}^{\bar{a}\bar{b}}$ and $f(x) = (\Delta_i^{\bar{a}})^2$ scale as $O(N^4)$ and $O(N^2)$, respectively. The former thus is too expensive for its use, while for the latter only an insignificant amount of time in comparison to the rest of the

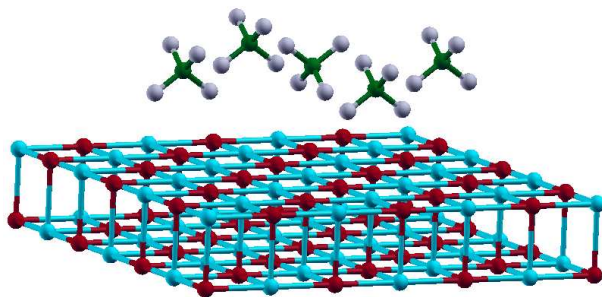


Figure 4.4: Two-layer MgO cluster, consisting of 98 atoms, with 5 adsorbed methane molecules. The distance between neighbouring Mg and O atoms was set to 2.105 Å. The methane molecules are placed on top of the Mg atoms in the dipole orientation. The distance between the carbon atoms and the surface was set to 3.25 Å and the C-H bond length to 1.0854 Å.

calculation has to be spent.

As test systems we have chosen (i) the dye dyad solvent cluster above (cf. Fig. 4.1), (ii) linear chains of polyglycine peptides $[\text{gly}]_n$, $\text{C}_{2n}\text{H}_{3n+2}\text{N}_n\text{O}_{n+1}$ (cf. Ref. 38), and (iii) a two-layer MgO cluster with five adsorbed methane molecules (cf. Fig. 4.4, such a system is studied in our group in the context of periodic LMP2 calculations of physisorption [102]). These systems represent three rather different situations for the application of the method. The results of these test calculations are compiled in Table 4.1. The relative deviations (in %) from the corresponding reference value based on $n_q = 10$ quadrature points are given for calculations involving $n_q = 2 \dots 7$ points. Ordinary, as well as augmented Boughton-Pulay (BP) domains (by all next nearest neighbour atoms) were used. As a criterion for the construction of the BP domains the default value of 0.98 was generally used. As AO basis sets the cc-pVDZ, aug-cc-pVDZ, and cc-pVTZ basis sets of Dunning were employed, together with the related fitting basis sets of Hättig and Weigend. A comparison of these relative deviations obtained at $n_q = 4$ or $n_q = 5$ between the different variants of $f(x)$ shows that the uniform distribution is inferior to $f(x) = \Delta_{ij}^{\bar{a}\bar{b}}$ and $f(x) = (\Delta_i^{\bar{a}})^2$, while the latter two show, as expected, nearly the same performance (shown for the $[\text{gly}]_6$ case). We therefore advocate the use of $f(x) = (\Delta_i^{\bar{a}})^2$ due to its much lower cost. For $n_q = 6$ or $n_q = 7$ all three distributions lead to well converged energies with deviations of a few μE_H from the $n_q = 10$ reference value. In contrast to the findings of Ref. 33 we did not find in all cases a systematic convergence pattern for $f(x) = \Delta_{ij}^{\bar{a}\bar{b}}$ and $f(x) = (\Delta_i^{\bar{a}})^2$. Since in Ref. 33 just one partic-

System	[gly] ₆			[gly] ₁₈						DA			CH ₄ /MgO
Basis	cc-pVDZ			cc-pVDZ		aug-cc-pVDZ		cc-pVTZ		cc-pVDZ			cc-pVDZ
Domains	BP			iext=1		BP		iext=1		BP			BP
<i>f</i> (<i>x</i>)	1	Δ ^{ab} _{<i>ij</i>}	(Δ ^a _{<i>i</i>}) ²	1	(Δ ^a _{<i>i</i>}) ²	(Δ ^a _{<i>i</i>}) ²	(Δ ^a _{<i>i</i>}) ²	1	(Δ ^a _{<i>i</i>}) ²	1	(Δ ^a _{<i>i</i>}) ²	(Δ ^a _{<i>i</i>}) ²	(Δ ^a _{<i>i</i>}) ²
Δ <i>E</i> ₁ ^a , %	1.20185	-0.36667	-0.36239	1.32132	-0.32443	-0.72008	-0.73212	1.41899	0.21044	8.85062	0.46403	0.45904	-1.41712
Δ <i>E</i> ₂ ^a , %	0.01256	0.00570	0.00645	0.00632	0.00625	-0.03598	-0.03753	0.15002	0.02522	-0.45237	0.06177	0.06055	-0.04778
Δ <i>E</i> ₃ ^a , %	-0.00303	-0.00049	-0.00029	-0.00293	-0.00019	-0.00358	-0.00404	-0.00006	0.00330	0.01707	0.00618	0.00612	0.00572
Δ <i>E</i> ₄ ^a , %	0.00007	-0.00004	-0.00002	0.00007	-0.00001	-0.00061	-0.00094	-0.00149	0.00011	-0.00157	0.00092	0.00090	0.00027
Δ <i>E</i> ₅ ^a , %	-0.00001	-0.00000	0.00001	0.00002	0.00002	-0.00037	-0.00064	0.00004	-0.00015	0.00021	0.00023	0.00022	-0.00019
Δ <i>E</i> ₇ ^a , %	0.00000	0.00000	0.00000	0.00000	-0.00004	-0.00009	-0.00015	-0.00005	0.00001	0.00002	0.00001	0.00001	0.00000
<i>E</i> _{<i>n</i><i>q</i>=10} ^a	-3.756888			-11.038798		-11.386892	-11.594812	-13.758256		-13.261057		-13.446021	-11.526849
<i>E</i> _{<i>n</i><i>q</i>=10} ^b	-3.756899			-11.038798		-11.386600	-11.594720	-13.758252		-13.261054		-13.446020	-11.526613
<i>E</i> _{LMP2} ^c	-3.748798			-11.036429		-11.404204	-11.605419	-13.751505		-13.235349		-13.439857	-11.430101

a) LT-DF-LMP2 calculation, B_P^{dk} defined in eq. (4.18) is restricted to $d \in [U(k)]$.

b) LT-DF-LMP2 calculation, no *a priori* restrictions apply for B_P^{dk} defined in eq. (4.18).

c) DF-LMP2 calculation.

Table 4.1: Convergence of the energy with respect to the number of points taken for the numerical Laplace quadrature. ΔE_n is the deviation from a reference calculation using 10 quadrature points, calculated as $\Delta E_n = \frac{E(N_q=n) - E(N_q=10)}{|E(N_q=10)|} \times 100\%$. The B_P^{dk} quantity defined in eq. (4.18) was *a priori* restricted to the united pair domains $[U(k)]$, except explicitly stated otherwise. The convergence has been analyzed for standard Boughton-Pulay domains [56] (denoted as BP) and Boughton-Pulay domains, extended by the nearest neighbours (denoted as iext=1). For the function $f(x)$, involved in optimizing the quadrature weights and points (4.23) the uniform (denoted as 1) and the true distribution of the denominator Δ_{ij}^{ab} energies (denoted as Δ_{ij}^{ab}) were tested, as well as the distribution defined as the “sum” of two Δ_i^a distributions (denoted as $(\Delta_i^a)^2$). Absolute energies are given in E_H . For details see Sect. 4.2.

ular example was examined we conclude that this behaviour cannot be anticipated generally.

LT-DF-LMP2 vs. DF-LMP2: energies and efficiency

The correlation energies as obtained with DF-LMP2 and LT-DF-LMP2 for the different test systems, domains, and basis sets, are included in Tables 4.1 and 4.2. For the present implementation based on DF the most severely truncated set of ERIs which is possible includes all LMO pairs and all PAOs within the related *united pair domains*,

$$(ck|dl) = \sum_p B_p^{ck} B_p^{dl}, \quad \forall k, \forall l, c \in [U(k)], d \in [U(l)]. \quad (4.33)$$

This corresponds to a much larger restricted local space than that of the local amplitudes, the latter being confined to the restricted local pair list and the related *pair domains*. The four-index ERIs $(ck|dl)$ are of course never constructed explicitly, cf. eqs.(4.20) and (4.22). Most of the calculations presented in Table 4.1 are based on such a restricted ERI set and it can be seen that the deviations from results of calculations based on the full ERI set are indeed very small. Without much higher cost though it is also possible to abandon any *a priori* restrictions on the ERIs altogether (only the calculation of the B_p^{ck} quantities are be affected), and all calculations reported in Table 4.2 actually employed the full ERI set.

It can be seen that LT-DF-LMP2 recovers for all basis sets (including the aug-cc-pVTZ basis, as calculations on smaller molecules reveal) apart from the aug-cc-pVDZ case a somewhat larger fraction of the correlation energy than DF-LMP2. This directly reflects the special feature of LT-DF-LMP2 discussed in the previous section, which, for the case of a larger set of ERIs than amplitudes always provides a better fit to the canonical amplitudes than DF-LMP2 does (the latter entirely disregards non-zero residual elements outside the amplitude domain boundaries). For ordinary BP domains LT-DF-LMP2 usually recovers about 0.2 % more of the correlation energy than DF-LMP2. The two-layer MgO cluster appears to represent a case where the BP domains are particularly insufficient. Here, LT-DF-LMP2 recovers almost 1 % more than DF-LMP2. With augmented BP domains the discrepancy decreases by almost an order of magnitude to 0.02 – 0.05 % (0.09 % for the MgO cluster). For the aug-cc-pVDZ basis set a rather large fraction of the functions has diffuse character. As a consequence, numerous energetically low-lying Rydberg like diffuse MOs may occur, which do not contribute significantly to the correlation energy,

System	[gly] ₁₈				DA				CH ₄ /MgO			
Basis	cc-pVTZ				aug-cc-pVDZ				cc-pVDZ			
<i>N</i> _{AO} , <i>N</i> _{AUX}	2974, 7593				2905, 8703				1738, 7028			
Domains	text=1				text=1				text=1			
	BP				BP				BP			
	text=1				text=1				text=1			
DF-LMP2												
<i>E</i> _{LOC} ⁽²⁾	-13.751505	-13.236139	-13.440706	-13.813185	-14.006510	-16.243006	-16.407678	-11.430101	-11.956126	-12.697749	-	
Min Mem. ^a /MW	377	70	221	298	889	318	1038	57	1166	134	2835	
No. of iter.	7	8	8	8	8	8	8	9	9	9	-	
CPU Time ^b /min												
ERIs/FCs	104	67	89	336	374	431	520	130	199	289	562	
ITER	13	10	20	51	118	67	172	13	109	36	-	
TOTAL	189	146	232	706	1232	914	1738	232	1108	585	-	
LT-DF-LMP2												
<i>E</i> _{LOC} ⁽²⁾	-13.758237	-13.261747	-13.446759	-13.793212	-13.991243	-16.279686	-16.416874	-11.526571	-11.967917	-12.693230	-12.869608	
CPU Time ^b /min												
SIMPLEX	4	1	1	5	6	9	9	1	1	2	2	
ERIs/FCs	200	120	127	609	636	734	784	181	232	365	534	
Q-POINT	31	21	27	93	124	183	235	25	64	58	163	
TOTAL(<i>n</i> _q = 5)	325	201	234	986	1134	1474	1733	281	488	598	1189	

^a Memory needed to hold the local amplitudes (1 MW = 8MByte).^b Intel Xeon 5150, 2.66 GHz

Table 4.2: DF-LMP2 and LT-DF-LMP2 correlation energies (in E_H) obtained for the individual test molecules with different basis sets and domains. For the LT-DF-LMP2 calculations five quadrature points were used. CPU times are also given for individual steps of the calculations.

even though the related denominators can be small. Since the LT-DF-LMP2 method is based on a least-squares fit of the canonical MP2 residual weighted by the inverse of the related denominators (*vide supra*) the importance of such amplitudes in the fit is overrated, which may lead to the observed behaviour.

The CPU times of the individual relevant steps of the DF-LMP2 and LT-DF-LMP2 calculations are compiled in Table 4.2. Comparing the overall times it can be seen that the efficiency of LT-DF-LMP2 is comparable to that of DF-LMP2. For small compact domains DF-LMP2 is quicker, for large extended domains LT-DF-LMP2 is faster. For the case of the MgO cluster with extended domains even a single quadrature point is cheaper than a single LMP2 iteration. For the same system a calculation within the aug-cc-pVDZ basis was not possible with the present DF-LMP2 implementation due to a memory bottleneck, whereas the same calculation could be easily performed with the LT-DF-LMP2 method, which has only very modest memory requirements.

Table 4.3 compares the orbital-unrelaxed LT-DF-LMP2 and DF-LMP2 dipole moments of [gly]₆ calculated with different basis sets. This shall serve as a first illustration for our discussion about LT-DF-LMP2 properties in the previous section. Ordinary BP domains were used for these calculations (with extended domains there would hardly be any visible difference), for the reference calculations the BP domains were extended with all centres within a range of 10 Bohr from the core BP domains. The LT-DF-LMP2 density matrices were calculated according to eq. (4.32), i.e., using the symmetrical approach. Evidently, even for non-extended BP domains the DF-LMP2 and LT-DF-LMP2 are very close with the latter being slightly closer to the reference value. This is most pronounced for the biggest basis set, for the two other basis sets the differences between LT-DF-LMP2 and DF-LMP2 are hardly noticeable. From this first preliminary example it appears that the simple symmetrical approach provides LT-DF-LMP2 properties which are at least as accurate as than those provided by

μ_α	cc-pVDZ			aug-cc-pVDZ			cc-pVTZ		
	rext=10	LMP2	LT	rext=10	LMP2	LT	rext=10	LMP2	LT
μ_Y	-0.00998	-0.00895	-0.00916	-0.00999	-0.00854	-0.00876	-0.01073	-0.01018	-0.01040
μ_Z	-0.03260	-0.03526	-0.03505	-0.03093	-0.03230	-0.03214	-0.02782	-0.03064	-0.02965

Table 4.3: DF-LMP2 and LT-DF-LMP2 correlation contributions to the dipole moment (in a.u.) for the case of [gly]₆ using different basis sets. The reference calculations were performed with extended domains by augmenting the BP domains (criterion 0.98) by all atoms within a range of 10 Bohr (rext=10). The LT-DF-LMP2 calculations were performed with 10 quadrature points and by using eq. (4.32) to calculate the correlated density matrix. The X-component of the dipole moment is zero due to symmetry.

the original DF-LMP2 method.

4.4 Conclusions

A new local method based on the Laplace transform ansatz of Almlöf is presented. As the previous local methods based on the local ansatz of Pulay the occupied and virtual orbital spaces are spanned by mutually orthogonal localized MOs and non-orthogonal projected AOs, respectively, and the set of wavefunction parameters (amplitudes) is *a priori* restricted. An implementation for local second-order Møller-Plesset perturbation theory is described, which is utilizing Density Fitting for factorizing the electron repulsion integrals. A detailed analysis of the relation between the original and the new Laplace based local method reveals that the two methods are complementary: The former corresponds to a projection of the canonical residual onto the *a priori* restricted local space with the requirement that this projection is exactly vanishing, and the latter to a least-squares minimization weighted with the inverse of the related energy denominators. The Laplace based local method generally recovers a slightly larger fraction of the correlation energy. Properties and energy gradients can also be calculated, gradients though at a somewhat higher cost compared to ordinary local MP2 due to an asymmetry in the related density matrices. The computational efficiency for calculating correlation energies is comparable for local MP2 and the Laplace based local method, the former being more efficient for calculations involving small –, the latter for calculations involving large domains. The primary purpose of this work though was not to present yet another efficient local MP2 method, but to investigate generally the usefulness of the Laplace transform ansatz in local methods with *a priori* restricted sets of wavefunction parameters.

Chapter 5

Integration Points for Laplace Transform

In electron correlation methods the energy denominators appear in the canonical formulation of perturbation theory within the Møller-Plesset partitioning. The Laplace transformation, suggested originally by Almlöf [45], is an attractive way to factorize this denominator, which is used in various methods like MP2 [33,46,93,95,98,99], MP4 [33], CC2 [103] and CCSD(T) [104]. The accuracy and cost of numerical quadrature for the Laplace transformation is of major concern.

Recently, Takatsuka *et al.* [105] suggested the minimax technique, previously developed for numerical evaluation of the Laplace representation of $1/x$ function, [106,107] to be employed in this context. The minimax approach has some nice features, such as uniformity of the error along the whole range, or alternating sign of the error possibly leading to an error cancellation. It was shown in Ref. 105 that it remarkably outperforms classical quadrature techniques like Gauss-Laguerre and Gauss-Legendre [98]. Unfortunately, the authors have not discussed the most commonly used Least-Square (LS) quadrature [33,46,93,95,104]. It is mentioned only briefly and only in conjunction with an (in fact not necessary, cf. Refs. 33,46) explicit treatment of the distribution of the denominators.

Conventionally, the roots and weights are obtained by minimizing the self-overlap of the quadrature error function, which corresponds to the LS optimization. Optionally, this function can be multiplied by a weight function $f(x)$ describing the actual distribution of the denominators, thus accentuating the energy regions where high accuracy of the quadrature is desirable. Calculating the real distribution of the denominators scales for MP2 quartically with the system size, which for large systems becomes expensive. Therefore, in practice the trivial choice $f(x) = 1$ is commonly

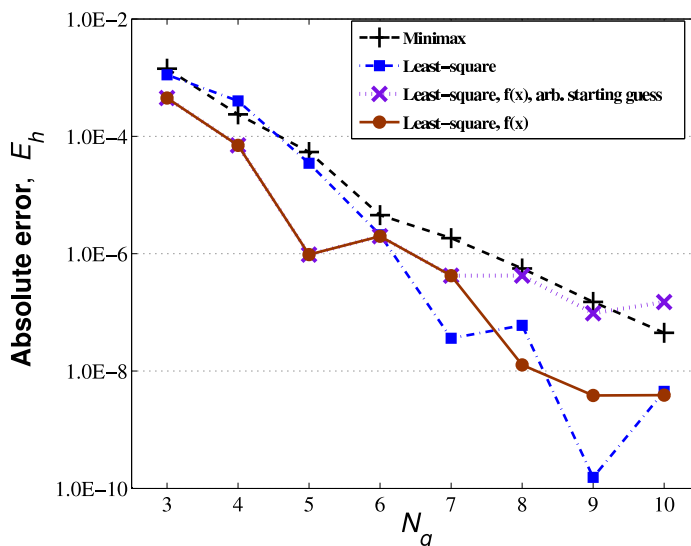


Figure 5.1: Error in valence-only correlation energy of benzene

utilized, which still is sufficiently accurate [33, 93]. However, it is also feasible to obtain a close approximation to the distribution $f(x)$ at the cost of $\mathcal{O}(N_{occ}N_{virt})$ (see Chp. 4 or Ref. 46). Specifically, the function $f(x)$, counting the number of denominators $\Delta_{ij}^{\bar{a}\bar{b}}$ in the vicinity of a certain x can be approximated by generating the histogram of all $\Delta_i^{\bar{a}}$ and then taking the product of two identical histograms $\Delta_i^{\bar{a}}$ and $\Delta_j^{\bar{b}}$. This inexpensive procedure relative to the subsequent MP2 calculation (see Chp. 4 or Ref. 46 for measured timings) completely eliminates the issue of the computationally unfavorable quartic denominators in the quadrature, brought up by Takatsuka *et al.* as an argument in favor of the minimax scheme. In principle the use of a histogram might introduce discontinuities in the potential surface, yet our tests indicate this effect to be insignificant.

The minimax is sometimes referred to as “best approximation” in the sense that the *possible* error in the approximated function is smaller than that from any other quadrature. However, when applied to the MP2 method, where *all* the approximated determinants are *accumulated* in the energy, the LS technique, which deals not with the maximal *possible*, but rather *integrated* error, seems to be at least not less adequate. Besides, the LS procedure similarly to the minimax tends to a uniform distribution of the error. However, it can sacrifice this uniformity in order to minimize the *integrated* error, which is more closely related to the MP2 energy.

To compare the performance of minimax and self-overlap optimizations we present results from Laplace-DF-LMP2 [46] calculations performed

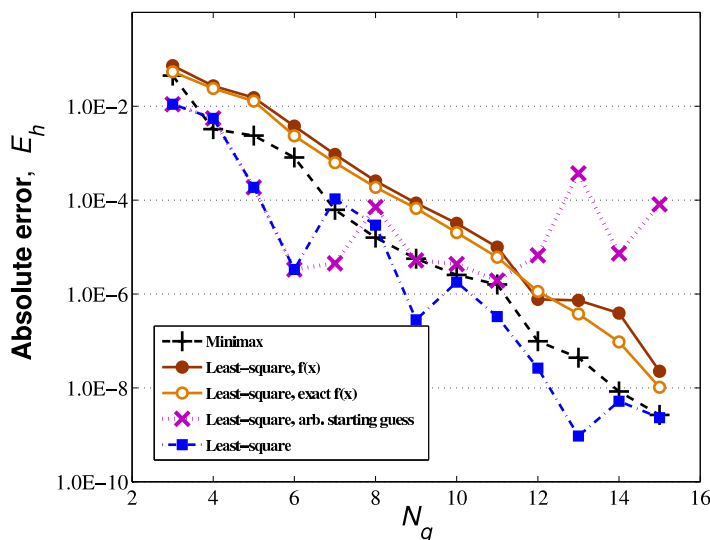


Figure 5.2: Error in all-electron correlation energy for benzene

for the benzene molecule, also considered by Takatsuka *et al.*. In all our calculations we used full domains such that the local MP2 reproduces the canonical MP2 correlation energies.

Fig. 5.1 displays the errors in the correlation energy of the different quadrature schemes for the most common valence-only case (aug-cc-pVTZ basis). Our minimax results coincide with those from Ref. 105. It is evident that the LS fit employing the approximated distribution function $f(x)$ is on average slightly better than the LS fit with $f(x) = 1$ and competitive to the minimax technique. As a second example we consider an all-electron calculation of benzene in the aug-cc-pCVTZ basis (Fig. 5.2). When excitations from the core orbitals are included the range R for the possible denominators

$$R = \frac{\epsilon_{\max} - \epsilon_{\min}}{\epsilon_{\text{LUMO}} - \epsilon_{\text{HOMO}}} \quad (5.1)$$

noticeably increases (278 vs 56 in the valence-only case) (ϵ are the orbital energies). The worse performance of the weighted fit (note that the exact and the approximate $f(x)$ yield basically the same result) can be attributed to the non-uniformity of the integrals with core and valence orbitals, which makes the denominator-only distribution not an adequate estimate of the important energy regions. On the other hand, the unweighted LS fit performs quite well and for most of the points is somewhat better than the minimax.

For these calculations the starting guesses reported in Ref. 21 of Ref. 105 were used. It turned out that the choice of good starting guesses is really

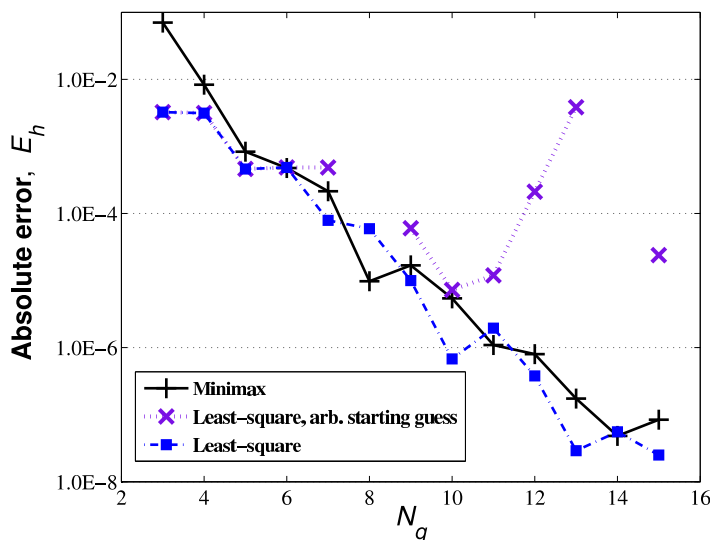


Figure 5.3: Error in all-electron correlation energy for ozone. For $N_q = 8$ and $N_q = 14$ the least-square procedure with an arbitrary starting guess did not converge.

essential to obtain high accuracy, both for the LS and the minimax method. This is demonstrated by performing additional calculations where the LS optimization was started from a set of roots equidistantly distributed over the range $[0, 1]$ (the minimax equations with such starting guesses could not be converged at all). As is evident from Fig. 5.2 in all-electron case not even 10^{-4} H accuracy can be reached, regardless, how many integration points N_q are used. A proper starting guess (for the LS procedure) is particularly important for very high accuracy, or in cases with a large range R (big basis sets, all-electron calculations). Up to $N_q = 6$ the initial guess has little effect on the outcome of the LS fit, while for a larger number of optimization points non-global optimization procedures may converge to a local rather than the global minimum and good starting guesses become vital.

Additional calculations were performed for the ozone molecule (all-electron calculation in the aug-cc-pCVQZ basis, another test case of Ref. 105 with an extensive denominator range $R = 2058$) and for a polypeptide chain involving 12 glycine monomers (local valence-only calculation in the cc-pVTZ basis, $R = 32.3$). The resulting error curves, provided in Fig. 5.3 and 5.4, are similar to those of the corresponding benzene calculations.

To conclude, the claim made in Ref. 105 for the minimax to be the "best" quadrature scheme w.r. to accuracy and efficiency is not supported by our calculations on these test molecules. From the Figs. 5.1-5.4 it is evident that, apart from few points in the benzene valence-only case, the LS method with $f(x) = 1$ provides on average the same or better

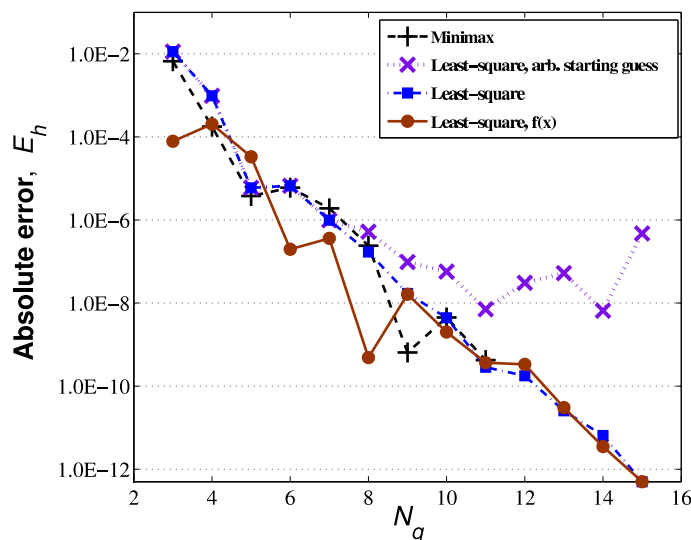


Figure 5.4: Error in valence-only correlation energy for a poly-glycine chain comprising 12 units

accuracy relative to the minimax, and in the valence only calculations the inexpensive weighted LS technique improves the results further. In all-electron calculations the distribution of the integral values, entering the amplitude expression, might become important, which reflects in the better performance of the uniformly weighted quadrature compared to the denominator-only weighted one. On the other hand, the weighted LS method allows to include also the integral weighting [33], which might be not very expensive if density fitting and Schwarz estimates are used. Such a weighting is not straight-forward in the minimax scheme.

Chapter 6

Local CC2 with Laplace Transform

6.1 Introduction

In chapters 2 and 3 (Refs. 10,89) the restricted pair lists and domains for the amplitude response were determined by analysis of un-truncated wavefunctions obtained at a simpler level of theory, i.e., CCS wavefunctions. However, such an approach is bound to fail if the simpler level of theory provides qualitative wrong wavefunctions for the individual excited states. A further flaw of our previous local response method was the fact, that it functioned exclusively as a single-state method, using a root-homing procedure to follow the desired state defined by the CCS start vector, during the Davidson diagonalization. As a consequence there was a rather strong dependence on the initial un-truncated wavefunction, rendering the method as somewhat fragile.

In this chapter we present a new local response method which avoids all these shortcomings of the previous approach. It utilizes the Laplace transform [33,45,92] to decompose the energy denominators occurring in the double-doubles block of the CC2 Jacobian. In a previous study we have already explored the use the Laplace transform in the context of local correlation methods for the case of Local Møller-Plesset perturbation theory of second order (LMP2) (Chps. 4 and 5) [46,108]. Due to the fact that the PAO domains (spanning the pair-specific virtual subspace) naturally have lower rank than the full virtual space this is more involved than for AO Laplace methods [93,95,109,110]. The use of the Laplace transform ansatz in the context of local CC2 linear response theory allows for a partitioning of the CC2 eigenvalue problem exactly as in the case of the canonical theory [27], yet with integrals and amplitudes in a local, rather than a delocalized canonical orbital basis. Hence, an *effective* eigenvalue

problem involving only the un-truncated singles vector has to be solved and the doubles amplitude part entering the effective Jacobian \times singles vector product can be computed on-the-fly and does not enter the Davidson diagonalization. This, in turn, can be exploited to devise a multi-state diagonalization procedure with much improved convergence behavior, which still maintains state-specific pair domains for the individual states. Furthermore, in combination with Density Fitting of the ERIs it is possible without much effort to utilize the un-truncated information of diagonal pair amplitudes for constructing suitable pair lists and domains for the pair amplitude response in an adaptive way, i.e., during the diagonalization. Hence the truncation of the pair amplitude response is specified by analyzing directly the object which is to be approximated. The multi-state treatment of several states, together with the adaptive determination of pair lists and domains for the amplitude response repairs the shortcomings of our previous approach. The new method is much less dependent on the initial un-truncated wavefunction (hardly more than canonical CC2 response) and thus much more robust.

6.2 Theory

The (non-symmetric) CC2 Jacobian, which has to be diagonalized to get the CC2 excitation energies $\omega_{\bar{m}}$ of the individual states $\Psi^{\bar{m}}$, can be written as

$$A_{\mu_i \nu_j} = \begin{pmatrix} \langle \tilde{\mu}_1 | [\hat{H}, \tau_{\nu_1}] \exp(T_2) | 0 \rangle & \langle \tilde{\mu}_1 | [\hat{H}, \tau_{\nu_2}] | 0 \rangle \\ \langle \tilde{\mu}_2 | [\hat{H}, \tau_{\nu_1}] | 0 \rangle & \langle \tilde{\mu}_2 | [F, \tau_{\nu_2}] | 0 \rangle \end{pmatrix}, \quad (6.1)$$

where the τ_{μ_i} are covariant one- or two-particle excitation operators, and the $\langle \tilde{\mu}_i |$ contravariant configuration state functions (CSFs) ($i = 1, 2$ is the related excitation class). H and F denote the (normal ordered) Hamiltonian and Fock operator, respectively. Decoration of an operator with a hat implies similarity transformation of that operator with $\exp(T_1)$, i.e., $\hat{H} = \exp(-T_1) H \exp(T_1)$. T_1 and T_2 represent the singles and doubles cluster operators involving the precomputed ground state amplitudes.

In canonical CC2 response theory the double-doubles block $A_{\mu_2 \nu_2}$ is diagonal [21]. Consequently, the right eigenvalue problem can be partitioned

as

$$\begin{aligned}
A_{\mu_1\nu_1}^{\text{eff}}(\omega_{\bar{m}})R_{\nu_1}^{\bar{m}} &= A_{\mu_1\nu_1}R_{\nu_1}^{\bar{m}} + A_{\mu_1\xi_2}\frac{A_{\xi_2\nu_1}R_{\nu_1}^{\bar{m}}}{\omega_{\bar{m}} - \Delta\epsilon_{\xi_2}} \\
&= \omega_{\bar{m}}M_{\mu_1\nu_1}R_{\nu_1}^{\bar{m}}, \\
\text{with } \Delta\epsilon_{\mu_2} &= \Delta\epsilon_{\bar{i}\bar{j}}^{\bar{a}\bar{b}} = \epsilon_{\bar{a}} + \epsilon_{\bar{b}} - \epsilon_{\bar{i}} - \epsilon_{\bar{j}},
\end{aligned} \tag{6.2}$$

and an analogous equation holds for the left eigenvalue problem. The matrix \mathbf{M} represents the metric of contra- and covariant CSFs. Here and in the following canonical orbitals are indexed by characters decorated with a bar, i.e., $\bar{i}, \bar{j}, \bar{k}, \dots$ and $\bar{a}, \bar{b}, \bar{c}, \dots$ denote canonical occupied and virtual orbital indices, respectively. For LMOs and PAOs, on the other hand, we use un-bared indices. Furthermore, the Einstein convention is employed, i.e., repeated indices are summed up. Explicit summations are put in the equations only where we find it useful for clarity.

Utilizing the Laplace transform identity $1/x = \int_0^\infty \exp(-xt)dt$ eq. (6.2) can also be written as

$$\begin{aligned}
A_{\mu_1\nu_1}^{\text{eff}}(\omega_{\bar{m}})R_{\nu_1}^{\bar{m}} &= \omega_{\bar{m}}M_{\mu_1\nu_1}R_{\nu_1}^{\bar{m}} \\
&= A_{\mu_1\nu_1}R_{\nu_1}^{\bar{m}} - A_{\mu_1\xi_2} \int_0^\infty dt e^{-\Delta\epsilon_{\xi_2}t} e^{\omega_{\bar{m}}t} A_{\xi_2\nu_1}R_{\nu_1}^{\bar{m}} \\
&\approx A_{\mu_1\nu_1}R_{\nu_1}^{\bar{m}} - A_{\mu_1\xi_2} \sum_{q=1}^{n_q} w_q e^{-\Delta\epsilon_{\xi_2}t_q} e^{\omega_{\bar{m}}t_q} A_{\xi_2\nu_1}R_{\nu_1}^{\bar{m}},
\end{aligned} \tag{6.3}$$

where the t_q and w_q are the points and corresponding weights of the numerical Laplace integration. Only a few points are required for a sufficiently accurate quadrature (cf. section 6.3). Points and related weights can be determined by a Simplex optimization procedure, as described in Refs. 46,108.

Eq. (6.3) is the springboard for an *orbital invariant* formulation of CC2 response theory, which also holds for a non-canonical local LMO/PAO basis and thus allows to exploit the sparsity in integrals, amplitudes, and diagrams, without giving away the possibility to partition the eigenvalue problem.

Adopting the formalism devised previously for Laplace transformed

LMP2 [46] eq. (6.3) can be cast in the form

$$\begin{aligned}
A_{\mu_1\nu_1}^{\text{eff}}(\omega_{\bar{m}})R_{\nu_1}^{\bar{m}} &= A_{\mu_1\nu_1}R_{\nu_1}^{\bar{m}} - A_{\mu_1iajb} \sum_{q=1}^{n_q} \text{sgn}(w_q)e^{\omega_{\bar{m}}t_q} \\
&\times Y_{ac}^v(q)Y_{bd}^v(q)\left(A_{ckdl\nu_1}R_{\nu_1}^{\bar{m}}\right)X_{ki}^o(q)X_{lj}^o(q) \\
&= \omega_{\bar{m}}M_{\mu_1\nu_1}R_{\nu_1}^{\bar{m}}, \tag{6.4}
\end{aligned}$$

where the doubles index ξ_2 of the $A_{\mu_1\xi_2}$ and $A_{\xi_2\nu_1}$ blocks of the Jacobi matrix is written explicitly in terms of LMO and PAO indices. The quadrature point dependent transformation matrices,

$$\begin{aligned}
X_{ij}^o(q) &= W_{ii}^\dagger e^{(\epsilon_i - \epsilon_F)t_q + \frac{1}{4} \ln|w_q|} W_{ij}, \\
X_{ab}^v(q) &= Q_{aa}^\dagger e^{(-\epsilon_a + \epsilon_F)t_q + \frac{1}{4} \ln|w_q|} Q_{ab}, \\
Y_{ab}^v(q) &= V_{ac}X_{cd}^v(q)V_{db}^\dagger, \tag{6.5}
\end{aligned}$$

correspond to those introduced previously (eq. (4.17)) with the slight deviation that the weight w_q here is incorporated into the exponential. It turns out that this is numerically more stable for larger n_q , where negative t_q with small w_q or large t_q and w_q sometimes do occur. In eq. (6.5) the transformation matrices \mathbf{W} and \mathbf{Q} , and the matrix \mathbf{V} do appear. \mathbf{W} is the usual unitary transformation matrix specified by the chosen localization criterion (Boys [54], Pipek-Mezey [55], *etc.*) and transforms the canonical occupied orbitals ϕ_i^{CAN} to LMOs ϕ_i^{LMO} . The matrix \mathbf{Q} , on the other hand, is defined as

$$\mathbf{Q} = \mathbf{C}^{v\dagger} \mathbf{S}_{\text{AO}} \tag{6.6}$$

(with \mathbf{C}^v and \mathbf{S}_{AO} representing virtual block of the canonical MO coefficient matrix and AO overlap matrix, respectively), transforms canonical virtuals to PAOs. It has the property $\mathbf{Q}^\dagger \mathbf{Q} = \mathbf{S}_{\text{PAO}}$ (with \mathbf{S}_{PAO} being the metric of the PAOs). The matrix \mathbf{V} , finally, is a pseudo-inverse of \mathbf{S}_{PAO} (cf. eq. (4.11)). \mathbf{V} is obtained by (i) diagonalizing \mathbf{S}_{PAO} , (ii) inverting the elements of the diagonal matrix so obtained, which are above a given threshold defining redundancies, and zeroing the remaining ones, and (iii) back-transforming the resulting diagonal matrix. For the amplitude response restricted to pair domains, as done at a later stage, \mathbf{V} corresponds to a pseudo-inverse of *the corresponding block* of the PAO metric $\mathbf{S}_{\text{PAO}}^{ij}$ and thus is (along with \mathbf{Y}^v) *pair specific*.

$\epsilon_F = (\epsilon_{\text{HOMO}} + \epsilon_{\text{LUMO}})/2$ appearing in the exponentials, cancels in eq. (6.4), but ensures that the individual exponential factors are always smaller

than one (for positive t_q). Since the excitation energy ω , as well as the quadrature points t_q are not large the evaluation of $e^{\omega \bar{m} t_q}$ in (6.4) does not cause any numerical problem either. For a detailed derivation and discussion of the Laplace transformation matrices in eq. (6.5) we refer to chapter 4 (Ref. 46).

6.2.1 Direct diagonalization of the Jacobian

The effective singles eigenvalue problem is solved iteratively using a Davidson method [60] generalized to non-symmetric matrices [61]. Since the singles remain un-truncated in our local approach the Davidson subspace is spanned by basis vectors $u_a^i(m)$ in canonical orbital basis. The matrix-vector product $v_{\mu_1}(m) = A_{\mu_1 \nu_1}^{\text{eff}}(\omega_{\bar{m}}) U_{\nu_1}(m)$, on the other hand, is computed in the local basis, thus

$$\begin{aligned} u_a^i(m) &= W_{ii}^\dagger u_a^{\bar{i}}(m) Q_{\bar{a}c} V_{ca}^\dagger, \\ v_a^i(m) &= A_{aijb}^{\text{eff}}(\omega_{\bar{m}}) u_b^j(m), \\ v_a^{\bar{i}}(m) &= Q_{\bar{a}c} V_{ca}^\dagger v_a^i(m) W_{ii}^\dagger. \end{aligned} \quad (6.7)$$

Here, $m = 1 \dots N_{\text{Dav}}$ runs over all present basis vectors of the Davidson subspace, while $\bar{m} = 1 \dots N_{\text{stat}} \leq N_{\text{Dav}}$, as already defined above, just runs over all states of the multi-state calculation. Furthermore, $u_a^i(m)$ belongs to a particular state $\Psi^{\bar{m}}$, i.e., is calculated according to eqs. (6.11) and (6.12) for that state index \bar{m} . Initially, the CCS singles amplitude eigenvectors are employed as the first N_{stat} basis vectors of the Davidson subspace, along with the related CCS eigenvalues in the matrix-vector product according to eq. (6.4).

With the matrix-vector products $v_a^{\bar{i}}(m)$ at hand the small effective Jacobian living in the Davidson subspace,

$$A'_{mn}(\omega_{\bar{n}}) = \tilde{u}_a^{\bar{i}}(m) v_a^{\bar{i}}(n), \text{ with } \tilde{u}_a^{\bar{i}}(m) = 2u_a^{\bar{i}}(m) \quad (6.8)$$

can be set up. Solving the eigenvalue problem

$$\mathbf{A}' \mathbf{c} = \mathbf{S}' \mathbf{c} \omega', \text{ with } S'_{mn} = \tilde{u}_a^{\bar{i}}(m) u_a^{\bar{i}}(n) \quad (6.9)$$

yields the approximation

$$R_a^{\bar{i}}(\bar{m}) = u_a^{\bar{i}}(n) c_{n\bar{m}} \quad (6.10)$$

and $\omega'_{\bar{m}}$ to the eigenvector and eigenvalue of $\mathbf{A}^{\text{eff}}(\omega_{\bar{m}})$ for state $\Psi_{\bar{m}}$ with residual

$$r_a^{\bar{i}}(\bar{m}) = v_a^{\bar{i}}(n) c_{n\bar{m}} - \omega'_{\bar{m}} R_a^{\bar{i}}(\bar{m}). \quad (6.11)$$

It is understood that here and in the following equations (6.12) and (6.13) the state index \bar{m} is excluded from the summations. From the residual vectors corresponding to the individual states further basis vectors (for an enlarged Davidson subspace) are obtained via first-order perturbation theory as

$$u_{\bar{a}}^{\bar{i}}(m) = \frac{r_{\bar{a}}^{\bar{i}}(\bar{m})}{\epsilon_{\bar{i}} - \epsilon_{\bar{a}} + \omega'_{\bar{m}}}, \quad (6.12)$$

and from those the related matrix-vector products $v_{\mu_1}(m)$.

If the norm of a residual vector $r(\bar{m})$ exceeds $|\omega_{\bar{m}} - \omega'_{\bar{m}}|$ then the related eigenvector $\mathbf{R}(\bar{m})$ has converged in the present macro-iteration ($\omega_{\bar{m}}$ is the (previous) approximation to the related eigenvalue used in the matrix-vector product according to eq. (6.4)). If all eigenvectors have converged a *refresh* of the Davidson procedure is carried out, i.e., the Davidson subspace is reset to comprise just N_{stat} basis vectors calculated as

$$u_{\bar{a}}^{\bar{i}}(\bar{m}) = R_{\bar{a}}^{\bar{i}}(\bar{m}) + \frac{r_{\bar{a}}^{\bar{i}}(\bar{m})}{\epsilon_{\bar{i}} - \epsilon_{\bar{a}} + \omega'_{\bar{m}}}, \quad (6.13)$$

$\omega_{\bar{m}}$ is set to $\omega'_{\bar{m}}$, and a new macro-iteration is commenced.

If for all eigenvectors the norm of the corresponding residuals and $|\omega_{\bar{m}} - \omega'_{\bar{m}}|$ are smaller than 0.001 then the Davidson diagonalization has converged and the eigenvectors and corresponding eigenvalues are converged further individually using a Direct Inversion of the Iterative Subspace (DIIS) scheme [59, 111]. In the DIIS scheme used here the original normalization constraint of the DIIS coefficients $\sum_i c_i = 1$ is replaced by a normalization constraint for the new approximation to the eigenvector. Hence the error functional to be minimized is

$$f(c) = \sum_{ij}^n c_i \langle \Delta \mathbf{R}_i | \Delta \mathbf{R}_j \rangle c_j \quad (6.14)$$

$$- \lambda \sum_{ij}^n \left(c_i \langle \mathbf{R}_i + \Delta \mathbf{R}_i | \mathbf{R}_j + \Delta \mathbf{R}_j \rangle c_j - 1 \right),$$

where \mathbf{R}_i is the i -th DIIS approximation to the eigenvector $\mathbf{R}(\bar{m})$, $\Delta \mathbf{R}_i$ its update, calculated according to eq.(6.12), and n the actual size of the DIIS subspace. Minimization of eq. (6.14) w.r. to the DIIS coefficients yields the eigenvalue equation

$$\mathbf{Bc} = \mathbf{Sc}\lambda, \text{ with } B_{ij} = \langle \Delta \mathbf{R}_i | \Delta \mathbf{R}_j \rangle \quad (6.15)$$

$$\text{and } S_{ij} = \langle \mathbf{R}_i + \Delta \mathbf{R}_i | \mathbf{R}_j + \Delta \mathbf{R}_j \rangle.$$

Positive definiteness of \mathbf{S} is enforced by correcting small negative eigenvalues (which may occur due to numerics) to small positive ones. The eigenvectors \mathbf{c} corresponding to the lowest λ are chosen as the new set of DIIS coefficients and the new approximation to $\mathbf{R}(\bar{m})$ is calculated as

$$\mathbf{R}_{n+1} = \sum_i^n (\mathbf{R}_i + \Delta \mathbf{R}_i) c_i. \quad (6.16)$$

For the case that the lowest λ becomes very small ($< 10^{-16}$) and the second lowest λ still is small enough the eigenvector corresponding to the latter is chosen as the new set of DIIS coefficients. This strategy helps to avoid linear dependencies in the DIIS space (cf. Ref. 112).

The new approximation to the excitation energy $\omega_{\bar{m}}$ is calculated as the Rayleigh quotient

$$\omega^{n+1} = \frac{\langle \tilde{\mathbf{R}}_{n+1} | \mathbf{v}_{n+1} \rangle}{\langle \tilde{\mathbf{R}}_{n+1} | \mathbf{R}_{n+1} \rangle}, \text{ with } \mathbf{v}_{n+1} = \mathbf{A}^{\text{eff}}(\omega^n) \mathbf{R}_{n+1} \quad (6.17)$$

6.2.2 The right matrix-vector product

The right transform of the LCC2 Jacobian $\mathbf{v}_{\mu_1}(m) = A_{\mu_1 \nu_1}^{\text{eff}}(\omega_{\bar{m}}) U_{\nu_1}(m)$ is computed in the local basis. The doubles amplitude response is truncated according to restricted pair lists and domains, which are adapted on-the-fly in the course of the Davidson diagonalization (*vide infra*). As in our previous work [10, 89] density fitting is employed to decompose the four-index ERIs in three-index objects, i.e.,

$$(pq|\hat{r}s) = (pq|P)\hat{c}_{rs}^P, \text{ with } \hat{c}_{rs}^P = (J^{-1})_{PQ} (Q|\hat{r}s), \quad (6.18)$$

with P, Q indexing the auxiliary fitting functions, while p, q, r, s are general (occupied or virtual) molecular orbitals. $J_{PQ} = (P|Q)$ is the Coulomb metric of the auxiliary fitting functions. Here and in the following all objects decorated with hat involve dressed integrals (produced by the similarity transform of the related operators with $\exp(T_1)$, *vide supra*), cf. eqs. (2.7-2.9). For example, \hat{c}_{pq}^P and c_{pq}^P represent the fitting coefficients involving dressed three-index integrals $(P|\hat{p}q)$, and bare integrals $(P|pq)$, respectively.

The final working equation for $\mathbf{v}_{\mu_1}(m)$ is identical to eq. (2.20), i.e.,

$$\begin{aligned} v_a^i = & \hat{f}_{ac} u_c^i + S_{aa'} \left(\tilde{U}_{a'c}^{ik} \hat{f}_{kc} - u_{a'}^k \hat{f}_{ki} \right) - \hat{c}_{ki}^P \hat{Y}_{ak}^P \\ & + 2(\hat{c}_{ai}^P + V_{ia'}^P S_{a'a}) b_P + W_{ic}^P (ac|P) - S_{aa'} W_{ka'}^P (ki|P) \\ & - S_{aa'} \left(u_{a'}^k V_{ic}^P (kc|P) + V_{ka'}^P Y_{ki}^P + \tilde{T}_{a'c}^{ik} x_{kc} \right), \end{aligned} \quad (6.19)$$

with the intermediates

$$\begin{aligned} Y_{ij}^P &= (P|ic)u_c^j, \quad \hat{Y}_{ai}^P = (P|\hat{a}c)u_c^i, \quad b_P = (P|kc)u_c^k, \\ x_{ia} &= c_{ka}^P Y_{ik}^P, \\ V_{ia}^P &= \tilde{T}_{ac}^{ik} c_{kc}^P, \quad W_{ia}^P = \tilde{U}_{ac}^{ik} c_{kc}^P, \end{aligned} \quad (6.20)$$

and the object U_{μ_2} , defined in canonical basis as

$$U_{\mu_2} = \frac{A_{\mu_2 \nu_1} U_{\nu_1}(m)}{\omega_{\bar{m}} - \Delta \epsilon_{\mu_2}}. \quad (6.21)$$

The $\tilde{\mathbf{T}}^{ij} = 2\mathbf{T}^{ij} - \mathbf{T}^{ji}$ is the contravariant CC2 amplitude matrix of pair ij , and $\tilde{\mathbf{U}}^{ij}$ is analogously defined. The evaluation of the quantities V_{ia}^P and W_{ia}^P in eq. (6.20) nominally scales as $\mathcal{O}(\mathcal{N}^5)$ with molecular size \mathcal{N} , yet by virtue of the local approximation imposed on the (ground state) CC2 amplitudes T_{μ_2} , and on U_{μ_2} the summation and index ranges in these expressions are restricted to pair lists and domains (cf. eq. (2.13)), eliminating this computational bottleneck. Note that for the method presented in chapter 2 (Ref. 10) the object U_{μ_2} has a different meaning and stands for the doubles basis vector of the Davidson subspace. Here, by virtue of the Laplace trick it is possible to partition the eigenvalue problem also in the local basis, hence no doubles basis vectors are required to span the Davidson subspace. Instead, U_{μ_2} directly enters the effective Jacobian \times singles basis vector product according to eqs. (6.2,6.3). It can directly be calculated as

$$\begin{aligned} U_{ab}^{ij} &= -V_{ac}^{ij} V_{bd}^{ij} \left(1 + \mathcal{P}(ij)\mathcal{P}(cd)\right) \sum_q^{n_q} \text{sgn}(w_q) e^{\omega_{\bar{m}} t_q} \\ &\quad \times X_{ce'}^v(q) V_{e'e}^{\dagger} X_{df'}^v(q) V_{f'f}^{\dagger} \left(\hat{B}_{ek}^P \hat{c}_{fl}^P\right) X_{ki}^o(q) X_{lj}^o(q), \\ &= V_{ac}^{ij} V_{bd}^{ij} \tilde{U}_{cd}^{ij} \end{aligned} \quad (6.22)$$

with the permutation operator $\mathcal{P}(pq)$ (permuting the orbital indices p and q), and

$$\hat{B}_{ai}^P = \hat{Y}_{ai}^P - S_{aa'} u_{a'}^k (ki|P). \quad (6.23)$$

In eq. (6.22) we have implicitly defined the object \tilde{U}_{μ_2} for later use. Furthermore, the specificity of the pseudo-inverse \mathbf{V} on the LMO pair ij is explicitly indicated, and it is understood that the summation does not run over the repeated indices i, j . The index ranges a, b, c, d thus are restricted to the individual pair domains $[ij]$, and the pair index ij is confined to the

restricted pair list (*vide infra*). Furthermore, as was shown in chapter 4 (Ref. 46) the Laplace transformation and pseudo-inverse matrices are all sparse, thus extensive prescreening is applied to the individual steps of evaluating eq. (6.22). The 3-index objects \hat{B}_{ek}^P and $\hat{C}_{fl'}^P$, of course, are transformed individually and just assembled to the four-index object for the individual pairs where the domain restrictions apply.

6.2.3 Local approximations for excited states

In the previous work the restricted pair lists and domains for the amplitude response were determined initially by analysis of the un-truncated eigenvectors of the CCS Jacobian and kept fixed during the response calculation [10, 89]. This was a severe flaw of the method making it frail due to the dependence on the quality of the initial CCS wavefunction. In the method presented here the domains and restricted pair lists for the object U_{μ_2} are (re)determined on-the-fly for each Davidson refresh. This can be done by examining the current singles Davidson basis vector $U_{\mu_1}(\bar{m})$, which, at the refresh, is an approximation to the singles part of the eigenvector of the related state (cf. eq. (6.13)) by employing a scheme analogous to that used previously [10, 89]. Alternatively, domains and pair lists for $U_{\mu_2}(\bar{m})$ could be obtained directly by analysis of the doubles object itself, i.e., of its *unrestricted* diagonal pair part U_{ab}^{ii} . The latter is calculated from eq. (6.22) for all diagonal pairs and full domains. Since U_{ab}^{ii} is a three-index object its evaluation, in spite of full domains, is not too expensive. Again, at the refresh, $U_{\mu_2}(\bar{m})$ is an approximation to the doubles part of the eigenvector of the Jacobian.

A Löwdin alike analysis of U_{ab}^{ii} ,

$$d_A^i = \sum_{a \in [A]} S_{ab}^{\frac{1}{2}} U_{bc}^{ii} S_{cc'} U_{c'd}^{ii} S_{da}^{\frac{1}{2}}, \quad (6.24)$$

condenses the information to individual LMOs i and centers A . Again, it is understood that the summation does not run over the repeated index i . d_A^i then is normalized to unity, i.e., $\sum_{i \in A} d_A^i = 1$.

As in chapters 2 and 3 (Refs. 10, 89) a set of *important* LMOs is specified for each state \bar{m} , which then is used to construct the restricted list of pairs for $U_{\mu_2}(\bar{m})$. The important LMOs are determined by (i) summing up d_A^i over the centers A , (ii) resorting the resulting object in order of descending size, (iii) considering all LMOs i as important until the sum over i reaches the threshold κ_e set in the input. After that, the d_A^i is normed and resorted for individual LMOs i .

To truncate the PAO ranges of $U_{\mu_2}(\bar{m})$ state specific *LMO domains* are constructed, which then are unified to state specific *pair domains*. In a first step, initial LMO domains are generated by just adopting the corresponding ground-state LMO domains, and, for the important LMOs, by augmenting the latter by centers A until the sum $\sum_A d_A^i$ reaches a certain intermediate threshold. These rough LMO domains are refined thereafter by employing a least-squares optimization reminiscent of the Boughton-Pulay procedure [56]. The functional

$$f(U_{ab}^{ii}) = \int (\phi'_i - \phi_i^{\text{full}})^2 d\mathbf{r}, \text{ with} \\ \phi'_i = \sum_{abcd \in [ii]} \varphi_c \varphi_d V_{ca}^{ii} V_{db}^{ii} \bar{U}_{ab}^{ii} \quad (6.25)$$

is minimized w.r. to the elements of the restricted $U_{\mu_2}(\bar{m})$ in local basis, yielding

$$df(U_{ab}^{ii})/dU_{ab}^{ii} = 0 = 2 \sum_{cdc' d' \in [ii]} S_{ac} S_{bd} V_{cc'}^{ii} V_{dd'}^{ii} \bar{U}_{c'd'}^{ii} \\ - 2 \sum_{cdc' d'} S_{ac} S_{bd} V_{cc'} V_{dd'} \bar{U}_{c'd'}^{ii}. \quad (6.26)$$

In eq. (6.25) the φ_c, φ_d are PAOs of the (diagonal) pair domain $[ii]$. ϕ_i^{full} and ϕ'_i represent, for a given excited state \bar{m} , the whole double excitation from the LMO i for un-truncated and pair domain-truncated $U_{\mu_2}(\bar{m})$, respectively. Eq. (6.26) delimitates the matrices \mathbf{V}^{ii} to pseudo-inverses of the PAO overlap matrices for pair domain $[ii]$ (cf. eq. (4.10)). Thus the optimal U_{ab}^{ii} (restricted to pair domain $[ii]$) are obtained by choosing \mathbf{V}^{ii} as a pseudo-inverse of the related $[ii]$ domain part of \mathbf{S} . Expanding eq. (6.25) and utilizing eq. (6.26), as well as the definition of the pseudo-inverse (eq. (4.11)) yields

$$f(U_{ab}^{ij}) = D_{\text{full}}^i - D^i, \quad D^i = \sum_{abcd \in [ii]} \bar{U}_{ab}^{ii} V_{ac}^{ii} V_{bd}^{ii} \bar{U}_{cd}^{ii}, \quad (6.27)$$

with D_{full}^i corresponding to unrestricted summation over the PAOs. So, in the domain construction approach proposed here the initial rough LMO domains are augmented by further centers, one by one, according to the ordered list, until D^i/D_{full}^i exceeds the domain threshold set in the input. After each addition of a center \mathbf{V}^{ii} is re-calculated to get the corresponding new D^i .

Since the $U_{\mu_2}(\bar{m})$, truncated according to state specific pair lists and domains, do not enter the Davidson diagonalization, multi-state calculations are easily possible. Basically, the restricted pair lists and domains of $U_{\mu_2}(\bar{m})$ are re-determined at each Davidson refresh. A further criterion for carrying out a refresh (apart from the norm of the residual vector, cf. section 6.2.1) is the overlap $\sigma_{\bar{m}\bar{m}'} = S'_{\bar{m}\bar{m}'} c_{n\bar{m}'}$ between the first Davidson basis vector $\mathbf{U}(\bar{m})$ of a particular state and the actual approximation $\mathbf{R}(\bar{m}')$ of that state (see eqs. (6.9) and (6.10)). A new refresh is triggered, if $\sigma_{\bar{m}\bar{m}'}$ falls below a certain threshold (of 0.5 in our calculations). This signals a significant change in the character of the eigenstate, hence the domains and pair lists should be re-determined. $\sigma_{\bar{m}\bar{m}'}$ is also used to identify root flips. In such a situation domains and pair lists are just exchanged and not re-determined, i.e., no refresh is triggered. If the eigenvectors are not yet converged in the present macro-iteration, then, before any Davidson refresh, at least three (micro)iterations are always performed.

A critical phase of the calculation is the initial search for the lowest states. Therefore, during the first few Davidson iterations, individual restricted pair lists and domains are also generated for the Davidson basis vectors $m > \bar{m}$. Since the basis vectors $m > \bar{m}$ usually contain much smaller values the square of the regular domain threshold was employed as the criterion. In later iterations, the corresponding pair lists and domains of the individual states \bar{m} (determined at the Davidson refresh) are employed for the individual basis vectors $m > \bar{m}$.

6.2.4 Complex eigenvalues and -vectors

In the course of the Davidson diagonalization complex eigenvalues and vectors may appear. The CC2 Jacobian by itself is non-symmetric and hence it is no warranted that its eigenvalues are real. Furthermore, even if that would be fulfilled, as e.g. for the ADC(2) method [113] (ADC(2), even though conceptionally very different from CC2, has very similar working equations as CC2 response [114] such that an existing CC2 implementation can easily be modified to do ADC(2)) the resulting Davidson matrix would still be non-symmetric. According to eqs. (6.7) and (6.8) we have

$$\begin{aligned} A'_{mn} &= \tilde{u}_a^i(m) Q_{\bar{a}c} V_{ca}^\dagger \left(A_{aijb}^{\text{eff}}(\omega_{\bar{n}}) u_b^j(n) \right) W_{\bar{n}}^\dagger \\ &\neq A'_{nm} = \tilde{u}_a^i(n) Q_{\bar{a}c} V_{ca}^\dagger \left(A_{aijb}^{\text{eff}}(\omega_{\bar{m}}) u_b^j(m) \right) W_{\bar{n}}^\dagger, \end{aligned} \quad (6.28)$$

i.e., excitation energy of \mathbf{A}^{eff} , as well as the state specific domains are different for the two matrix-vector products.

The complex eigenvalues and -vectors come in conjugated pairs, i.e., $\omega_{\bar{m},\bar{m}+1} = \omega_{\bar{m}}^{(r)} \pm i\omega_{\bar{m}}^{(i)}$, and $\mathbf{R}_{\bar{m},\bar{m}+1} = \mathbf{R}_{\bar{m}}^{(r)} \pm i\mathbf{R}_{\bar{m}}^{(i)}$. Such a pair of eigenvectors can be rotated by multiplication with a complex number. The angle of the rotation can be chosen such that the rotated eigenvectors $\check{\mathbf{R}}_{\bar{m},\bar{m}+1} = \check{\mathbf{R}}_{\bar{m}}^{(r)} \pm i\check{\mathbf{R}}_{\bar{m}}^{(i)}$ possess some certain properties, e.g. maximum overlap of the real part with the previous eigenvector of the \bar{m} -th state (from refresh), which is equivalent to orthogonality of imaginary part with the \bar{m} -eigenvector:

$$\check{\mathbf{R}}_{\bar{m}} = \mathbf{R}_{\bar{m}} (\cos(\phi) + i \sin(\phi)) \quad (6.29)$$

$$\check{\mathbf{R}}_{\bar{m}}^{(r)} = \mathbf{R}_{\bar{m}}^{(r)} \cos(\phi) - \mathbf{R}_{\bar{m}}^{(i)} \sin(\phi) \quad (6.30)$$

$$\check{\mathbf{R}}_{\bar{m}}^{(i)} = \mathbf{R}_{\bar{m}}^{(r)} \sin(\phi) + \mathbf{R}_{\bar{m}}^{(i)} \cos(\phi) \quad (6.31)$$

$$\check{\mathbf{R}}_{\bar{m}}^{(r)} \mathbf{U}_{\bar{m}} \rightarrow \max \quad \text{or} \quad \check{\mathbf{R}}_{\bar{m}}^{(i)} \mathbf{U}_{\bar{m}} = 0 \quad (6.32)$$

In this case the angle of the rotation ϕ is calculated as

$$\phi = \arctan \left(-\frac{\mathbf{R}_{\bar{m}}^{(i)} \mathbf{U}_{\bar{m}}}{\mathbf{R}_{\bar{m}}^{(r)} \mathbf{U}_{\bar{m}}} \right) = \arctan \left(-\frac{\sum_n S'_{\bar{m}n} c_{n\bar{m}}^{(i)}}{\sum_n S'_{\bar{m}n} c_{n\bar{m}}^{(r)}} \right). \quad (6.33)$$

When a complex pair appears a refresh of the Davidson is carried out. All the domains are re-determined (as in any refresh) and the domains of real and imaginary part of the new basis vectors (related to the complex pair) are *unified*. The residuals $\mathbf{r}_{\bar{m},\bar{m}+1}$ for the pair of complex conjugate vectors then are calculated as

$$\begin{aligned} \mathbf{r}_{\bar{m}}^{(r)} &= \mathbf{A}^{\text{eff}} \mathbf{R}_{\bar{m}}^{(r)} - \omega_{\bar{m}}^{(r)} \mathbf{R}_{\bar{m}}^{(r)} + \omega_{\bar{m}}^{(i)} \mathbf{R}_{\bar{m}}^{(i)} \\ \mathbf{r}_{\bar{m}}^{(i)} &= \mathbf{A}^{\text{eff}} \mathbf{R}_{\bar{m}}^{(i)} - \omega_{\bar{m}}^{(r)} \mathbf{R}_{\bar{m}}^{(i)} - \omega_{\bar{m}}^{(i)} \mathbf{R}_{\bar{m}}^{(r)}, \end{aligned} \quad (6.34)$$

which substitutes eq. (6.11). Furthermore, the excitation energies entering eqs. (6.21) and (6.22) are corrected, according to Ref. 115, as

$$\begin{aligned} \omega_{\bar{m},\bar{m}+1} &= \omega_{\bar{m}}^{(r)} \pm \omega_{\bar{m}}^{(i)} s \frac{\sqrt{1 - \Sigma^2}}{\sqrt{1 - s^2}}, \\ s &= \frac{\sqrt{(|\mathbf{R}_{\bar{m}}^{(r)}|^2 - |\mathbf{R}_{\bar{m}}^{(i)}|^2)^2 + 4(\mathbf{R}_{\bar{m}}^{(i)} \mathbf{R}_{\bar{m}}^{(r)})^2}}{|\mathbf{R}_{\bar{m}}^{(r)}|^2 + |\mathbf{R}_{\bar{m}}^{(i)}|^2}, \\ \Sigma &= s_{\max} \tanh \left(\frac{1}{s_{\max} s} \right), \quad s_{\max} = 0.2. \end{aligned} \quad (6.35)$$

For the most of the cases studied so far the complex eigenvalues vanish after the Davidson refresh. If the complex eigenvalues persist then the real and imaginary parts of the complex pair take over the role of the \bar{m} , and $\bar{m} + 1$ state, respectively.

6.2.5 Rescaling of matrix-vector product after refresh

After each Davidson refresh the first N_{stat} matrix-vector products $\mathbf{v}(\bar{m})$ are calculated with the $\omega_{\bar{m}}$ obtained in the previous macro-iteration (cf. eq.(6.7)). However, these $\omega_{\bar{m}}$ refer to domains and pair lists *before* the refresh. It is preferable to instead use the new $\omega'_{\bar{m}}$ from the first diagonalization of \mathbf{A}' (with dimension N_{stat} , cf. eq. (6.9)) for the actual macro-iteration in the matrix-vector products of eq.(6.7). In order not to have to recompute the first N_{stat} matrix-vector products such that they correspond also to the new $\omega'_{\bar{m}}$ they are *rescaled*: according to eq. (6.3) the matrix-vector product for a single Laplace quadrature point t_1 can be written as

$$\begin{aligned} \mathbf{A}^{\text{eff}}(\omega'_{\bar{m}})\mathbf{U}(\bar{m}) &\approx \mathbf{v}_{11} + \mathbf{v}_{12}(\omega'_{\bar{m}}) = \mathbf{v}_{11} + \mathbf{v}_{12}(\omega_{\bar{m}})e^{(\omega'_{\bar{m}} - \omega_{\bar{m}})t_1}, \\ \text{with} \quad \mathbf{v}_{11} &= A_{\mu_1\nu_1}U_{\nu_1}(\bar{m}), \\ \text{and} \quad \mathbf{v}_{12}(\omega) &= -A_{\mu_1\xi_2}w_1e^{-\Delta\epsilon_{\xi_2}t_1}e^{\omega t_1}A_{\xi_2\nu_1}U_{\nu_1}(\bar{m}). \end{aligned} \quad (6.36)$$

$\exp((\omega'_{\bar{m}} - \omega_{\bar{m}})t_1)$ in eq. (6.36) is the desired scaling factor used to rescale the matrix-vector product after the refresh. The optimal single quadrature point t_1 is determined via Simplex optimization (*vide supra*).

6.3 Test Calculations

The new method based on the Laplace transform described in section 6.2, termed LT-DF-LCC2 response in the following, is implemented in the MOLPRO package [64]. Most of the relevant subroutines are parallelized, yet the scratch files containing integrals and amplitudes reside on a common shared file system. In this section we present results from test calculations performed with the new LT-DF-LCC2 response code for a test set of different molecules involving different excited states. This test set essentially comprises those molecules already used previously in Refs. 10,89 for testing the preceding DF-LCC2 response method. Of those, the phenothiazine-isoalloxazine dyad and the phenothiazine-isoalloxazine-pyrene triad (cf. Fig.6.1) constitute particularly difficult cases for which the initial CCS start vectors do not bear any resemblance to the converged CC2 eigenstates. It turns out that the previous DF-LCC2 response method, in contrast to the new LT-DF-LCC2 approach, fails to find the important CT state corresponding to a shift of electron density from the phenothiazine to the isoalloxazine subunit. As two further test molecules the bis-indole-cyclohexene (BICH), and its photo product solvated by a H_3O^+ molecule ($\text{BICH}^+\cdot\text{H}_3\text{O}^+$), which was studied in our group in the context of an application project, are in-

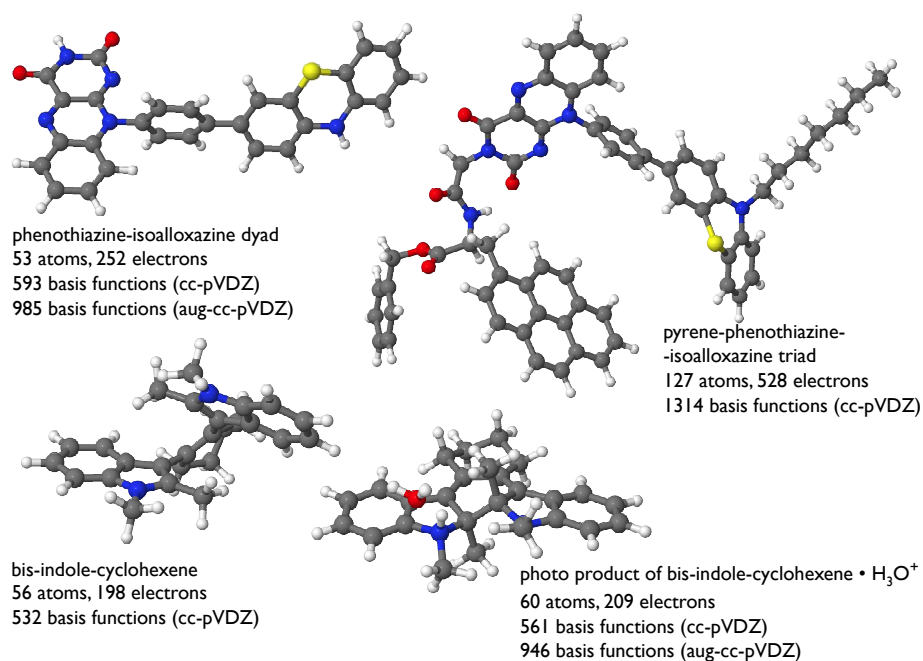


Figure 6.1: Structures of the phenothiazine-isoalloxazine dyad, the pyrene-phenothiazine-isoalloxazine triad, the bis-indole-cyclohexene (BICH), and the H_3O^+ complex of the photoproduct of the latter ($\text{BICH}^+ \cdot \text{H}_3\text{O}^+$). The first two structures were taken from Ref. 10, the last two were optimized in the course of the present work at the level of local MP2 employing the aug-cc-pVDZ basis set.

cluded. These two structures were optimized at the level of local MP2 [43] within the aug-cc-pVDZ AO basis set.

The LCC2 response calculations were performed with the cc-pVDZ and aug-cc-pVDZ AO basis sets, along with the related fitting basis sets optimized for DF-MP2. The LMOs were constructed according to Pipek-Mezey (PM) localization. For the aug-cc-pVDZ basis the most diffuse functions were discarded in the PM localization.

For the LCC2 ground state calculations the pair lists were truncated at an LMO interorbital distance of 10 bohrs, and the orbital domains determined according to the Boughton-Pulay (BP) procedure with a criterion of 0.98. All response calculations were carried out for pair lists denoted in chapter 2 (Ref. 10) as $\forall(ij), (im) \leq 5, (mn) \leq 5$, i.e., pair lists which include *all* pairs of *important orbitals* and other pairs up to an LMO interorbital distance of 5 bohr. For the DF-LCC2 calculations and the LT-DF-LCC2 calculations involving BP domains for the local approximation of the excited states the important LMOs i, j, \dots were specified as described in chapter 2 (Ref. 10) with a criterion of $\kappa_e = 0.995$, while for the BP domains again a cri-

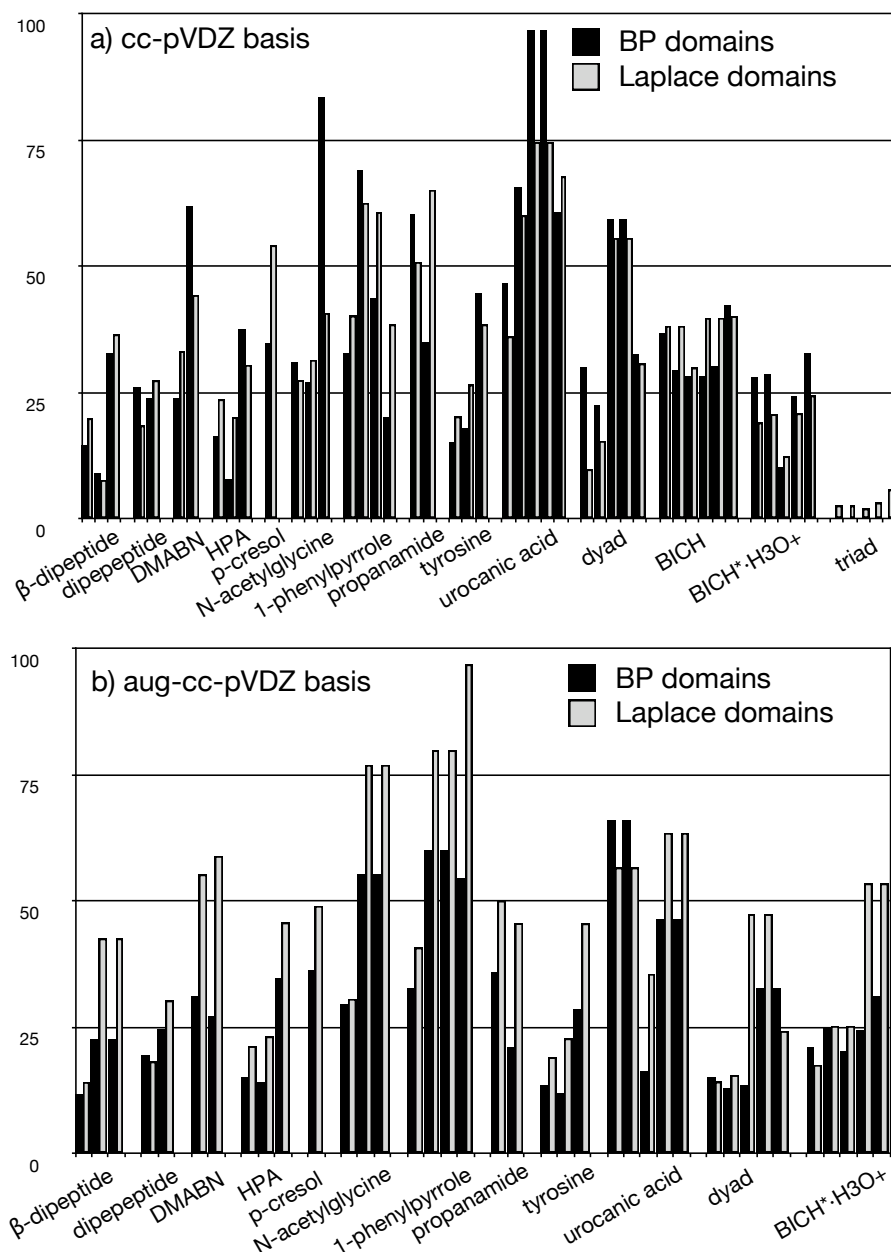


Figure 6.2: Ratios (local vs. canonical) of the number of unique elements of object U_{μ_2} as defined in eqs. (6.21,6.22) for the individual converged eigenstates, (a) for the cc-pVDZ basis, and (b) for the aug-cc-pVDZ basis.

terion of 0.98 was used. For the LT-DF-LCC2 calculations based on Laplace domains for the excited states, on the other hand, the important orbitals were determined by employing a criterion of $\kappa_e = 0.999$, while for the domains a threshold of 0.98 for important centers was used (cf. section 6.2.3). These parameters determine the number of elements of object U_{μ_2} , which is defined in eqs. (6.21,6.22) and enters eqs. (6.19,6.20). The ratios (local vs. canonical) of the number of unique elements of U_{μ_2} for the individual converged eigenstates are displayed in Fig.6.2. These ratios are intimately connected to the computational savings of the local response calculation. Evidently, they depend sensitively on the related eigenstate. In particular, if domains and pair lists of two energetically close-lying eigenstates have to be merged in the course of the Davidson diagonalization (cf. section 6.2.4) the ratios may eventually get larger. For example, for the case of the phenothiazine-isoalloxazine dyad the domains and pair lists of the S_3 and S_4 states are merged. Since the important LMOs and PAOs are localized at different ends of the molecule the unified pair lists and domains (and with this the ratios) of these two states become comparatively large: The S_4 state corresponds to a $\pi \rightarrow \pi^*$ excitation on phenothiazine with some charge transfer character shifting charge towards the linking phenyl subunit. The S_3 state, on the other hand, corresponds either to the CT state transferring electron density from phenothiazine to isoalloxazine (cc-pVDZ) or to an $n \rightarrow \pi^*$ excitation localized on the isoalloxazine subunit (aug-cc-pVDZ). Note that CT character alone, despite its non-local character, not necessarily leads to enlarged ratios: For example, the ratio of the S_2 state of the dyad (aug-cc-pVDZ), which here represents the CT state transferring electron density from phenothiazine to isoalloxazine, but remains un-merged, is only slightly larger than that of the local $\pi \rightarrow \pi^*$ excitation within isoalloxazine, i.e., S_1 . The target molecules of the present method are of course larger, as an example we calculated here the lowest five states of the phenothiazine-isoalloxazine-pyrene triad. Evidently, for such a case the ratios are all very low, implying heavy computational savings for the local method.

The calculated excitation energies ω are compiled in Table 6.1. The canonical reference values are taken from Ref. 10 when available, or (for the new molecules) computed with the TURBOMOLE implementation of CC2 response [27]. For the LT-DF-LCC2 response calculations three Laplace integration points were used, which is sufficiently accurate for exploratory calculations of excitation energies (*vide infra*). Evidently, the deviations from the canonical reference values do not exceed, and, in most of the cases are well below 0.1 eV, which in our view is quite acceptable for an expected accuracy of the canonical CC2 response method itself of about

Basis	cc-pVDZ						aug-cc-pVDZ					
			ω_{ref}	$\Delta\omega$					ω_{ref}	$\Delta\omega$		
	Molecule	st	char.	can.	BP	BP-LT	LD-LT	char.	can.	BP	BP-LT	LD-LT
" β -dipeptide"	S ₁	$n \rightarrow \pi^*$	4.861	-0.030	-0.042	-0.012		$n \rightarrow \pi^*$	4.715	-0.013	-0.023	-0.005
	S ₂	$n \rightarrow \pi^*$	5.825	-0.012	-0.020	0.017		$\pi \rightarrow \text{Ry}$	5.635	0.032	-0.003	-0.033
	S ₃	$\pi \rightarrow \text{Ry}$	6.908	0.033	0.013	-0.009		$n \rightarrow \pi^*$	5.665	0.010	-0.022	-0.030
"Dipeptide"	S ₁	$n \rightarrow \pi^*$	5.871	-0.019	-0.026	-0.004		$n \rightarrow \pi^*$	5.743	0.002	-0.025	-0.001
	S ₂	$n \rightarrow \pi^*$	6.106	0.000	-0.019	-0.005		$n \rightarrow \pi^*$	5.953	-0.005	-0.025	-0.016
DMABN	S ₁	$\pi \rightarrow \pi^*$	4.525	0.038	0.033	-0.033		$\pi \rightarrow \text{Ry}$	4.495	0.013	0.004	-0.014
	S ₂	$\pi \rightarrow \pi^*$	4.891	-0.064	-0.061	-0.055		$\pi \rightarrow \text{Ry}$	5.085	0.026	0.023	-0.022
HPA	S ₁	$\pi \rightarrow \pi^*$	4.984	0.013	0.010	-0.035		$\pi \rightarrow \pi^*$	4.816	0.005	0.013	-0.013
	S ₂	$n \rightarrow \pi^*$	6.148	0.011	0.002	0.005		$\pi \rightarrow \text{Ry}$	5.216	-0.001	0.023	-0.024
	S ₃	$\pi \rightarrow \pi^*$	6.285	-0.024	-0.053	-0.024		$\pi \rightarrow \text{Ry}$	5.726		0.037	0.006
p -cresol	S ₁	$\pi \rightarrow \pi^*$	4.981	0.011	0.002	-0.042		$\pi \rightarrow \text{Ry}$	5.145	0.005	0.018	-0.029
N-acetyl-glycine	S ₁	$n \rightarrow \pi^*$	5.862	-0.013	-0.020	-0.006		$n \rightarrow \pi^*$	5.732	0.013	-0.020	-0.005
	S ₂	$n \rightarrow \pi^*$	6.252	0.013	-0.003	-0.006		$n \rightarrow \text{Ry}$	5.989		-0.023	-0.031
	S ₃	$\pi \rightarrow \pi^*$	7.373	0.005	0.010	-0.005		$n \rightarrow \pi^*$	6.275	0.025	-0.032	-0.035
1-phenyl-pyrrole	S ₁	$\pi \rightarrow \pi^*$	5.072	0.012	0.008	-0.029			4.921	0.023	0.019	-0.020
	S ₂	$\pi \rightarrow \pi^*$	5.555	-0.002	0.006	-0.030		$\pi \rightarrow \pi^*$	5.309	0.011	0.009	-0.037
	S ₃	$\pi \rightarrow \pi^*$	5.771	0.014	0.000	-0.007		$\pi \rightarrow \text{Ry}$	5.434	0.008	0.011	-0.027
	S ₄	CT	6.091	0.135	0.205	-0.001		CT	5.489	-0.004	-0.005	-0.044
Propanamide	S ₁	$n \rightarrow \pi^*$	5.926	0.001	-0.032	0.003		$n \rightarrow \pi^*$	5.657	0.012	0.013	0.001
	S ₂	$\pi \rightarrow \pi^*$	7.776	0.022	0.048	0.026		$\pi \rightarrow \text{Ry}$	6.267	0.043	0.031	-0.009
Tyrosine	S ₁	$\pi \rightarrow \pi^*$	4.995	0.022	0.025	-0.013		$\pi \rightarrow \pi^*$	4.834	0.013	0.029	-0.008
	S ₂	$n \rightarrow \pi^*$	5.824	-0.001	-0.014	0.032		$\pi \rightarrow \text{Ry}$	5.292	-0.014	0.036	-0.020
	S ₃	$\pi \rightarrow \pi^*$	6.205	-0.003	-0.033	-0.011		$\pi \rightarrow \text{Ry}$	5.488		0.041	0.005
$trans$ -urocanic acid	S ₁	$n \rightarrow \pi^*$	4.987	0.010	-0.036	0.006		$n \rightarrow \pi^*$	4.863	-0.028	-0.023	-0.034
	S ₂	$\pi \rightarrow \pi^*$	5.207	-0.024	-0.021	-0.031		$\pi \rightarrow \pi^*$	4.931	-0.008	-0.011	-0.021
	S ₃	$\pi \rightarrow \pi^*$	6.233	-	-0.057	-0.037		$\pi \rightarrow \text{Ry}$	5.285	0.059	0.054	-0.016
	S ₄	$\pi \rightarrow \pi^*$	6.269	0.033	0.062	0.021		$\pi \rightarrow \pi^*$	5.953		0.038	-0.010
	S ₅	$\pi \rightarrow \text{Ry}$	6.877	0.027	0.006	-0.017		$\pi \rightarrow \text{Ry}$	6.009	0.031	0.036	-0.005
dyad	S ₁	$\pi \rightarrow \pi^*$	3.190	-0.024	-0.024	-0.040		$\pi \rightarrow \pi^*$			3.050 ^a	3.029 ^a
	S ₂	$n \rightarrow \pi^*$	3.412	-0.032	-0.059	-0.051		CT			3.275 ^a	3.198 ^a
	S ₃	CT	3.513	-	-0.013	-0.071		$n \rightarrow \pi^*$			3.386 ^a	3.382 ^a
	S ₄	$\pi \rightarrow \pi^*$	-	3.557 ^a	3.547 ^a	3.534 ^a		$\pi \rightarrow \pi^*$			3.452 ^a	3.421 ^a
	S ₅	$n \rightarrow \pi^*$	3.629	-	3.604 ^a	3.662 ^a		$n \rightarrow \pi^*$			3.522 ^a	3.593 ^a
BICH	S ₁	$\pi \rightarrow \pi^*$	4.281		-0.023	-0.054						
	S ₂	$\pi \rightarrow \pi^*$	4.382		-0.002	-0.046						
	S ₃	$\pi \rightarrow \pi^*$	4.577		0.032	-0.004						
	S ₄	$\pi \rightarrow \pi^*$	4.662		0.022	-0.046						
	S ₅	$\pi \rightarrow \pi^*$	4.737		0.031	-0.036						
	S ₆	$\pi \rightarrow \pi^*$	5.223		0.006	-0.021						
BICH ⁺ ·H ₃ O ⁺	S ₁	$\pi \rightarrow \pi^*$	2.561		-0.082	-0.072		$\pi \rightarrow \pi^*$			2.452 ^a	2.496 ^a
	S ₂	$\pi \rightarrow \pi^*$	3.716		-0.031	-0.032		$\pi \rightarrow \pi^*$			3.609 ^a	3.590 ^a
	S ₃	CT	3.983		0.059	0.015		CT			3.789 ^a	3.774 ^a
	S ₄	$\pi \rightarrow \pi^*$	4.266		0.022	0.006		$\pi \rightarrow \pi^*$			4.128 ^a	4.062 ^a
	S ₅	$\pi \rightarrow \pi^*$	4.784		-0.021	-0.002		$\pi \rightarrow \pi^*$			4.239 ^a	4.193 ^a

a) Excitation energy instead of its deviation from ω_{ref} .

Table 6.1: Excitation energies in [eV] for different molecules and excited states. For the local calculations the deviations from the related canonical reference values $\Delta\omega = \omega_{\text{loc}} - \omega_{\text{ref}}$ are given (except explicitly stated otherwise). The labels BP and BP-LT stand for DF-LCC2 and LT-DF-LCC2 results employing BP domains, LD-LT for LT-DF-LCC2 results employing Laplace domains.

0.3 eV (cf. Tables IV and V in Ref. 116). Notably, also the hiccup occurring for the CT state of 1-phenylpyrrole when BP domains in conjunction with the cc-pVDZ basis are used, vanishes for the new Laplace domains. As already mentioned above, the phenothiazine-isoalloxazine dyad represents a particularly difficult case since the initial CCS start vectors are entirely different from the CC2 solution. Especially, the important CT state (shifting electron density from phenothiazine to isoalloxazine) could not be located with the previous DF-LCC2 single-state approach (what was assigned in Ref. 10 as the CT state emerged later as only a partial CT state shifting electron density from phenothiazine to the linking benzene ring, i.e., state S_4 in Table 6.1). The LT-DF-LCC2 multistate method, on the other hand, is able to find the CT state for the cc-pVDZ and the aug-cc-pVDZ basis, certainly so if Laplace domains are used. Using BP domains there are still some problems for the case of the aug-cc-pVDZ basis. First of all the Davidson diagonalization with adaptive domains has difficulties to converge at all. Moreover, there is no state with clear HOMO \rightarrow LUMO CT character as the S_3 for the cc-pVDZ calculations, or the S_2 for the aug-cc-pVDZ calculation involving Laplace domains, but rather than that, the S_2 state and S_3 states are essentially plus/minus combinations of CT and $n \rightarrow \pi^*$ determinants with nearly equal weight. Also the S_5 state contains to lesser extend some CT component. The S_4 state of the dyad was not found by the corresponding canonical reference calculation. Notably, there are also rather pronounced differences in the character and properties of the individual states when comparing canonical CC2 response and ADC(2) [113], which usually yield quite similar results. It appears that this dyad constitutes a difficult case indeed, not only for the local methods.

Fig.6.3 presents, for a subset of the test molecules, the convergence of the LT-DF-LCC2 excitation energies with respect to the number of Laplace quadrature points. Plotted are the deviations of the excitation energies computed for the individual molecules/states by using three or five quadrature points, from the result of the corresponding reference calculations involving eight points. The domains and pair lists were kept fixed in these calculations. For many molecules and states (including the dyad) the difference between five and eight points is not visible on the scale of the plot. Using just three quadrature points leads to deviations below 0.01 eV for most cases and therefore yields sufficient accuracy for exploratory calculations. Yet for calculations of potential energy surfaces (which should be carried out with domains and pair lists fixed for different geometries to avoid steps in the surface) an increased number of quadrature points (for the DIIS step only) may be more appropriate.

In Table 6.2 CPU/core and elapsed times of individual key steps of LT-

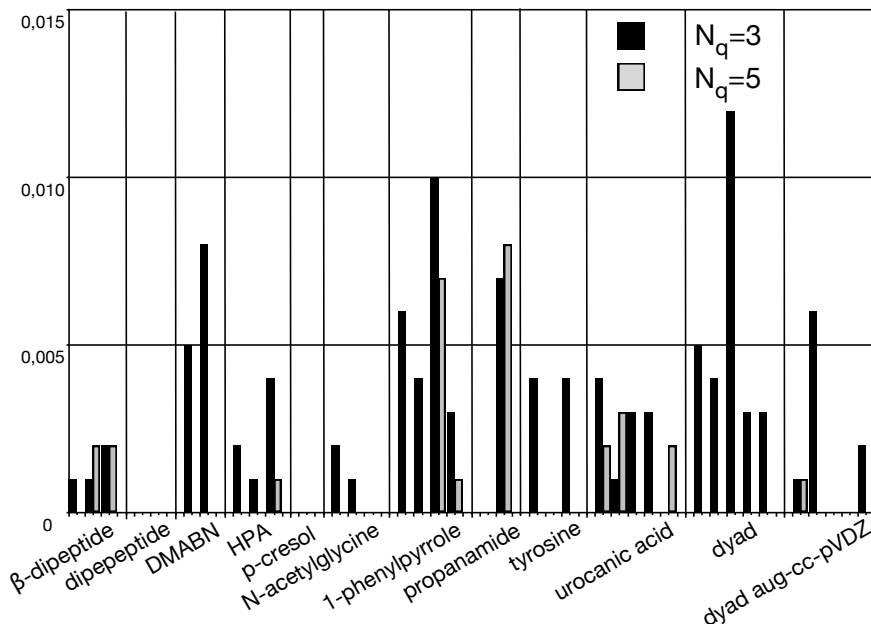


Figure 6.3: Deviations (in eV) of calculated LT-DF-LCC2 excitation energies involving three and five Laplace quadrature points from corresponding reference values involving eight quadrature points. Except explicitly stated otherwise the cc-pVDZ basis was used.

Molecule(Basis)	State	char.	omega	#batch ^a	$t(U_{ab}^{ii})^b$	$t(U_{ab}^{ij}(q))^c$	$t(U_{ab}^{ij})^d$	$t(W_{ia}^P)^e$	$t(v_a^i)^f$	$t(\text{iter})^g$
Dyad (cc-pVDZ)	S_1	$\pi \rightarrow \pi^*$	3.150	1	3(3)	30(46)	124(146)	45(56)	132(146)	1547(1773)
	S_2	$n \rightarrow \pi^*$	3.361	1	3(4)	60(69)	177(216)	65(79)		
	S_3	CT	3.442	1	3(4)	98(107)	295(326)	116(131)		
	S_4	$\pi \rightarrow \pi^*$	3.534	1	3(4)	96(105)	295(327)	295(327)		
	S_5	$n \rightarrow \pi^*$	3.662	1	3(4)	42(48)	125(149)	125(149)		
Dyad (aug-cc-pVDZ)	S_1	$\pi \rightarrow \pi^*$	3.029	2	14(26)	443(470)	1334(1508)	565(618)	330(1280)	13125(14993)
	S_2	CT	3.198	2	16(27)	558(591)	1681(1799)	682(729)		
	S_3	$n \rightarrow \pi^*$	3.382	2	17(26)	732(788)	2185(2313)	923(978)		
	S_4	$\pi \rightarrow \pi^*$	3.421	2	16(26)	725(779)	2170(2294)	896(956)		
	S_5	$n \rightarrow \pi^*$	3.593	2	14(24)	554(585)	1667(1768)	686(740)		
Triad (cc-pVDZ)	S_1	$\pi \rightarrow \pi^*/\text{CT}$	2.974	2	37(96)	340(500)	1015(1529)	277(434)	1886(3105)	9567(14337)
	S_2	$\pi \rightarrow \pi^*/\text{CT}$	3.057	2	39(99)	335(499)	996(1511)	285(447)		
	S_3	CT	3.233	3	41(97)	405(600)	1217(1734)	353(559)		
	S_4	$n \rightarrow \pi^*$	3.320	2	41(100)	332(496)	993(1505)	311(459)		
	S_5	CT	3.481	3	39(97)	560(752)	1679(2268)	545(774)		

a) Number of batches in calculation of the doubles vector and of W_{ia}^P

b) CPU (elapsed) time for calculation of full U_{ab}^{ii} ; eq. (6.22)

c) CPU (elapsed) time for calculation of U_{ab}^{ij} for one quadrature point; eq. (6.22)

d) CPU (elapsed) time for calculation of the doubles vector; eq. (6.22)

e) CPU (elapsed) time for calculation of W_{ia}^P ; eq. (6.20)

f) CPU (elapsed) time for calculation of v_a^i (only multi-state part); eq. (6.19)

g) CPU (elapsed) time for one Davidson iteration

Table 6.2: Timings (in seconds) for dyad and triad (Laplace domains) (6 CPUs, Intel(R) Xeon(R) CPU E5462 @ 2.80GHz)

DF-LCC2 excitation energy calculations are compiled. As representative examples the dyad in cc-pVDZ and aug-cc-pVDZ basis, and the triad in cc-pVDZ are given. The calculations were run in parallel mode on 6 Intel Xeon E5462 2.80GHz cores, and the common shared file system was striped over four SAS disks. It can be seen that the calculation of the *unrestricted* diagonal pair part of $U_{\mu_2}(\bar{m})$, i.e., U_{ab}^{ii} , according to eq. (6.22), is inexpensive. Since the latter is solely used for the construction of the Laplace domains (cf. section 6.2.3), only a single quadrature point is required and a much larger product prescreening threshold (10^{-5} instead of 10^{-9}) than in the "real" calculation of the $U_{\mu_2}(m)$ can be employed.

The lion's share of the computing time indeed goes into the "real" calculation of the $U_{\mu_2}(m)$ according to eq. (6.22). The subsequent contraction of $U_{\mu_2}(m)$ with the fitting coefficients to the object $W_{ia}^P(m)$ according to eq. (6.20) is independent of the number of quadrature points and costs less. $W_{ia}^P(m)$ is stored for each individual state $\Psi^{\bar{m}}$. The calculation of the matrix-vector product $v_{\mu_1}(m)$ according to eq. (6.19) proceeds simultaneously for all states such that e.g. the two-external ERIs $(ab|P)$ only have to be read twice per Davidson iteration, i.e., once for the contraction with all $W_{ia}^P(m)$ and once for the formation of the objects $\hat{Y}_{ai}^P(m)$ according to eq. (6.20). Nevertheless, the I/O cost for that step still is rather heavy compared to the CPU cost. The overall elapsed time for a single Davidson iteration involving the lowest five states of the triad (127 atoms, 370 correlated electrons, 1314 basis functions) is about four hours, which makes it possible to calculate the excitation energies of such a molecule within about a week using a computational setup as described.

6.4 Conclusions

In this contribution we present a new multi-state local CC2 response method for calculating excitation energies of extended molecular systems, ironing out the fragility of the earlier single state local CC2 response method presented in Refs. 10, 89. The Laplace transform trick is applied to the doubles-doubles block of the LCC2 Jacobian (being diagonal in canonical orbital basis) in order to decompose the CC2 eigenvalue problem into an effective eigenvalue problem involving only the singles part. In contrast to the canonical case, where such a decomposition is straightforwardly possible, the orbital basis is still localized and the sparsity in the amplitude and integral supermatrices is maintained. The new approach furthermore works with adaptive pair lists and domains for the doubles parts of the eigenvectors of the Jacobian (and generally, the basis

vectors of the Davidson subspace), which are computed on the fly when calculating the effective Jacobian \times singles vector matrix-vector products in the Davidson or DIIS iterations. This removes the dependency of the result on the initial CCS starting vectors, which were used to specify the local approximation in our earlier approach. Furthermore a new variant to specify the local approximation, i.e., the domains of the doubles part of the Davidson basis vectors is proposed. These Laplace domains are determined by analysis of the quantity itself, which is to be approximated. The performance of the new method, for which we introduce the acronym LT-DF-LCC2 response is tested for a set of molecules including the difficult case of a phenothiazine-isoalloxazine dyad, for which the earlier method failed to produce the important HOMO \Rightarrow LUMO charge transfer state. It is demonstrated that the new method indeed is able to catch this charge transfer state. The deviations between local and canonical excitation energies are well below 0.1 eV for the molecules of the test set. With the new LT-DF-LCC2 response we now have a robust tool at hand which can be used to investigate excited states of extended molecular systems.

Chapter 7

LCC2 vs. LT-LCC2

7.1 Introduction

Over the past few years a *local* CC2 response method with reduced scaling behavior was developed in our group [10,89]. Local correlation approaches have been used before with great success in the context of *ab initio* theories for electronic ground states to circumvent the inherent scaling problem of these methods [35–43,117,118]. The essential idea of local correlation approaches is to exploit the short-range character of dynamic electron correlation effects and to work with the naturally sparse, rather than artificially dense (an artifact of the delocalized canonical MO basis) data objects. Hence, the de-localized canonical MOs are replaced by spatially *localized* orbitals. In our local CC2 response method we employ the ansatz proposed by Pulay [36]. Mutually orthogonal localized molecular orbitals (LMOs) and non-orthogonal projected atomic orbitals (PAOs) are used to span the occupied and virtual orbital spaces of the underlying Hartree-Fock reference. Strong orthogonality thus is conserved, yet among the PAOs there are redundancies which must be eliminated at some stage of the calculation. *A priori* restrictions then are imposed on the amplitudes of doubly substituted configuration state functions (single substitutions remain un-truncated): Restricted LMO pair lists and pair specific excitation subspaces of PAOs (domains) are specified and amplitudes outside these lists/domains are *a priori* set to zero. For the amplitudes (of the electronic ground state) such a truncation is based on spatial locality arguments, in analogy to the previous local correlation methods for ground states. Only LMO pairs up to a certain inter-orbital distance and only double substitutions of LMOs by nearby PAOs are considered. For the amplitude response (subject to the frequency dependent perturbation), on the other

hand, *a priori* truncations are far more complicated and the specification of proper pair lists and domains actually is one of the key challenges in the formulation of a local method for excited states. Excited states may have substantial non-local CT character, thus spatial locality is an improper criterion for setting up restricted pair lists and domains. In the first version of our *local* CC2 response method, presented in chapters 2 and 3 (Refs. 10,89), the pair lists and domains for the amplitude response were determined by analysis of un-truncated wavefunctions obtained at a simpler level of theory, e.g., CCS wavefunctions. The method yet turned out to be frail for cases where the simpler level of theory provides qualitatively wrong wavefunctions for the individual excited states of interest. Relevant states then might be missed.

Recently [103], we presented a new local CC2 response method, which is utilizing the Laplace transform [33,45,92] to decompose the energy denominators occurring in the doubles-doubles block of the CC2 Jacobian. This allows for a partitioning of the CC2 eigenvalue problem exactly as in the case of the canonical theory [27], yet with integrals and amplitudes in a local, rather than a delocalized canonical orbital basis. As a result, an *effective* eigenvalue problem involving only the un-truncated singles vector has to be solved, while the contribution of the doubles amplitude response to the effective Jacobian - singles vector product can be computed on-the-fly and does not enter the Davidson diagonalization. On this basis a multi-state diagonalization procedure with much improved convergence behavior (compared to the single-state root-homing procedure of the previous approach) can be devised, which still maintains state-specific pair domains for the individual states. Furthermore, in combination with Density Fitting of the ERIs it is possible without much effort to utilize the un-truncated information of diagonal pair amplitudes for constructing suitable pair lists and domains for the pair amplitude response in an adaptive way in the course of the diagonalization. This new Laplace based method (termed LT-DF-LCC2 response) repairs the shortcomings of our initial DF-LCC2 response method. It faithfully finds the relevant excited states also for cases where the initial un-truncated wavefunction obtained at lower level of theory is qualitatively wrong.

In this chapter the new LT-DF-LCC2 response method is compared to the previous DF-LCC2 response. For a particularly pathological case it is demonstrated that LT-DF-LCC2 response, contrary to DF-LCC2 response, finds all the relevant excited states. Some first results on first-order properties and oscillator strengths obtained via LT-DF-LCC2 response are also presented and compared to the corresponding results of DF-LCC2 response.

7.2 Theory

In this section we briefly outline the basic theory of DF-LCC2 and LT-DF-LCC2 response. For a detailed discussion and the working equations we refer to Refs. 10,89,103 (Chps. 2,3,6).

7.2.1 Excitation energies

The LCC2 model is specified by the amplitude equations

$$\begin{aligned} 0 &= \Omega_{\mu_1} = \langle \tilde{\mu}_1 | \hat{H} + [\hat{H}, T_2^{\text{loc}}] | 0 \rangle \\ 0 &= \Omega_{\mu_2}^{\text{loc}} = \langle \tilde{\mu}_2^{\text{loc}} | \hat{H} + [F, T_2^{\text{loc}}] | 0 \rangle, \end{aligned} \quad (7.1)$$

where doubles substitution operators T_2^{loc} and the related contravariant projection manifold $\langle \tilde{\mu}_2^{\text{loc}} |$ are *a priori* confined to local subspaces (specified by restricted pair lists and domains). F and $\hat{H} = \exp(-T_1)H\exp(T_1)$ are the Fock $-$, and the similarity transformed Hamilton operators, respectively. Here and in the following all objects decorated with a hat involve dressed integrals (produced by the similarity transform of the related operators with $\exp(T_1)$), i.e., the T_1 contractions are absorbed in the transformed integrals. The excitation energies $\omega_{\bar{m}}$ of state $\Psi^{\bar{m}}$ are obtained by solving either the left or the right eigenvalue problem

$$\mathbf{A}\mathbf{R}^{\bar{m}} = \omega_{\bar{m}}\mathbf{M}\mathbf{R}^{\bar{m}}, \quad \mathbf{L}^{\bar{m}}\mathbf{A} = \omega_{\bar{m}}\mathbf{L}^{\bar{m}}\mathbf{M}, \quad (7.2)$$

involving the non-symmetric LCC2 Jacobian

$$A_{\mu_i\nu_j} = \begin{pmatrix} \langle \tilde{\mu}_1 | [\hat{H}, \tau_{\nu_1}] \exp(T_2^{\text{loc}}) | 0 \rangle & \langle \tilde{\mu}_1 | [\hat{H}, \tau_{\nu_2}] | 0 \rangle \\ \langle \tilde{\mu}_2 | [\hat{H}, \tau_{\nu_1}] | 0 \rangle & \langle \tilde{\mu}_2 | [F, \tau_{\nu_2}] | 0 \rangle \end{pmatrix}, \quad (7.3)$$

and the metric \mathbf{M} . The τ_{μ_i} are covariant one- or two-particle excitation operators. Eqs. (7.2) are solved by Davidson diagonalization [60,61]. In each iteration the left/right matrix–vector product of the Jacobian \times a basis vector of the Davidson subspace, e.g., for the right eigenvalue equation,

$$\mathfrak{B}_{\mu_i}^m = A_{\mu_i\nu_i} U_{\nu_i}^m \quad (7.4)$$

is calculated (m enumerates the basis vectors of the Davidson subspace). Here and in the following the Einstein convention is employed, i.e., repeated indices are summed up. Explicit summations are put in the equations only where we find it useful for clarity. In eq. (7.4) the doubles parts

of the basis vector, $U_{\mu_2}^m$ and of the corresponding matrix–vector product, $\mathfrak{B}_{\mu_2}^m$ are confined to the specific local subspace of state $\Psi^{\bar{m}}$, which is related to basis vector \mathbf{U}^m . These state specific local subspaces obviously differ from those of the ground state calculation (cf. eq. (7.1)). In the original DF-LCC2 response method these subspaces are determined *a priori* once by analyses of the related initial (un-truncated) CCS eigenstate. Working equations for the left/right matrix–vector products, based on the DF approximation for the ERIs, are given in chapters 2 and 3 (Refs. 10, 89).

From the matrix–vector products the Davidson Jacobian

$$A'_{mn} = \tilde{U}_{\mu_i}^m \mathfrak{B}_{\mu_i}^n \quad (7.5)$$

is constructed/extended ($\tilde{U}_{\mu_i}^m$ denotes the contravariant of $U_{\mu_i}^m$). Solving the eigenvalue equation

$$\mathbf{A}'\mathbf{c} = \mathbf{S}'\mathbf{c}\omega', \text{ with} \quad (7.6)$$

$$S'_{mn} = \tilde{u}_a^i(m)S_{ab}u_b^i(n) + \tilde{U}_{ab}^{ij}(m)S_{aa'}U_{a'b'}^{ij}(n)S_{bb'},$$

yields the approximations

$$R_{\mu_i}^{\bar{m}} = U_{\mu_i}^n c_{n\bar{m}} \quad (7.7)$$

and $\omega'_{\bar{m}}$ to eigenstate and eigenvalue of \mathbf{A} for state $\Psi^{\bar{m}}$ with residual

$$\begin{aligned} r_a^i(\bar{m}) &= v_a^i(n)c_{n\bar{m}} - \omega'_{\bar{m}}S_{aa'}r_{a'}^i(\bar{m}), \\ \mathfrak{R}_{ab}^{ij}(\bar{m}) &= \mathfrak{B}_{ab}^{ij}(n)c_{n\bar{m}} - \omega'_{\bar{m}}S_{aa'}R_{a'b'}^{ij}(\bar{m})S_{bb'}. \end{aligned} \quad (7.8)$$

In eqs. (7.6-7.8) we used capital and small letters for doubles and singles parts of basis–, eigen–, and residual vectors, respectively, e.g., $R_{\mu_1}^{\bar{m}} = r_a^i(\bar{m})$, $R_{\mu_2}^{\bar{m}} = R_{ab}^{ij}(\bar{m})$, etc. Furthermore, we used the conventional notation for the orbital indices, i.e., i, j, k, \dots and a, b, c, \dots label occupied LMOs, and virtual PAOs, respectively. \mathbf{S} represents the PAO metric. The residuals, calculated according to eq. (7.8), determine the new (additional) basis vectors via first-order perturbation theory.

In the LT-DF-LCC2 response method presented recently [103] the Laplace transform identity $1/x = \int_0^\infty \exp(-xt)dt$ is utilized to partition the eigenvalue problem in eq. (7.2) along the doubles–doubles block $A_{\mu_2\nu_2}$, which is diagonal in the canonical orbital basis. A new eigenvalue equation then is

obtained, which involves only the singles parts of the vectors,

$$\begin{aligned}
 A_{\mu_1\nu_1}^{\text{eff}}(\omega_{\bar{m}})R_{\nu_1}^{\bar{m}} &= \omega_{\bar{m}}M_{\mu_1\nu_1}R_{\nu_1}^{\bar{m}} = \\
 &= A_{\mu_1\nu_1}R_{\nu_1}^{\bar{m}} - A_{\mu_1\xi_2} \int_0^\infty dt e^{-\Delta\epsilon_{\xi_2}t} e^{\omega_{\bar{m}}t} A_{\xi_2\nu_1}R_{\nu_1}^{\bar{m}} \\
 &\approx A_{\mu_1\nu_1}R_{\nu_1}^{\bar{m}} - A_{\mu_1\xi_2} \sum_{q=1}^{n_q} w_q e^{-\Delta\epsilon_{\xi_2}t_q} e^{\omega_{\bar{m}}t_q} A_{\xi_2\nu_1}R_{\nu_1}^{\bar{m}}.
 \end{aligned} \tag{7.9}$$

The *effective* Jacobian $\mathbf{A}^{\text{eff}}(\omega_{\bar{m}})$ now depends on the excitation energies of the individual states $\Psi^{\bar{m}}$. In eq. (7.9) $\Delta\epsilon_{\xi_2}$ denotes the canonical orbital energy denominator, whereas the t_q and w_q are the points and corresponding weights of the numerical Laplace integration. Only a few points are required for a sufficiently accurate quadrature. The doubles part of the eigenvector $R_{\mu_2}^{\bar{m}}$, manifested in the Laplace quadrature, no longer enters the Davidson diagonalization, and can be computed on the fly. Eq. (7.9), as it stands, holds for canonical orbitals only, and little appears to have been achieved over the original formulation in terms of the doubles energy denominators. However, eq. (7.9) is the springboard for a formulation in terms of local orbitals. After some algebraic manipulations it can be cast in the computationally amenable form of

$$\begin{aligned}
 A_{\mu_1\nu_1}^{\text{eff}}(\omega_{\bar{m}})R_{\nu_1}^{\bar{m}} &= A_{\mu_1\nu_1}R_{\nu_1}^{\bar{m}} - A_{\mu_1iajb} \sum_{q=1}^{n_q} \text{sgn}(w_q) e^{\omega_{\bar{m}}t_q} \\
 &\times Y_{ac}^{\text{v}}(q) Y_{bd}^{\text{v}}(q) (A_{ckdl\nu_1} R_{\nu_1}^{\bar{m}}) X_{ki}^{\text{o}}(q) X_{lj}^{\text{o}}(q) \\
 &= \omega_{\bar{m}} M_{\mu_1\nu_1} R_{\nu_1}^{\bar{m}}.
 \end{aligned} \tag{7.10}$$

Here, the doubles index ξ_2 of the singles–doubles and doubles–singles blocks of the Jacobi matrix is written explicitly in terms of LMO and PAO indices. The quadrature point dependent transformation matrices occurring in eq. (7.10) are defined as

$$\begin{aligned}
 X_{ij}^{\text{o}}(q) &= W_{ii}^{\dagger} e^{(\epsilon_i - \epsilon_F)t_q + \frac{1}{4} \ln |w_q|} W_{ij}, \\
 X_{ab}^{\text{v}}(q) &= Q_{aa}^{\dagger} e^{(-\epsilon_a + \epsilon_F)t_q + \frac{1}{4} \ln |w_q|} Q_{ab}, \\
 Y_{ab}^{\text{v}}(q) &= V_{ac} X_{cd}^{\text{v}}(q) V_{db}^{\dagger},
 \end{aligned} \tag{7.11}$$

where the matrices \mathbf{W} , \mathbf{Q} , and \mathbf{V} do appear. \mathbf{W} is the usual unitary transformation matrix specified by the chosen localization criterion and transforms from canonical occupied orbitals to LMOs, while \mathbf{Q} transforms from canonical virtuals to PAOs ($\bar{i}, \bar{j}, \bar{k} \dots$ and $\bar{a}, \bar{b}, \bar{c} \dots$ refer to canonical occupied –

and virtual orbitals). The matrix \mathbf{V} is a pseudo-inverse of \mathbf{S}_{PAO} (cf. eq. (4.11)). Since $R_{\mu_2}^m$, calculated as the sum over the quadrature points, is confined to a pair specific local subspace (pair domains), \mathbf{V} corresponds to a pseudo-inverse of *the corresponding block* of the PAO metric $\mathbf{S}_{\text{PAO}}^{ij}$ and thus is (along with \mathbf{Y}^v) *pair specific*. For simplicity this pair dependence is not explicitly written out in eqs. (7.10, 7.11). It has been shown before [46] that quadrature point dependent transformation matrices as defined in eq.(7.11) are sparse.

$\epsilon_F = (\epsilon_{\text{HOMO}} + \epsilon_{\text{LUMO}})/2$, finally, appearing in the exponentials, cancels in eq. (7.10), but ensures that the individual exponential factors are always smaller than one (for positive t_q).

Eq. (7.10) is solved by Davidson diagonalization, yet only singles basis vectors $U_{\mu_1}^m$ now are used to span the Davidson subspace. Hence, since the singles remain un-truncated in the LT-DF-LCC2 response method as specified, any reference to local subspaces is absent. Multi-state calculations are now straight forwardly possible, which is mandatory to reliably find all the relevant low-lying states and also helps to improve the convergence behavior. In our program the whole Davidson procedure is carried out in the canonical basis, transforming basis vectors $U_{\mu_1}^m$ to local basis just for calculating the matrix–vector product $\mathfrak{B}_{\mu_1}^m$, and back-transforming the latter again to canonical basis for further processing in the Davidson procedure. For the working equations of the matrix–vector product, again based on the DF approximation for the ERIs, we refer to chapter 6 (Ref. 103). Of relevance here is the intermediate U_{μ_2} , defined in canonical basis as

$$U_{\mu_2} = \frac{A_{\mu_2\nu_1} U_{\nu_1}^m}{\omega_{\bar{m}} - \Delta\epsilon_{\mu_2}}. \quad (7.12)$$

It can be calculated directly in the local basis as

$$\begin{aligned} U_{ab}^{ij} &= -V_{ac}^{ij} V_{bd}^{ij} \sum_q^{n_q} \text{sgn}(w_q) e^{\omega_{\bar{m}} t_q} \\ &\quad \times X_{ce'}^v(q) V_{e'e} X_{df'}^v(q) V_{f'f} \left(A_{ekfl\nu_1} U_{\nu_1}^m \right) X_{ki}^o(q) X_{lj}^o(q), \\ &= V_{ac}^{ij} V_{bd}^{ij} \bar{U}_{cd}^{ij} \end{aligned} \quad (7.13)$$

The U_{μ_2} is confined to a local subspace, i.e., restricted pair lists and pair domains are specified for it. The index ranges a, b, c, d in eq. (7.13) thus are restricted to individual pair domains $[ij]$, and the pair index ij is confined to the restricted pair list. The dependence of the pseudo-inverse \mathbf{V} on a

specific LMO pair ij now is explicitly indicated, and it is understood that the summation does not run over the repeated indices i, j .

In multi-state calculations it is necessary to dynamically adapt the state specific local subspaces to changes of the approximate eigenvectors in the course of the Davidson diagonalization. For example, the individual eigenstates may come energetically close and mix, or switch the energetical order (root flip). Pair lists and domains for U_{μ_2} thus should dynamically be re-specified. In our program this is done *in each refresh* of the Davidson diagonalization, i.e., when the Davidson subspace is reset to comprise just as many basis vectors as there are eigenstates to be calculated. Pair lists and domains then can be determined by (i) analysis of the singles part of the present approximation to the eigenstate $R_{\mu_1}^{\bar{m}}$, or (ii) by analysis of the *unrestricted* quantity \bar{U}_{cd}^{ii} (diagonal pairs only), implicitly defined in eq. (7.13), and evaluated with the actual $R_{\mu_1}^{\bar{m}}$. For this second variant we use the acronym *Laplace domains*. It has the advantage that pair lists and domains are constructed directly from the data object, which is to be approximated. Even without local restrictions \bar{U}_{cd}^{ii} can be calculated without too much effort by virtue of the DF approximation. For all the details about the (more complicated) Davidson procedure, including pair list and domain construction in the context of the new LT-DF-LCC2 response method we refer to chapter 6 (Ref. 103).

7.2.2 Transition strengths and first-order properties

The calculation of transition strengths and (orbital-unrelaxed) first-order properties in the framework of the original DF-LCC2 response approach is extensively discussed in chapter 3 (Ref. 89). Here we will just provide the most relevant equations to indicate the modifications related to the LT-DF-LCC2 response method.

In order to compute transition strength and first-order properties of state $\Psi^{\bar{m}}$ also the left eigenvector $\mathbf{L}^{\bar{m}}$ and the ground state multipliers $\mathbf{\Lambda}$ are needed. The former is obtained for the LT-DF-LCC2 case by solving the left eigenvalue equation analogue of (7.10), which is of course much easier to converge, since the eigenvalues now are already known. The $\mathbf{\Lambda}$ are determined by the linear equation system

$$0 = \Lambda_{vj} A_{vj\mu_i} + \eta_{\mu_i}, \quad \text{with} \quad \eta_{\mu_i} = \langle 0 | [\hat{H}, \tau_{\mu_i}] | 0 \rangle. \quad (7.14)$$

Again, by virtue of the Laplace trick, it can be partitioned to yield a linear

equation system just for the singles part only, i.e.,

$$\begin{aligned} -\eta_{\mu_1} = & \Lambda_{v_1} A_{v_1 \mu_1} - \left(\sum_{q=1}^{n_q} \text{sgn}(w_q) X_{ki}^o(q) X_{lj}^o(q) \right. \\ & \times \left(\eta_{iajb} + \Lambda_{v_1} A_{v_1 iajb} \right) Y_{ac}^v(q) Y_{bd}^v(q) \Big) A_{ckdl\mu_1}. \end{aligned} \quad (7.15)$$

The Λ_{μ_2} , manifesting in the Laplace quadrature (as negative sum over q), is computed on the fly and kept after convergence for later use (cf. eq. (7.18)).

The transition strength of a one-photon excitation $\bar{m} \leftarrow 0$ is computed as

$$S_{XY}^{0\bar{m}} = \frac{1}{2} \left(\mathbf{M}_X^{0\bar{m}} \mathbf{M}_Y^{\bar{m}0} + (\mathbf{M}_Y^{0\bar{m}} \mathbf{M}_X^{\bar{m}0})^* \right), \quad (7.16)$$

with the left and right transition moments defined as

$$\mathbf{M}_X^{0\bar{m}} = \eta^X \mathbf{R}^{\bar{m}} + \bar{\mathbf{M}}^{\bar{m}}(\omega_{\bar{m}}) \xi^X, \quad \mathbf{M}_X^{\bar{m}0} = \mathbf{L}^{\bar{m}} \xi^X. \quad (7.17)$$

The quantities η^X and ξ^X appearing in the definitions of the transition moments are

$$\begin{aligned} \eta_{\mu_1}^X = & \left(\langle 0 | + \Lambda_{v_i} \langle \tilde{v}_i | \right) [\hat{X}, \tau_{\mu_1}] | 0 \rangle + \Lambda_{v_2} \langle \tilde{v}_2 | [[\hat{X}, \tau_{\mu_1}], T_2^{\text{loc}}] | 0 \rangle, \\ \eta_{\mu_2}^X = & \Lambda_{v_i} \langle \tilde{v}_i | [\hat{X}, \tau_{\mu_2}] | 0 \rangle, \quad \text{and} \end{aligned} \quad (7.18)$$

$$\xi_{\mu_i}^X = \langle \tilde{\mu}_i | \hat{X} + [\hat{X}, T_2^{\text{loc}}] | 0 \rangle, \quad (7.19)$$

with $\hat{X} = \exp(-T_1) X \exp(T_1)$ representing the similarity transformed position operator. The multipliers $\bar{\mathbf{M}}^{\bar{m}}(\omega_{\bar{m}})$ appearing in eq. (7.17) are the solutions of the linear equation system

$$0 = \bar{M}_{v_j}^{\bar{m}}(\omega_{\bar{m}}) \left(A_{v_j \mu_i} + \omega_{\bar{m}} M_{v_j \mu_i} \right) + F_{\mu_i v_j} R_{v_j}^{\bar{m}}, \quad (7.20)$$

which again involves the left vector–matrix product with \mathbf{A} , and additionally, as the *rhs*, the right matrix–vector product of the matrix \mathbf{F} with the right eigenvector. The matrix \mathbf{F} is defined as

$$\begin{aligned} F_{\mu_1 v_1} = & \left(\langle 0 | + \Lambda_{\rho_i} \langle \tilde{\rho}_i | \right) [[\hat{H}, \tau_{\mu_1}], \tau_{v_1}] | 0 \rangle, \quad F_{\mu_2 v_2} = 0, \\ F_{\mu_1 v_2} = & \Lambda_{\rho_1} \langle \tilde{\rho}_1 | [[\hat{H}, \tau_{\mu_1}], \tau_{v_2}] | 0 \rangle, \quad F_{\mu_2 v_1} = F_{\mu_1 v_2}, \end{aligned} \quad (7.21)$$

The partitioning of equation system (7.20) by application of the Laplace trick yields here

$$\begin{aligned}
 -F_{\mu_1\nu_j}R_{\nu_j}^{\bar{m}} &= \bar{M}_{\nu_1}^{\bar{m}}(\omega_{\bar{m}}) \left(A_{\nu_1\mu_1} + \omega_{\bar{m}} M_{\nu_1\mu_1} \right) \\
 &- \left(\sum_{q=1}^{n_q} \text{sgn}(w_q) e^{-\omega_{\bar{m}} t_q} X_{ki}^o(q) X_{lj}^o(q) \left((FR)^{\bar{m}} \right)_{iajb} \right. \\
 &\quad \left. + \bar{M}_{\nu_1}^{\bar{m}}(\omega_{\bar{m}}) A_{\nu_1iajb} \right) Y_{ac}^v(q) Y_{bd}^v(q) A_{ckdl\mu_1}, \tag{7.22}
 \end{aligned}$$

again reducing it to an equation just for the singles part of the multipliers $\bar{\mathbf{M}}^{\bar{m}}(\omega_{\bar{m}})$. The doubles part of $\bar{M}_{\mu_2}^{\bar{m}}(\omega_{\bar{m}})$, calculated on the fly as the negative of the sum over q part in eq. (7.22), is kept at the end for the converged equation for use in eq. (7.17).

The (orbital unrelaxed) first-order properties of state $\Psi^{\bar{m}}$ related to perturbations Y (e.g. position operator for dipole moments) are calculated as

$$\langle Y \rangle_{\bar{m}} = \langle Y \rangle + \mathbf{L}^{\bar{m}} \mathbf{A}^Y \mathbf{R}^{\bar{m}} + \mathbf{\Lambda}^{\bar{m}} \xi^Y. \tag{7.23}$$

$\langle Y \rangle = \mathbf{\Lambda} \xi^Y$ is the corresponding ground-state property (e.g. ground-state dipole moment). The vector $\mathbf{L}^{\bar{m}} \mathbf{A}^Y = {}^L\eta^Y$ is almost identical to η^Y defined in eq. (7.18), with the sole difference that the first term of the singles part (which involves the bra reference state) is dropped and the ground-state multipliers $\mathbf{\Lambda}$ are replaced by the left eigenvector $\mathbf{L}^{\bar{m}}$. The multipliers for the excited state $\mathbf{\Lambda}^{\bar{m}}$ occurring in eq. (7.23) are obtained by solving the linear equation system

$$\Lambda_{\nu_j}^{\bar{m}} A_{\nu_j\mu_i} = -L_{\nu_j}^{\bar{m}} B_{\nu_j\mu_i\rho_k} R_{\rho_k}^{\bar{m}}. \tag{7.24}$$

Again, the matrix $\mathbf{L}^{\bar{m}} \mathbf{B} = {}^L\mathbf{F}$ is almost identical to the matrix \mathbf{F} defined in eq. (7.21) with the sole difference of dropping the first term with the bra reference state in the singles-singles block and substituting $\mathbf{\Lambda}$ by $\mathbf{L}^{\bar{m}}$. Hence, the *rhs* of eq. (7.24) can be calculated using the same machinery as for $\mathbf{F}\mathbf{R}^{\bar{m}}$ in eq. (7.20). Application of the Laplace trick and partitioning of equation system (7.24) finally yields

$$\begin{aligned}
 -{}^L F_{\mu_1\nu_j} R_{\nu_j}^{\bar{m}} &= \Lambda_{\nu_1}^{\bar{m}} A_{\nu_1\mu_1} - \left(\sum_{q=1}^{n_q} \text{sgn}(w_q) X_{ki}^o(q) X_{lj}^o(q) \right. \\
 &\quad \left. \times \left({}^L F_{iajb\ \nu_1} R_{\nu_1}^{\bar{m}} + \Lambda_{\nu_1}^{\bar{m}} A_{\nu_1iajb} \right) Y_{ac}^v(q) Y_{bd}^v(q) \right) A_{ckdl\mu_1}. \tag{7.25}
 \end{aligned}$$

7.3 Test Calculations

The formalism outlined in Sec.7.2 for calculating excitation energies, transition strengths, and orbital-unrelaxed first-order properties is implemented in the MOLPRO package [64]. For a detailed discussion we refer to chapters 2 and 3 (Refs. 10 and 89) (DF-LCC2), and chapter 6 (Ref. 103) (LT-DF-LCC2 excitation energies). In this section we present results performed for a test set of different molecules and different excited states, in order to compare LT-DF-LCC2 and DF-LCC2 response. As a particularly difficult case we consider the lowest five excited states of the phenothiazine-isoalloxazine dyad studied recently [11], for which the initial CCS wavefunctions are entirely wrong. The previous DF-LCC2 response method fails to find the important CT state, whereas LT-DF-LCC2 indeed finds the five lowest states.

The calculations were performed with the cc-pVDZ and aug-cc-pVDZ AO basis sets, along with the related fitting basis sets optimized for DF-MP2. The LMOs were constructed according to Pipek-Mezey (PM) localization (for the aug-cc-pVDZ basis the most diffuse functions were discarded in the PM localization). The Laplace quadratures were carried out over three points, which turned out to be sufficient for quite accurate excitation energies [103]. For the LCC2 ground state calculations the pair lists were truncated at an LMO interorbital distance of 10 bohr, and the orbital domains determined according to the Boughton-Pulay (BP) procedure with a criterion of 0.98. All response calculations were carried out for pair lists denoted in chapter 2 (Ref. 10) as $\forall(ij), (im) \leq 5, (mn) \leq 5$, i.e., pair lists which include *all* pairs of *important orbitals* and other pairs up to an LMO interorbital distance of 5 bohr. For the DF-LCC2 calculations and the LT-DF-LCC2 calculations involving BP domains the important LMOs i, j, \dots were specified as described in chapter 2 (Ref. 10) with a criterion of $\kappa_e = 0.995$, while for the BP domains again a criterion of 0.98 was used. For the LT-DF-LCC2 calculations involving Laplace domains, on the other hand, the important orbitals were determined according to chapter 6 (Ref. 103) employing a criterion of $\kappa_e = 0.999$. For the domains a threshold of 0.98 for important centers was used. With these specifications the sizes of the truncated pair lists and the domains were quite similar for DF-LCC2 and LT-DF-LCC2 response. All canonical reference calculations were calculated with the TURBOMOLE implementation of CC2 response [27,28]. The assignment of the individual states is based on the analysis of the related singles vectors in canonical basis.

Table 6.1 in the previous chapter compares the excitation energies of canonical CC2 vs. the three different local variants investigated here,

i.e., DF-LCC2 and LT-DF-LCC2 employing the local approximations for excited states (involving BP domains) presented earlier [10], the latter in the context of an adaptive multi-state scheme [103], and LT-DF-LCC2 employing the newly proposed Laplace domains [103]. The deviations are all considerably below 0.1 eV with the sole exception of the CT state of 1-phenylpyrrole in the cc-pVDZ basis. For that very case LT-DF-LCC2 with Laplace domains is the only local method which remains well within this error bar. Another special case is the S_3 state of *trans*-urocanic acid, which was not located with the previous DF-LCC2 approach, but now, within the framework of the new multi-state approach no longer constitutes a problem. A particular nasty example is the dyad mentioned above, where the initial CCS eigenvectors have hardly any resemblance to the converged CC2 solution. Especially, the important CT state (shifting electron density from phenothiazine to isoalloxazine) could not be located with the previous DF-LCC2 single-state approach (what was assigned in Ref. 10 as the CT state emerged later as only a partial CT state shifting electron density from phenothiazine to the linking benzene ring, i.e., state S_4 in Table 6.1). The LT-DF-LCC2 multistate method, on the other hand, is able to find the CT state for the cc-pVDZ and the aug-cc-pVDZ basis, and for both domain and pair list variants. The S_4 state of the dyad was not found by the canonical reference calculation. The S_5 state, according to the local methods, carries a considerable (though not dominant) amount of CT character, which is absent in the canonical reference calculation. This is also reflected in a much smaller transition strength vector for the local case. However, the canonical ADC(2) method [113], which usually yields results rather similar to CC2 response, also features two states, i.e., S_2 and S_4 , with dominant CT character. It appears that the dyad constitutes a difficult case indeed, not only for the local methods. The dyad calculation in the aug-cc-pVDZ basis involving five states takes about 219 (250) minutes CPU (elapsed) time per Davidson iteration on six cores Intel(R) Xeon(R) E5462 @ 2.80 GHz. For more detailed timings we refer to chapter 6 (Ref. 103).

Table 7.1 compares the transition strength, computed for the test set with the three local variants, to the corresponding canonical CC2 reference results. The norm of the deviation vector, $|\delta \mathbf{S}^{0\bar{m}}| = |\mathbf{S}^{0\bar{m}}(\text{loc.}) - \mathbf{S}^{0\bar{m}}(\text{can.})|$, is about 10% or less of the norm of the canonical reference, except for cases with tiny transition strengths. For some cases like the S_3 ($\pi \rightarrow \pi^*$) state of N-acetyl-glycine (cc-pVDZ), or the S_3 ($n \rightarrow \pi^*$) state of " β -dipeptide" (aug-cc-pVDZ) there is a marked improvement between the previous DF-LCC2 and the new LT-DF-LCC2 approach with Laplace domains.

Table 7.2 finally presents an analogous comparison for the changes in

Basis	cc-pVDZ						aug-cc-pVDZ				
			$ S^{0\bar{m}} $		$ \delta S^{0\bar{m}} $			$ S^{0\bar{m}} $		$ \delta S^{0\bar{m}} $	
Molecule	st	char.	can.	BP	BP-LT	LD-LT	char.	can.	BP	BP-LT	LD-LT
"β-dipeptide"	S ₁	$n \rightarrow \pi^*$	0.0041	0.0002	0.0001	0.0001	$n \rightarrow \pi^*$	0.0001	0.0001	0.0001	0.0002
	S ₂	$n \rightarrow \pi^*$	0.0114	0.0000	0.0000	0.0008	$\pi \rightarrow Ry$	0.1046	0.0106	0.0273	0.0005
	S ₃	$\pi \rightarrow Ry$	0.0964	0.0089	0.0046	0.0096	$n \rightarrow \pi^*$	0.0180	0.0113	0.0291	0.0002
"Dipeptide"	S ₁	$n \rightarrow \pi^*$	0.0104	0.0005	0.0005	0.0002	$n \rightarrow \pi^*$	0.0092	0.0006	0.0003	0.0005
	S ₂	$n \rightarrow \pi^*$	0.0068	0.0002	0.0001	0.0003	$n \rightarrow \pi^*$	0.0015	0.0001	0.0001	0.0004
DMABN	S ₁	$\pi \rightarrow \pi^*$	0.3043	0.0226	0.0197	0.0085	$\pi \rightarrow Ry$	0.2130	0.0052	0.0074	0.0036
	S ₂	$\pi \rightarrow \pi^*$	5.3951	0.2645	0.2208	0.2509	$\pi \rightarrow Ry$	0.0000	0.0000	0.0000	0.0000
HPA	S ₁	$\pi \rightarrow \pi^*$	0.1903	0.0052	0.0040	0.0025	$\pi \rightarrow \pi^*$	0.1842	0.0038	0.0015	0.0048
	S ₂	$n \rightarrow \pi^*$	0.0023	0.0009	0.0008	0.0009	$\pi \rightarrow Ry$	0.0015	0.0006	0.0009	0.0007
	S ₃	$\pi \rightarrow \pi^*$	1.1457	0.1238	0.0405	0.0601	$\pi \rightarrow Ry$	0.0990		0.0045	0.0055
p-cresol	S ₁	$\pi \rightarrow \pi^*$	0.2036	0.0076	0.0053	0.0051	$\pi \rightarrow Ry$	0.0001	0.0001	0.0001	0.0001
N-acetyl-glycine	S ₁	$n \rightarrow \pi^*$	0.0112	0.0003	0.0003	0.0005	$n \rightarrow \pi^*$	0.0084	0.0003	0.0003	0.0004
	S ₂	$n \rightarrow \pi^*$	0.0044	0.0002	0.0000	0.0001	$n \rightarrow Ry$	0.1329		0.0041	0.0041
1-phenyl-pyrrole	S ₃	$\pi \rightarrow \pi^*$	0.2627	0.1001	0.0654	0.0229	$n \rightarrow \pi^*$	0.0000	0.0001	0.0000	0.0000
	S ₁	$\pi \rightarrow \pi^*$	0.0235	0.0007	0.0016	0.0018	$\pi \rightarrow \pi^*$	0.0359	0.0026	0.0042	0.0015
	S ₂	$\pi \rightarrow \pi^*$	2.2771	0.0524	0.0574	0.0709	$\pi \rightarrow \pi^*$	2.1535	0.0449	0.0340	0.0253
	S ₃	$\pi \rightarrow \pi^*$	0.0848	0.0191	0.0051	0.0045	$\pi \rightarrow Ry$	0.0003	0.0055	0.0003	0.0004
Propanamide	S ₄	CT	0.0103	0.0017	0.0013	0.0016	CT	0.1302	0.0276	0.0210	0.0053
	S ₁	$n \rightarrow \pi^*$	0.0066	0.0010	0.0000	0.0013	$n \rightarrow \pi^*$	0.0006	0.0001	0.0001	0.0000
Tyrosine	S ₂	$\pi \rightarrow \pi^*$	0.0363	0.0007	0.0007	0.0001	$\pi \rightarrow Ry$	0.1217	0.0037	0.0036	0.0013
	S ₁	$\pi \rightarrow \pi^*$	0.1654	0.0033	0.0039	0.0070	$\pi \rightarrow \pi^*$	0.1540	0.0045	0.0027	0.0086
trans-urocanic acid	S ₂	$n \rightarrow \pi^*$	0.0513	0.0242	0.0252	0.0088	$\pi \rightarrow Ry$	0.0111	0.0044	0.0092	0.0087
	S ₃	$\pi \rightarrow \pi^*$	1.5584	0.1178	0.0559	0.0820	$\pi \rightarrow Ry$	0.1516	0.1474	0.0071	0.0078
	S ₁	$n \rightarrow \pi^*$	0.0008	0.0001	0.0001	0.0000	$n \rightarrow \pi^*$	0.0000	0.0000	0.0000	0.0000
	S ₂	$\pi \rightarrow \pi^*$	5.2365	0.0724	0.0555	0.0239	$\pi \rightarrow \pi^*$	5.5697	0.0462	0.0367	0.0019
dyad	S ₃	$\pi \rightarrow \pi^*$	0.0067	—	0.0000	0.0002	$\pi \rightarrow Ry$	0.0029	0.0005	0.0005	0.0002
	S ₄	$\pi \rightarrow \pi^*$	0.5199	0.0029	0.0372	0.0424	$\pi \rightarrow \pi^*$	0.3640		0.0572	0.0536
	S ₅	$\pi \rightarrow Ry$	0.7529	0.0712	0.0169	0.0230	$\pi \rightarrow Ry$	0.0305	0.0052	0.0024	0.0041
	S ₁	$\pi \rightarrow \pi^*$	2.3948			0.1357					
	S ₂	$n \rightarrow \pi^*$	0.0325			0.0149					
	S ₃	CT	0.0968			0.0118					
	S ₄	$\pi \rightarrow \pi^*$	—			2.0273 ^a					
	S ₅	$n \rightarrow \pi^*$	1.1422			0.0853 ^a					

a) Norm of transition strength vector instead of the norm of its deviation from the canonical reference vector.

Table 7.1: Norms (in a.u.) of the transition strength vectors

$|S^{0\bar{m}}| = ((S_{XX}^{0\bar{m}})^2 + (S_{YY}^{0\bar{m}})^2 + (S_{ZZ}^{0\bar{m}})^2)^{1/2}$. The results for the different local calculations are given as the norm of the related difference vector $|\delta S^{0\bar{m}}| = |S^{0\bar{m}}(\text{loc.}) - S^{0\bar{m}}(\text{can.})|$. The labels BP and BP-LT stand for DF-LCC2 and LT-DF-LCC2 results employing BP domains, LD-LT for LT-DF-LCC2 results employing Laplace domains.

the dipole moment vectors on going from the ground- to the individual excited states. The dipole moments turn out to be more sensitive w.r. to the specification of the domains. Note that no domain extensions as in Ref. 89 are used here. Deviations of up to 20 % (or even more in a few cases) are observed. Particularly affected are states with Rydberg character. Somewhat disappointingly the Laplace domains presented here do not show an improvement over the BP domains over all, but rather the contrary. On the other hand, for quite some cases, the Laplace domains are indeed better, e.g., for the HPA, 1-phenylpyrrole, and tyrosine S₁ states, or the β-dipeptide S₃ state (aug-cc-pVDZ basis). Perhaps a merging of the two domain approaches may indeed lead to general improvement. Results from first test calculations already look quite promising.

Basis		cc-pVDZ					aug-cc-pVDZ				
			$ \mu^{0\bar{m}} $	$ \delta\mu^{0\bar{m}} / \mu^{0\bar{m}} $				$ \mu^{0\bar{f}} $	$ \delta\mu^{0\bar{m}} / \mu^{0\bar{m}} $		
Molecule	st	char.	can.	BP	BP-LT	LD-LT	char.	can.	BP	BP-LT	LD-LT
"β-dipeptide"	S ₁	$n \rightarrow \pi^*$	0.3875	1.68	1.42	22.48	$n \rightarrow \pi^*$	0.3721	7.40	5.78	28.63
	S ₂	$n \rightarrow \pi^*$	0.7600	6.25	5.63	3.11	$\pi \rightarrow \text{Ry}$	2.9470	7.26	6.84	5.36
	S ₃	$\pi \rightarrow \text{Ry}$	1.6283	2.86	0.69	9.25	$n \rightarrow \pi^*$	1.0765	7.54	25.38	5.60
"Dipeptide"	S ₁	$n \rightarrow \pi^*$	0.7353	5.44	4.63	2.61	$n \rightarrow \pi^*$	0.9629	1.94	0.91	6.77
	S ₂	$n \rightarrow \pi^*$	0.7401	5.74	4.25	4.29	$n \rightarrow \pi^*$	1.0227	16.58	14.50	5.90
DMABN	S ₁	$n \rightarrow \pi^*$	0.9348	0.34	0.17	5.88	$\pi \rightarrow \text{Ry}$	2.8072	0.61	0.32	4.04
	S ₂	$\pi \rightarrow \pi^*$	2.0718	4.49	3.47	3.91	$\pi \rightarrow \text{Ry}$	1.9141	4.21	0.03	1.79
HPA	S ₁	$\pi \rightarrow \pi^*$	0.2418	8.87	7.41	2.95	$\pi \rightarrow \pi^*$	0.2030	19.91	15.04	5.43
	S ₂	$n \rightarrow \pi^*$	0.6240	3.65	0.86	9.45	$\pi \rightarrow \text{Ry}$	4.5105	3.36	3.28	5.60
p-cresol	S ₃	$\pi \rightarrow \pi^*$	0.8985	3.70	0.96	8.05	$\pi \rightarrow \text{Ry}$	1.5189		30.95	31.93
	S ₁	$n \rightarrow \pi^*$	0.2562	9.73	6.81	4.22	$\pi \rightarrow \text{Ry}$	4.2811	1.78	4.20	6.73
N-acetyl-glycine	S ₁	$n \rightarrow \pi^*$	0.7408	3.74	3.12	3.55	$n \rightarrow \pi^*$	0.9480	0.90	0.84	6.40
	S ₂	$n \rightarrow \pi^*$	0.5942	3.50	4.18	0.83	$n \rightarrow \text{Ry}$	2.2175		0.45	3.22
	S ₃	$\pi \rightarrow \pi^*$	1.9856	27.11	20.17		$n \rightarrow \pi^*$	0.5878	13.22	3.48	2.58
	S ₁	$\pi \rightarrow \pi^*$	0.8822	4.36	7.49	3.48	$\pi \rightarrow \pi^*$	1.0998	8.71	10.22	1.29
1-phenyl-pyrrole	S ₂	$n \rightarrow \pi^*$	2.3809	3.74	5.47	1.81	$\pi \rightarrow \pi^*$	2.2354	4.91	5.84	2.26
	S ₃	$\pi \rightarrow \pi^*$	4.4506	1.78	0.48	0.28	$\pi \rightarrow \text{Ry}$	0.4478	71.74	36.42	37.80
	S ₄	CT	5.7148	0.65	0.75	1.34	CT	3.8053	4.14	8.29	7.26
	S ₁	$n \rightarrow \pi^*$	0.7889	5.99	0.84	6.80	$n \rightarrow \pi^*$	1.0260	11.10	11.52	10.58
Propanamide	S ₂	$\pi \rightarrow \pi^*$	2.0787	2.79	2.52	16.15	$\pi \rightarrow \text{Ry}$	3.1085	4.08	4.32	4.92
	S ₁	$\pi \rightarrow \pi^*$	0.2217	7.31	6.64	0.69	$\pi \rightarrow \pi^*$	0.1916	6.73	10.26	1.66
Tyrosine	S ₂	$n \rightarrow \pi^*$	0.5702	7.51	4.99	19.29	$\pi \rightarrow \text{Ry}$	4.1572	6.63	15.37	18.21
	S ₃	$\pi \rightarrow \pi^*$	1.0688	9.84	2.94	12.30	$\pi \rightarrow \text{Ry}$	4.4276		8.04	11.62
trans-urocanic acid	S ₁	$n \rightarrow \pi^*$	2.3098	1.12	1.50	1.87	$n \rightarrow \pi^*$	2.2847	1.49	0.57	0.45
	S ₂	$\pi \rightarrow \pi^*$	2.2610	2.68	2.53	1.08	$\pi \rightarrow \pi^*$	2.2021	2.85	2.65	1.81
	S ₃	$\pi \rightarrow \pi^*$	2.9996	–	0.93	1.73	$\pi \rightarrow \text{Ry}$	5.7190	2.74	2.78	1.12
	S ₄	$\pi \rightarrow \pi^*$	0.4262	5.97	2.35	14.45	$\pi \rightarrow \pi^*$	0.8143		6.33	28.47
	S ₅	$\pi \rightarrow \text{Ry}$	0.1163	282.60	37.36	31.79	$\pi \rightarrow \text{Ry}$	3.1825	8.48	3.36	3.27
	S ₁	$\pi \rightarrow \pi^*$	1.4090			8.59					
dyad	S ₂	$n \rightarrow \pi^*$	4.1830			17.27					
	S ₃	CT	8.3233			9.80					
	S ₄	$\pi \rightarrow \pi^*$	–			2.4015 ^a					
	S ₅	$n \rightarrow \pi^*$	2.9833			3.2401 ^a					

a) Norm of dipole difference vector instead of the norm of its deviation from the canonical reference vector.

Table 7.2: Norms (in a.u.) of the dipole difference vectors $|\mu^{0\bar{m}}|$ (excited state relative to ground state). The results for the different local calculations are given as the ratio (in %) $|\delta\mu^{0\bar{m}}|/|\mu^{0\bar{m}}|$ of the norm of the related difference vector (canonical minus local vector) relative to the canonical reference value. The labels BP and BP-LT stand for DF-LCC2 and LT-DF-LCC2 results employing BP domains, LD-LT for LT-DF-LCC2 results employing Laplace domains.

7.4 Conclusions

In this contribution we compare our new local CC2 response method, which is utilizing the Laplace transform approach to decompose the energy denominators in the doubles-doubles block of the Jacobian, to the previous local CC2 response method. The new approach, in contrast to the old, works with adaptive pair lists and domains for the eigenvectors of the Jacobian (and generally, the basis vectors of the Davidson subspace), which makes it less dependent on the initial un-truncated CCS wavefunction, and therefore, more robust. Two different variants of adaptive pair lists and domains are compared. Furthermore, multi-state calculations with state-specific local truncations now are possible. With the present implementation, calculations involving more than hundred atoms are routinely feasible [103]. Here we present excitation energies, transi-

tion strengths, and orbital-unrelaxed dipole moments, obtained for a set of different molecules and excited states. While the results obtained for excitation energies and transition strengths agree reasonably well with the canonical reference values, the situation is not yet satisfying for the dipole moments. Presently, work is in progress for improvements along this direction. A generalization to orbital-relaxed properties (and finally analytical gradients w.r. to nuclear displacements) generally is possible for Laplace transformed methods [92, 119].

Chapter 8

Summary

New local approaches for calculating energies and first-order properties of electronically excited states in extended molecular systems are presented. They are based on the CC2 model using Coupled Cluster linear-response theory and local approximations for the wave functions. In the proposed methods the singles excitations are treated non-locally and local restrictions are imposed on doubles amplitudes only.

In the first implementation of DF-LCC2 (Chp. 2) the appropriate local approximations for the amplitude response are determined by analysis of wavefunctions from a simpler level of theory (CCS). Within this method, molecular systems comprising hundred atoms and more can be treated with basis sets of a polarized double-zeta quality. The implementation was then expanded to calculations of the first-order properties and transition moments of excited states.

Despite a certain success, this method remained too inflexible and failed in cases where CCS wavefunctions were qualitatively wrong for the individual excited states of interest. These problems have been circumvented by applying the Laplace transform ansatz of Almlöf in the context of local correlation methods with *a priori* restricted sets of wavefunction parameters, which was first explored at the MP2 ground-state level, resulting in a new local MP2 scheme LT-DF-LMP2 (Chp. 4).

The experience from the LT-DF-LMP2 was then used to implement a new local CC2 program (LT-DF-LCC2), which allows to perform multi-state calculations with on-the-fly adapted local approximations for excited state double amplitudes (Chp. 6). The CC2 eigenvalue problem is partitioned like in the case of the canonical implementation [27], but the integrals and amplitudes stay in the local basis. Thus an effective eigenvalue problem with only singles eigenvector has to be solved, and a considerable reduction of the I/O rate and memory usage is achieved. Furthermore,

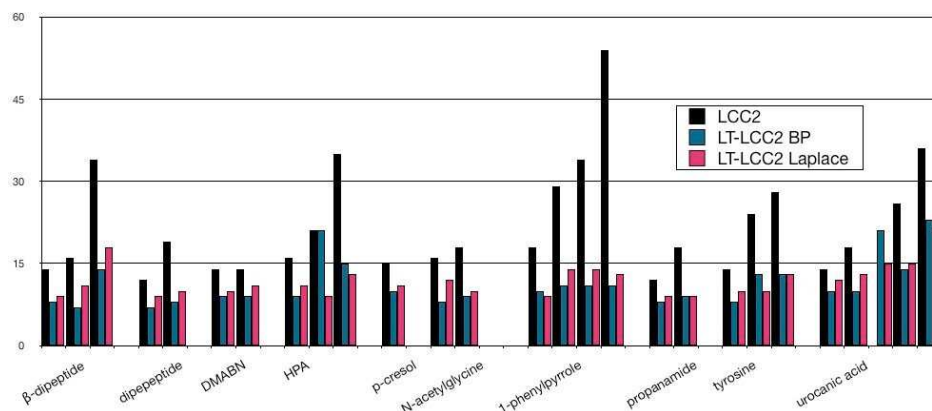


Figure 8.1: Number of iterations in the Davidson diagonalisation for different states and molecules in case of local CC2 (LCC2), LT-DF-LCC2 with Boughthon-Pulay domains (LT-LCC2 BP) and LT-DF-LCC2 with Laplace domains (LT-LCC2 Laplace).

a new procedure to specify the local approximations using intermediate Laplace transformed quantities, related to the CC2 doubles excitation amplitudes in the local basis is proposed. The multi-state calculations also improve the convergence of the iterative Davidson diagonalisation (Fig. 8.1).

In this new method the CCS wavefunctions are used as starting guesses only, and play an inferior role in the quality of the final results. The errors coming from local approximations in LT-DF-LCC2 are smaller than the error of the CC2 method itself (about 0.3 eV) and are usually well below 0.1 eV (Fig. 8.2). The first-order properties and the transition strengths can be also calculated. However the resulting numbers are virtually not

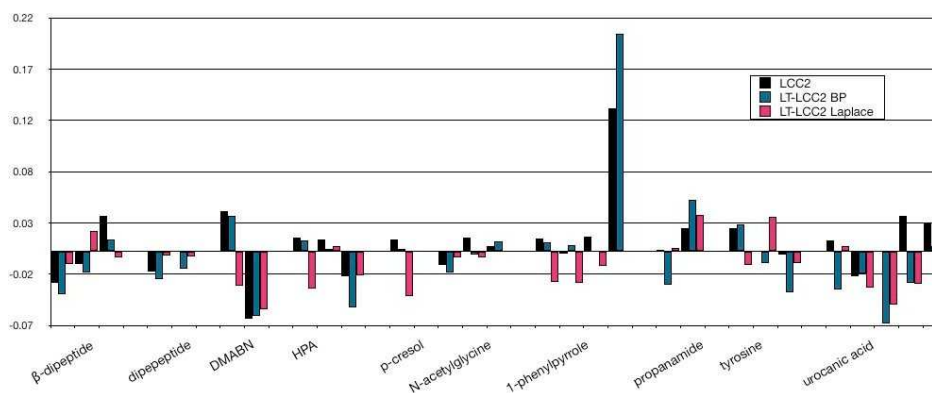


Figure 8.2: Deviations of excitation energies (in eV) from canonical CC2 reference calculations for local CC2 (LCC2), LT-DF-LCC2 with Boughthon-Pulay domains (LT-LCC2 BP) and LT-DF-LCC2 with Laplace domains (LT-LCC2 Laplace).

improved with the new local approximations, if the orbital domains are not further extended.

The LT-DF-LCC2 implementation was also adapted to the algebraic diagrammatic construction through second order ADC(2) [113], allowing one to evaluate the excitation energies at this level (LT-DF-LADC(2)).

The next step is the development of orbital-relaxed first-order properties for the ground and excited states. Thereby one has to add new conditions to the Lagrangians: the localization, the Brillouin ($f_{ai} = 0$) and the orthogonality ($\mathbf{C}^\dagger \mathbf{S} \mathbf{C} = \mathbf{1}$) conditions. For the new Lagrange multipliers additional equations have to be solved: the Coupled-Perturbed Localization Z-Vector (Z-CPL) and the Coupled-Perturbed Hartree-Fock Z-Vector (Z-CPHF) equations. Since these equations appear also in the DF-LMP2 gradient code [43], only the right-hand side of the equations has to be modified.

Developing analytical gradients with respect to nuclear displacements for the ground- and excited states is then a natural extension of the existing code, and geometry optimizations of large excited molecules on *ab-initio* level will become possible. That will open a large field of possible applications like QM/MM studies on biolocal systems [120] etc.

In addition, an extension for the calculation of energies and first-order properties of the triplet states can be performed. The theoretical fundamentals for the canonical methods have already been worked out [121–123] and an adaptation of the formalism for LT-DF-LCC2 should be rather straightforward. With this method, it will be possible to investigate processes in large molecular systems, where triplet states are involved, such as phosphorescence, etc., and will be useful e.g. for design of new organic light emitting diodes (OLEDs).

Bibliography

- [1] Foresman, J. B.; Head-Gordon, M.; Pople, J. A.; Frisch, M. J. *J. Phys. Chem.* **1992**, *96*, 135.
- [2] Buenker, R. J.; Peyerimhoff, S. D. *Theor. Chim. Acta* **1974**, *35*, 33.
- [3] Siegbahn, P. E. M. *Int. J. Quantum Chem.* **1980**, *18*, 1229.
- [4] Lischka, J.; Shepard, R.; Brown, F. B.; Shavitt, I. *Int. J. Quantum Chem. Symp.* **1981**, *15*, 91.
- [5] Werner, H.-J.; Knowles, P. J. *J. Chem. Phys.* **1988**, *89*, 5803.
- [6] Paldus, J.; Li, X. *Adv. Chem. Phys.* **1999**, *110*, 1.
- [7] Casida, M. E. Time-Dependent Density Functional Response Theory for Molecules. In *Recent Advances in Computational Chemistry*, Vol. 1; Chong, D. P., Ed.; World Scientific: Singapore, 1995.
- [8] Dreuw, A.; Head-Gordon, M. *Chem. Rev.* **2005**, *105*, 4009.
- [9] Grimme, S.; Parac, M. *ChemPhysChem* **2003**, *3*, 292.
- [10] Kats, D.; Korona, T.; Schütz, M. J. *Chem. Phys.* **2006**, *125*, 104106.
- [11] Sadeghian, K.; Schütz, M. J. *Am. Chem. Soc.* **2007**, *129*, 4068.
- [12] Yanai, T.; Tew, D. P.; Handy, N. C. *Chem. Phys. Lett.* **2004**, *393*, 51.
- [13] Kobayashi, R.; Amos, R. D. *Chem. Phys. Lett.* **2006**, *420*, 106.
- [14] Jacquemin, D.; Perpète, E. A.; Scalmani, G.; Frisch, M. J.; Kobayashi, R.; Adamo, C. J. *Chem. Phys.* **2007**, *126*, 144105.
- [15] Roos, B. O.; Andersson, K.; Fulscher, M. P.; Malmqvist, P. A.; Serrano-Andrés, L.; Pierloot, K.; Merchan, M. *Adv. Chem. Phys.* **1996**, *93*, 219-331.

- [16] Monkhorst, H. J. *Int. J. Quantum Chem. Symp.* **1977**, 11, 421.
- [17] Stanton, J. F.; Bartlett, R. J. *J. Chem. Phys.* **1993**, 98, 7029.
- [18] Koch, H.; Jørgensen, P. *J. Chem. Phys.* **1990**, 93, 3333.
- [19] Koch, H.; Jensen, H. J. A.; Jørgensen, P.; Helgaker, T. *J. Chem. Phys.* **1990**, 93, 3345.
- [20] Christiansen, O.; Jørgensen, P.; Hättig, C. *Int. J. Quantum Chem.* **1998**, 68, 1.
- [21] Christiansen, O.; Koch, H.; Jørgensen, P. *Chem. Phys. Lett.* **1995**, 243, 409.
- [22] Christiansen, O.; Koch, H.; Jørgensen, P. *J. Chem. Phys.* **1995**, 103, 7429.
- [23] Koch, H.; Kobayashi, R.; de Merás, A. S.; Jørgensen, P. *J. Chem. Phys.* **1994**, 100, 4393.
- [24] Helgaker, T.; Jørgensen, P.; Olsen, J. *Molecular Electronic-Structure Theory*; John Wiley & Sons, LTD: Chichester, 2000.
- [25] Kucharski, S. A.; Bartlett, R. J. *Adv. Quantum Chem.* **1986**, 18, 281.
- [26] Crawford, T. D.; Schaefer III, H. F. *Reviews in Computational Chemistry* **2000**, 14, 33.
- [27] Hättig, C.; Weigend, F. *J. Chem. Phys.* **2000**, 113, 5154.
- [28] Hättig, C.; Köhn, A. *J. Chem. Phys.* **2002**, 117, 6939.
- [29] Ahlrichs, R.; Bär, M.; Häser, M.; Horn, H.; Kölmel, C. *Chem. Phys. Lett.* **1989**, 162, 165.
- [30] Baerends, E. J.; Ellis, D. E.; Ros, P. *Chem. Phys.* **1973**, 2, 41.
- [31] Whitten, J. L. *J. Chem. Phys.* **1973**, 58, 4496.
- [32] Dunlap, B. I.; Connolly, J. W. D.; Sabin, J. R. *J. Chem. Phys.* **1979**, 71, 3396.
- [33] Häser, M.; Almlöf, J. *J. Chem. Phys.* **1992**, 96, 489.
- [34] Feyereisen, M.; Fitzgerald, G.; Komornicki, A. *Chem. Phys. Letters* **1993**, 208, 359.

- [35] Saebø, S.; Pulay, P. *Annu. Rev. Phys. Chem.* **1993**, *44*, 213.
- [36] Pulay, P. *Chem. Phys. Lett.* **1983**, *100*, 151.
- [37] Hampel, C.; Werner, H.-J. *J. Chem. Phys.* **1996**, *104*, 6286.
- [38] Schütz, M.; Hetzer, G.; Werner, H.-J. *J. Chem. Phys.* **1999**, *111*, 5691.
- [39] Schütz, M.; Werner, H.-J. *J. Chem. Phys.* **2001**, *114*, 661.
- [40] Schütz, M. *J. Chem. Phys.* **2000**, *113*, 9986.
- [41] Schütz, M. *J. Chem. Phys.* **2002**, *116*, 8772.
- [42] Schütz, M.; Manby, F. R. *Phys. Chem. Chem. Phys.* **2003**, *5*, 3349.
- [43] Schütz, M.; Werner, H.-J.; Lindh, R.; Manby, F. R. *J. Chem. Phys.* **2004**, *121*, 737.
- [44] Korona, T.; Werner, H.-J. *J. Chem. Phys.* **2003**, *118*, 3006.
- [45] Almlöf, J. *Chem. Phys. Letters* **1991**, *181*, 319.
- [46] Kats, D.; Usvyat, D.; Schütz, M. *Phys. Chem. Chem. Phys.* **2008**, *10*, 3430.
- [47] Crawford, T. D.; King, R. A. *Chem. Phys. Lett.* **2002**, *366*, 611.
- [48] Azhary, A. E.; Rauhut, G.; Pulay, P.; Werner, H.-J. *J. Chem. Phys.* **1998**, *108*, 5185.
- [49] Rauhut, G.; Werner, H.-J. *Phys. Chem. Chem. Phys.* **2001**, *3*, 4853.
- [50] Gauss, J.; Werner, H.-J. *Phys. Chem. Chem. Phys.* **2000**, *2*, 2083.
- [51] Pulay, P.; Saebø, S.; Meyer, W. *J. Chem. Phys.* **1984**, *81*, 1901.
- [52] Paldus, J. Many-Electron Correlation Problem: A Group Theoretical Approach. In *Theoretical Chemistry Advances and Perspectives*; Eyring, H.; Henderson, D., Eds.; Academic Press: New York, 1976.
- [53] Koch, H.; de Merás, A. S.; Helgaker, T.; Christiansen, O. *J. Chem. Phys.* **1996**, *104*, 4157.
- [54] Boys, S. F. . In *Quantum Theory of Atoms, Molecules, and the Solid State*; Löwdin, P. O., Ed.; Academic Press: New York, 1966.

- [55] Pipek, J.; Mezey, P. G. *J. Chem. Phys.* **1989**, *90*, 4916.
- [56] Boughton, J. W.; Pulay, P. *J. Comput. Chem.* **1993**, *14*, 736.
- [57] Hampel, C.; Peterson, K. A.; Werner, H.-J. *Chem. Phys. Lett.* **1992**, *190*, 1.
- [58] Werner, H.-J.; Manby, F. R.; Knowles, P. J. *J. Chem. Phys.* **2003**, *118*, 8149.
- [59] Pulay, P. *Chem. Phys. Lett.* **1980**, *73*, 393.
- [60] Davidson, E. R. *J. Comp. Phys.* **1975**, *17*, 87.
- [61] Hirao, K.; Nakatsuji, H. *J. Comp. Phys.* **1982**, *45*, 246.
- [62] Mata, R. A.; Werner, H.-J. *J. Chem. Phys.* **2006**, *125*, 184110.
- [63] Pflüger, K.; Werner, H.-J. unpublished.
- [64] Werner, H.-J.; Knowles, P.J.; Lindh, R.; Manby, F.R.; Schütz, M. *et al.* "MOLPRO, version 2009.2, a package of ab initio programs", 2009 see <http://www.molpro.net>.
- [65] Dunning, Jr., T. H.; Hay, P. J. Gaussian Basis Sets for Molecular Calculations. In *Methods of electronic structure theory*, Vol. 2; Schaefer III, H. F., Ed.; Plenum Press: , 1977.
- [66] Kendall, R. A.; Dunning, T. H.; Harrison, R. J. *J. Chem. Phys.* **1992**, *96*, 6796.
- [67] Weigend, F.; Köhn, A.; Hättig, C. *J. Chem. Phys.* **2002**, *116*, 3175.
- [68] Hättig, C. *Phys. Chem. Chem. Phys.* **2005**, *7*, 59.
- [69] Schütz, M.; Rauhut, G.; Werner, H.-J. *J. Phys. Chem. A* **1998**, *102*, 5997.
- [70] Shen, Z.; Procházka, R.; Daub, J.; Fritz, N.; Acar, N.; Schneider, S. *Phys. Chem. Chem. Phys.* **2003**, *5*, 3257.
- [71] Furche, F.; Ahlrichs, R. *J. Chem. Phys.* **2002**, *117*, 7433.
- [72] Schäfer, A.; Horn, H.; Ahlrichs, R. *J. Chem. Phys.* **1992**, *97*, 2571.
- [73] Nooijen, M.; Shamasundar, K. R.; Mukherjee, D. *Mol. Phys.* **2005**, *103*, 2277.

- [74] Dreuw, A.; Head-Gordon, M. *J. Am. Chem. Soc.* **2004**, *126*, 4007.
- [75] Meissner, L.; Bartlett, R. J. *J. Chem. Phys.* **1995**, *102*, 7490.
- [76] Fliegl, H.; Köhn, A.; Hättig, C.; Ahlrichs, R. *J. Am. Chem. Soc.* **2003**, *125*, 9821.
- [77] Barbarella, G.; Zarnbianchi, M.; Ventola, A.; Fabiano, E.; Sala, F. D.; Gigli, G.; Anni, M.; Bolognesi, A.; Polito, L.; Naldi, M.; Capobianco, M. *Bioconjugate Chem.* **2006**, *17*, 58.
- [78] Nooijen, M.; Bartlett, R. J. *J. Chem. Phys.* **1997**, *106*, 6441.
- [79] Nooijen, M.; Bartlett, R. J. *J. Chem. Phys.* **1997**, *107*, 6812.
- [80] Koch, H.; de Merás, A. S.; Helgaker, T.; Christiansen, O. *J. Chem. Phys.* **1996**, *104*, 4157.
- [81] Christiansen, O.; Koch, H.; Halkier, A.; Jørgensen, P.; Helgaker, T.; de Merás, A. *J. Chem. Phys.* **1996**, *105*, 6921.
- [82] Christiansen, O.; Halkier, A.; Koch, H.; Jørgensen, P.; Helgaker, T. *J. Chem. Phys.* **1998**, *108*, 2801.
- [83] Gauss, J. Molecular Properties. In *Modern Methods and Algorithms of Quantum Chemistry*; Grotendorst, J., Ed.; NIC Series 1; John von Neumann Institute for Computing (NIC): Jülich, 2000.
- [84] Azhary, A. E.; Rauhut, G.; Pulay, P.; Werner, H.-J. *J. Chem. Phys.* **1998**, *108*, 5185.
- [85] Trieflinger, C.; Rurack, K.; Daub, J. *Angew. Chem. Int. Ed.* **2005**, *44*, 2288.
- [86] Kats, D.; Schütz, M. unpublished.
- [87] Korona, T.; Pflüger, K.; Werner, H.-J. *Phys. Chem. Chem. Phys.* **2004**, *6*, 2059.
- [88] Werner, H.-J.; Knowles, P.; Manby, F. R. *J. Chem. Phys.* **2003**, *118*, 8149.
- [89] Kats, D.; Korona, T.; Schütz, M. *J. Chem. Phys.* **2007**, *127*, 064107.
- [90] Maschio, L.; Usvyat, D.; Manby, F.; Cassassa, S.; Pisani, C.; Schütz, M. *Phys. Rev. B* **2007**, *76*, 075101.

- [91] Usvyat, D.; Maschio, L.; Manby, F.; Cassassa, S.; Schütz, M.; Pisani, C. *Phys. Rev. B* **2007**, 76, 075102.
- [92] Häser, M. *Theor. Chim. Acta* **1993**, 87, 147.
- [93] Ayala, P. Y.; Scuseria, G. E. *J. Chem. Phys.* **1999**, 110, 3660.
- [94] Ayala, P. Y.; Kudin, K. N.; Scuseria, G. E. *J. Chem. Phys.* **2001**, 115, 9698.
- [95] Lambrecht, D.; Doser, B.; Ochsenfeld, C. *J. Chem. Phys.* **2005**, 123, 184102.
- [96] Rauhut, G.; Pulay, P. *Chem. Phys. Letters* **1996**, 248, 223.
- [97] Wilson, A.; Almlöf, J. *Theor. Chim. Acta* **1997**, 95, 49.
- [98] Nakajima, T.; Hirao, K. *Chem. Phys. Letters* **2006**, 427, 225.
- [99] Jung, Y.; Lochan, R.; Dutoi, A.; Head-Gordon, M. *J. Chem. Phys.* **2004**, 121, 9793.
- [100] Jung, Y.; Shao, Y.; Head-Gordon, M. *J. Comput. Chem.* **2007**, 28, 1953.
- [101] Cloizeaux, J. D. *Phys. Rev.* **1964**, 135, A685.
- [102] Pisani, C.; Maschio, L.; Casassa, S.; Halo, M.; Schütz, M.; Usvyat, D. *J. Comput. Chem.* **2008**, in press, .
- [103] Kats, D.; Schütz, M. *J. Chem. Phys.* **2009**, 131, 124117.
- [104] Constans, P.; Ayala, P.; Scuseria, G. *J. Chem. Phys.* **2000**, 113, 10451.
- [105] Takatsuka, A.; Ten-no, S.; Hackbusch, W. *J. Chem. Phys.* **2008**, 129, 044112.
- [106] Braess, D.; Hackbusch, W. *IMA J. Numer. Anal.* **2005**, 25, 685.
- [107] Braess, D. Nonlinear Approximation theory. In ; Springer-Verlag: Berlin, 1986.
- [108] Kats, D.; Usvyat, D.; Loibl, S.; Merz, T.; Schütz, M. *J. Chem. Phys.* **2009**, 130, 127101.
- [109] Häser, M. *Theor. Chim. Acta* **1993**, 87, 147.
- [110] Constans, P.; Ayala, P.; Scuseria, G. *J. Chem. Phys.* **2000**, 113, 10451.

- [111] Pulay, P. *J. Comput. Chem.* **1982**, *3*, 556.
- [112] Sellers, H. *Int. J. Quantum Chem.* **1993**, *45*, 31.
- [113] Trofimov, A.; Schirmer, J. *J. Phys. B-At. Mol. Opt.* **1995**, *28*, 2299–2324.
- [114] Hättig, C. Structure Optimizations for Excited States with Correlated Second-Order Methods: CC2 and ADC(2). In *Advances in Quantum Chemistry - Vol. 50*; Sabin, J.; Brändas, E., Eds.; Academic Press, Inc.: 2005.
- [115] Köhn, A.; Tajti, A. *J. Chem. Phys.* **2007**, *127*, 044105.
- [116] Schreiber, M.; Silva-Junior, M.; Sauer, S.; Thiel, W. *J. Chem. Phys.* **2008**, *128*, 134110.
- [117] Pisani, C.; Maschio, L.; Cassassa, S.; Halo, M.; Schütz, M.; Usvyat, D. *J. Comput. Chem.* **2008**, *29*, 2113.
- [118] Adler, T.; Werner, H.-J.; Manby, F. R. *J. Chem. Phys.* **2009**, *130*, 054106.
- [119] Schweizer, S.; Doser, B.; Ochsenfeld, C. *J. Chem. Phys.* **2008**, *128*, 154101.
- [120] Sadeghian, K.; Bocola, M.; Schütz, M. *J. Am. Chem. Soc.* **2008**, *130*, 12501.
- [121] Hald, K.; Hättig, C.; Yeager, D.; Jørgensen, P. *Chem. Phys. Lett.* **2000**, *328*, 291.
- [122] Hald, K.; Hättig, C.; Yeager, D.; Jørgensen, P. *J. Chem. Phys.* **2001**, *115*, 3545.
- [123] Hättig, C.; Köhn, A.; Hald, K. *J. Chem. Phys.* **2002**, *116*, 5401.

Erklärung

Ich erkläre hiermit an Eides statt, dass ich diese Arbeit selbst verfaßt und keine anderen als die angegebenen Hilfsmittel verwendet habe. Alle aus anderen Quellen direkt oder indirekt übernommenen Daten und Konzepte sind unter Angabe des Literaturzitats gekennzeichnet.

Regensburg, Januar 2010

Danylo Kats